UNIVERSITY OF OKLAHOMA

GRADUATE COLLEGE

SOIL-STRUCTURE INTERACTION STUDIES FOR UNDERSTANDING THE BEHAVIOR OF INTEGRAL ABUTMENT BRIDGES

A DISSERTATION

SUBMITTED TO THE GRADUATE FACULTY

in partial fulfillment of the requirements for the

Degree of

DOCTOR OF PHILOSOPHY

By

KARRTHIK KIRUPAKARAN
Norman, Oklahoma
2013

SOIL-STRUCTURE INTERACTION STUDIES FOR UNDERSTANDING THE BEHAVIOR OF INTEGRAL ABUTMENT BRIDGES

A DISSERTATION APPROVED FOR THE
SCHOOL OF CIVIL ENGINEERING AND ENVIRONMENTAL SCIENCE

BY

_____
Dr. Kanthasamy Muraleetharan, Chair

_____
Dr. Gerald Miller

_____
Dr. Christopher Ramseyer

_____
Dr. Kianoosh Hatami

_____
Dr. Luther White

Dedicated to My Wife, Antonette Kanishka Karrthik

Acknowledgements

I would like to express my sincere gratitude to my advisor, Dr. Kanthasamy K. Muraleetharan for recruiting me from Sri Lanka and guiding me over the past five years. He has served as a wonderful teacher and mentor to me, and spent countless hours working to help me develop as a researcher, student, and human being. His academic advice, guidance, financial support and personal communication are gratefully appreciated. Observing his tremendous knowledge has made me want to become a better thinker and push myself to learn new subjects. My great thanks go to Dr. Gerald A. Miller for his guidance and help to learn instrumentation. I would like to thank my committee members; Dr. Christopher C. Ramseyer, Dr. Kianoosh Hatami and Dr. Luther W. White for serving on my committee and for their guidance and encouragement. I am thankful to Bryce Hanlon for working on the instrumentation of the Oklahoma integral abutment bridge and helping me to familiarize myself with the instrumentation of the bridge.

My appreciation goes to the OU Foundation Fellowship and the Oklahoma Transportation Center (OkTC, Grant No. OTCREOS7.1-37) for the financial support that made my attendance of graduate school possible. The assistance provided by the Oklahoma Department of Transporation Bridge Engineer, Mr. Bob Rusch, and the Assistant Bridge Engineer, Mr. Walt Peters, in the instrumentation of the Oklahoma intergral abutment bridge is also gratefully acknowledged. Futhermore, the support provided by the

Materials Division of the Oklahoma Department of Transporation, and the Geotechnical Lab Supervisor, Mr. Christopher R. Clarke, in the subsurface investigation for the Oklahoma intergral abutment bridge is acknowledged.

I also want to thank the long string of teachers and mentors who have contributed to my learning over the years. Finally, I am profoundly grateful of my life's greatest blessings which are my adorable family members, especially my parents for their loving support and understanding. I would especially like to thank my beloved wife for her immense love and never ending care.

Table of Contents

List of Tables

List of Figures

Abstract

Integral Abutment Bridges (IABs) are increasingly being used to eliminate undesirable effects of bridge joints on the long-term performance of bridges. Behavior of abutments in IABs is, however, poorly understood. Soil-structure interactions at the abutments occurring during thermal loading of a bridge are complex, especially in skewed and long span IABs. This research describes an effort to understand the complex soil-structure interactions occurring in IABs and to propose design guidelines.

The North-bound I-44 Bridge over Medicine Bluff Creek in Comanche County near Lawton, Oklahoma, a 210 feet long, three span IAB with a 10^{o} skew was instrumented for the study and more than three years of data were collected. Instrumentation included pile strain gages, earth pressure cells, tiltmeters, crackmeters, and thermistors. The temperature variation across the depth of superstructure was not uniform and a thermal gradient existed. The field measured seasonal bridge temperatures agreed with the temperature range specified in AASHTO LRFD Specifications. Fairly significant abutment back pressures occurred during the summer and the majority of bridge translation was accommodated by the abutment pile movements in IABs. Abutment piles of IABs were experiencing bending moments beyond the yield bending moment at shallow depths.

Behavior of the Oklahoma IAB was studied using computer programs LPILE, GROUP and TeraDysac. Computed bending moments for abutment piles confirm that piles have yielded at shallow depths. Three-dimensional

model developed in GROUP shows biaxial bending of abutment piles occurs due to the skew of the bridge. Field measured bending moments for the south abutment pile have lower values than the computed bending moments; very likely due to the installation of these piles in pre-drilled holes and not considering the thermal gradient in modeling. Computed TeraDysac bending moments have better agreement with field measurements. A parametric study was conducted to propose design guidelines for IABs. According to this study, in order to accommodate thermal movement in IABs and to reduce bending moments in abutment piles, a smaller HP pile section should be placed in weak axis bending and in pre-drilled holes with low stiffness fill material, especially at shallow depths. Abutment piles for IABs should be checked for capacities under combined axial force and bending moments. Bridges built with longer spans and larger girders will increase the axial load on the abutment piles and concrete stresses in the superstructure, and therefore long-span IABs should be designed with caution. Inclusion of a compressible material and using a flowable fill (CLSM) or using a backfill with soil reinforcement will reduce the passive pressures and settlement of soil behind the abutments. For IABs with larger skew angles, abutment piles should be oriented in weak axis bending along transverse direction. Biaxial bending of abutment piles in skewed IABs increases stresses in the concrete superstructure and the structural components for IABs with larger skew angles have to be designed with caution to accommodate the thermally induced deformations and avoid distresses within the superstructure.

Chapter 1: Introduction

1.1 Overview of Research

Integral Abutment Bridges (IABs) are bridges without any joints within the bridge deck or between the superstructure (decks and girders) and the abutments. IABs have integrally constructed abutments with the bridge girders and deck at the end spans. Traditional bridges have an expansion joint between the abutment and bridge superstructure. Schematic diagrams of a traditional bridge and an IAB are shown in Figures 1.1 and 1.2, respectively. A conventional bridge has stub abutments supported by vertical and battered piles, however, an IAB has abutments supported by vertical piles only. The lateral flexibility of the vertical piles in an IAB permits longitudinal bridge movements that are induced by thermal expansion and contraction of the bridge superstructure subjected to temperature changes.

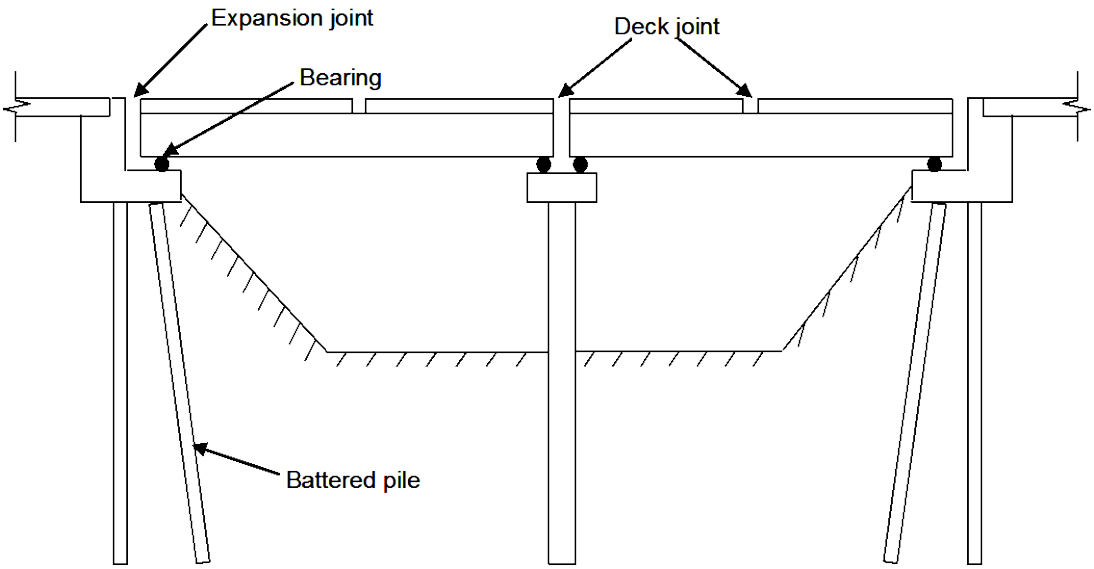

Figure 1.1: Schematic Diagram of a Traditional Bridge

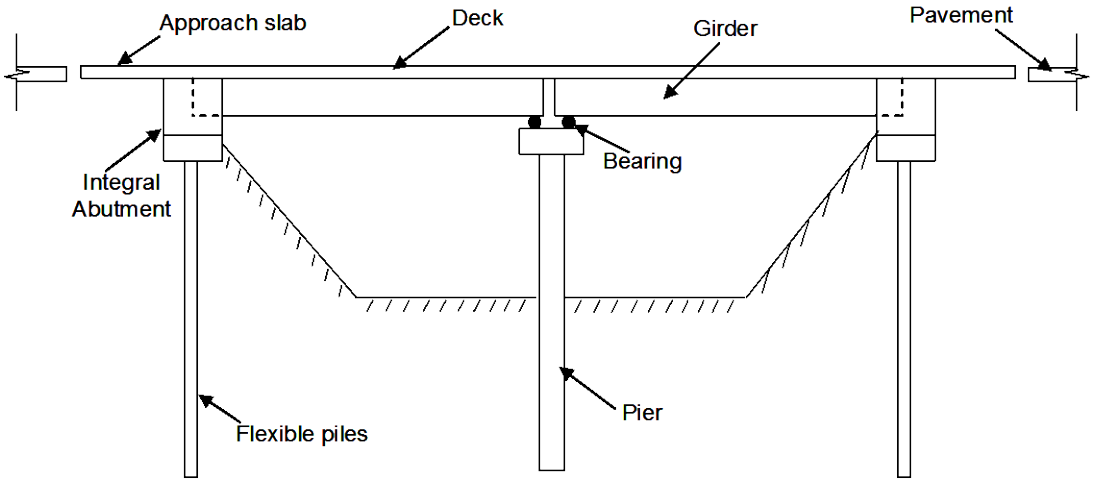

Figure 1.2: Schematic Diagram of an Integral Abutment Bridge

The use of integral abutment bridges has been increasing during the recent years. According to one estimate, more than 13, 900 IABs have been built by 40 bridge agencies in U.S. since 1987. An IAB provides many advantages during the construction and maintenance (Mistry, 2005). The main advantage of an IAB, which affects the structure's life and maintenance costs, is the elimination of roadway expansion joints and associated bearings. Joints and bearings are expensive to buy, install and difficult to maintain. Joints and bearings are also costly to repair and more costly to replace. Roadway runoff through open or leaking joints in a traditional bridge leads to deterioration of girders and bearings. Water within deck joints can also freeze during the cold weather and not be able to properly accommodate thermal contraction and expansion of the bridge. Bridge deck joints are subjected to continuous wear and heavy impact from live loads and seasonal thermal movements of bridge superstructure. Also, concrete creep and shrinkage, and long term movement effects such as settlement and soil pressure contribute to wear and heavy impact of joints. Therefore use of expansion joints and bearings to accommodate thermal movements introduces maintenance problems, hence avoiding expansion joints and bearings leads to lower maintenance costs.

Thermal loading in an IAB is accommodated by the movement of the abutments. In general, abutments are supported on steel piles that are oriented with their weak axis perpendicular to the longitudinal axis of the bridge to allow for translation of the abutments. Prestressed concrete piles,

and steel pipe piles filled with concrete and steel reinforcement at shallow depths are also used for abutment piles. Simple joints between approach slabs and pavements accommodate the relative movements between the bridge and pavement. In an IAB, a monolithic joint at each abutment is formed by casting: (i) concrete abutment pile cap around the upper portion of the abutment piles; and (ii) concrete abutment backwall around the ends of the bridge girders at the same time as the end portion of the bridge deck is cast, hence developing force and moment resistance at the construction joint between the pile cap and backwall of the abutment. Monolithic IABs also provide superior performance during extreme loading events such as earthquakes and blast loading.

In the design of IABs, it is essential to evaluate the induced forces in the abutment and abutment piles and establish the ductility requirements for the abutment piles due to longitudinal translation. Integral construction creates additional strains and stresses in the bridge elements due to thermal expansion and contraction of the bridge, and creep and shrinkage of concrete. Translation of the abutments into and away from the soil backfill behind an abutment wall creates pressures on the backwall and induces forces in the abutment piles. Passive earth pressures from the soil backfill and the horizontal reactions from the piles induce axial forces, shear forces, and bending moments in the bridge superstructure.

Soil-structure interactions at the abutments occurring during the thermal loading of a bridge are complex. It becomes more complex in

skewed and long span IABs. Interactions taking place in between the superstructure, abutments, piers, foundations and soils in IABs are not well understood. Because of the uncertainties in understanding these interactions, Oklahoma Department of Transportation (ODOT) has been reluctant to build longer and skewed IABs. These uncertainties also affect the ability of the agency to properly predict the long term behavior of these bridges. This research provides valuable insight into the complex soil-structure interactions occurring in IABs. Advanced computer simulation tools validated with field performance data are used to understand the soil-structure interactions in IABs. Validated computer simulation tools will be utilized to study the long term performance of existing IABs and propose guidelines to build new IABs with longer lengths and larger skew angles.

1.2 Objectives

The goal of this research is to understand the complex interactions occurring in IABs and to propose design guidelines to build new IABs with longer lengths and larger skew angles. The objectives of this research are: (i) to instrument a skewed IAB in Oklahoma and collect data which can provide valuable insight into the complex soil-structure interactions occurring in IABs for local conditions; (ii) utilize the field data to validate computer simulation tools for Oklahoma conditions and construction practices; and (iii) to use the validated computer simulation tools to understand the long-term behavior of IABs and propose design guidelines to build new IABs with longer lengths and larger skew angles. Understanding the long-term behavior of IABs will

reduce uncertainties in the long term performance of IABs and enhance the design and construction practices of IABs in Oklahoma.

1.3 Outline of Dissertation

This dissertation is organized into 9 chapters. General introduction laying out the objectives for the dissertation is included in Chapter 1. A literature review considering previous and relevant work related to IABs is provided in Chapter 2. A Description of the instrumentation and data collection is provided in Chapter 3. The subsurface exploration, in-situ testing and laboratory testing for the Oklahoma IAB are described in Chapter 4. The effect of temperature and solar radiation on the Oklahoma IAB is described in Chapter 5. Furthermore, Chapter 5 includes the behavior of the Oklahoma IAB for daily temperature variations. The behavior of the Oklahoma IAB for seasonal temperature variations is presented in Chapter 6. Numerical modeling of the Oklahoma IAB is described in Chapter 7. A parametric study conducted to extend the results of the Oklahoma IAB to more general IABs is detailed in Chapter 8. The concluding remarks from the behavior of the Oklahoma IAB and the parametric study are summarized in Chapter 9. Design recommendations and recommendations for future research are also provided in Chapter 9.

Chapter 2: Literature Review

2.1 Performance of IABs

A survey on the performance of IABs was conducted by Greimann et al. (1984) among twenty nine design agencies. According to the responses for the survey, more than half of the design agencies oriented the abutment piles in strong axis bending in order to accommodate the induced thermal loading due to the expansion and contraction of the bridge superstructure. The survey also revealed that there was a wide variation in the construction practices of IABs from state to state. Pile-head details were either fixed, hinged or partially restrained at the tops of abutment piles, and pile caps were or were not used. Approach slabs were tied to the abutment backwalls with the use of dowels in some states while expansion joints were provided between the approach slabs and bridge slabs in other states. A granular backfill material was used behind the abutments, however, some states do not provide any specification for the backfill material. Limitations on the length of IABs were established on the basis of experience and engineering judgment. Many agencies have progressively increased the bridge length limitations, primarily based on the observed satisfactory bridge performance. As of 1983, the bridge length limitations for non-skewed IABs were 150 ft to 400 ft for steel girder bridges, 150 ft to 800 ft for concrete girder bridges, and 200 ft to 800 ft for prestressed concrete girder bridges. The same length

limitations are used for skewed IABs in most states. Most agencies use their own empirically based limitations and criteria for the design of IABs.

Performance of IABs in Tennessee was presented by Loveall (1985) and Wasserman (1987). As of 1987, the maximum lengths of steel girder IABs and prestressed concrete girder IABs were 400 ft and 800 ft, respectively, in Tennessee. However, it was indicated that the longest IAB in Tennessee is a 927 ft long concrete IAB. It was noted that a temperature range of 0 ^{o}F to 120 ^{o}F for steel girder IABs and a temperature range of 20 ^{o}F to 90 ^{o}F for concrete girder IABs are used for bridge design in Tennessee. With these temperature ranges and maximum bridge lengths, the thermal movement of the superstructure is about 2 inches. Abutment pile translation and rotation capacities are considered and modified foundation conditions are used when feasible in order to establish the long bridge lengths. Furthermore, the following approaches are considered for establishing longer lengths: (i) using reduced modulus of elasticity for long term thermal loading on concrete substructures; (ii) allowing plastic hinges to form in the steel abutment piles and constructing internal hinges in parts of the structure; and (iii) using expansion bearings when required.

Performance of IABs in California, New York and Tennessee was discussed by Wolde-Tinsae et al. (1988). Some of the problems that were encountered in IABs were presented and the corrective measures that were used by these states to improve the performance of IABs were discussed by Wolde-Tinsae et al. (1988). It was noted that the evaluated IABs are

performing as intended and have not experienced major structural problems or long term serviceability problems in most cases. For IABs with the length of 450 ft or more, some of the problems encountered included the settlement of the approach slabs and the development of compression induced bumps in the roadway at the ends of the bridges.

Design considerations that need to be addressed for IABs were assessed by Russell and Gerken (1994). It was indicated IABs must accommodate the thermal movements that are induced by the expansion and contraction of bridge superstructure, and concrete creep and shrinkage. It was indicated that seasonal temperature variation primarily affects the longitudinal movement of the bridge and daily temperature variation primarily affects thermal gradients through the depth of the bridge superstructure. Resistance to bridge movements provided by the abutment stiffness and earth pressures behind the abutments were discussed in this study.

Performance of IABs in New York was presented by Alampalli and Yannotti (1998). A condition rating system was used in this study to present the findings of visual inspections of various bridge components in IABs. Statistical methods were applied by Alampalli and Yannotti (1998) to evaluate the performance of prestressed girder IABs in New York. The findings were that the condition of the bridge deck and abutments directly correlated with the span length for the bridge. Lower deck and abutment ratings occurred for bridges with long span lengths. The skew angle of the bridge significantly affected the performance of the deck slabs and the

approach slabs. Bridges with large skew angles produced lower condition ratings for both the bridge deck and the approach slabs. It was indicated that abutments with straight wingwalls performed better than abutments with flared wingwalls. Furthermore, the condition ratings for the bridge components were not significantly influenced by the type of abutment piles. It was concluded that IABs in New York have performed very well and the construction practices are quite satisfactory.

A detailed survey of current practices for the design of IABs was performed by Kunin and Alampalli (1999, 2000) for the New York State Department of Transportation. Thirty nine transportation agencies in the United States and Canada responded to the survey. A questionnaire targeting various aspects of the design and performance of IABs such as bridge length, skew angle, design assumptions, design and analysis procedures was circulated among the agencies. Most of the agencies indicated they had a good experience with IABs. Only minor problems were reported including minor cracking in the deck near the piers, cracking and spalling of concrete in bearing areas, drainage problems in the abutment backfill, and settlement of the approach slabs. It was indicated that the majority of the agencies use the American Association of State Highway and Transportation Officials (AASHTO) Specifications for the bridge design. The maximum length of IABs varied widely and different assumptions and limitations were applied in the design of IABs. Most design agencies limit the skew angle to 30 degrees. In General, a passive earth pressure is applied in

the design of IABs, however, some agencies neglect the effect of earth pressure on the abutments during thermal expansion of the bridge. Also, the effects of the bridge skew on earth pressures are neglected by most of the agencies. Special construction details are applied by many agencies to reduce backfill pressure on the abutment walls. Following approaches are practiced to reduce the backfill pressure: (i) using a granular embankment backfill with an underdrain; (ii) attaching a foam on the back of abutment wall; and (iii) providing a gap between the abutment wall and a geotextile reinforced backfill.

The survey conducted by Kunin and Alampalli (1999, 2000) indicated that most agencies use HP steel piles oriented in weak axis bending to support the abutments of IABs in order to accommodate the changes in the bridge length. However, some agencies use prestressed concrete piles and concrete filled steel shell piles to support abutments. Only few agencies consider combined axial load and bending moment for the design of the abutment piles. Depending on the pile to abutment connection details, fixed, pinned or free pile head conditions are used in the analysis. Some agencies use the pre-drilled holes for the abutment piles. These pre-drilled holes are filled with either bentonite slurry or sand, or sometimes left unfilled. Many agencies used both prestressed concrete girders and steel girders for IABs. Some agencies reported differences in bridge performance between prestressed concrete girder and steel girder bridges. Prestressed concrete girder bridges showed concrete creep and shrinkage problems while greater

girder rotations at the pier bearings were observed in steel girder bridges. The approach slabs of IABs have the largest number of incidences of poor performance. It was indicated that approach slab problems are settlement, transverse or longitudinal cracking and cracking of asphalt overlays at the ends of the approach slabs.

2.2 Field Instrumentation of IABs

An experimental monitoring program of a 450 ft long, six span IAB with five prestressed concrete box girders, was conducted by Jorgenson (1983). The bridge had a pressure relief system directly behind the abutment backwalls and an expansion joint in the approach slabs located at a distance of 20 ft from each abutment. To compensate for anticipated thermal movements, two unique features (pressure relief system) were built into the bridge. Expansion joint material was placed between the back side of the abutment and the soil backfill and compressible material was placed on the webs of the abutment piles to create low soil resistance to pile movement. Instrumentation included thermocouples to measure air and concrete deck temperatures and slope indicators to measure the change in the slope along the length of selected abutment piles. Displacements at the abutments were not equal even though the bridge appeared to be geometrically symmetric. Seasonal maximum movements at south and north abutments were 1.96 inches and 0.74 inches, respectively. Based on the results of the field monitoring and an analytical model of the bridge, it was concluded that the

abutment piles experienced yielding when the south abutment was fully displaced.

A field instrumentation study was performed by Girton et al. (1989, 1991) in Iowa to measure the performance of IABs. Instrumentation covered the monitoring of temperatures, displacements and strains in two skewed IABs. A steel girder bridge and a prestressed concrete girder bridge were monitored over a two year period of time for changes in bridge length, strains in one abutment pile, and temperatures in deck and girder. Bridge length changes and pile bending strains showed daily and seasonal variations associated with the thermal loading of the superstructure. For each bridge, a bilinear temperature distribution was established through the depth of the superstructure.

Thermally induced superstructure displacements in an IAB were measured by Pentas et al. (1994a, 1994b). A multi span bridge with both steel and prestressed concrete girders was instrumented with thermocouples and linear variable displacement transducers (LVDTs) in this study. LVDTs were used to measure the relative longitudinal movements between the adjoining girder sections at several expansion joint locations. The relative displacement measurements were made near the top and bottom of the bridge girders. These measurements were used to calculate relative rotations between the girder ends. Unsymmetrical movements were recorded for the expansion joint along the width of the bridge. These measurements were

believed to be caused due to the variability in the longitudinal stiffness of the neoprene supports for the bridge girders.

The behavior of skewed IABs had been discussed by Stanford and Elgaaly (1994). It was reported active soil pressures are normally considered in IAB design despite the movement of the abutments into the soil from thermal expansion of the deck. Furthermore, many abutments are located on a skew and possible effects of this skew on the backfill soil pressures behind the abutments are not considered in design. Passive soil pressures behind a skewed IAB was monitored by Sandford and Elgaaly (1994). It was reported that the skew effects on the earth pressure changes developed near the deck level behind the backwall of the abutments are substantial, however, the magnitude of earth pressure changes are lower than that of straight IABs. Furthermore, the horizontal variations of earth pressure changes are greater than the vertical variations.

Field monitoring of a steel girder IAB was performed by Oesterle et al. (1999) to determine the temperature gradients in the bridge superstructure. It was indicated the positive temperature gradient recommended by the AASHTO Load and Resistance Factor Design (LRFD) Specifications (1998) was conservative, however, the temperature gradient followed the general shape of the experimentally measured temperature gradients within the cross section for the bridge. Maximum experimentally measured temperatures were approximately 60 percent of the recommended AASHTO temperatures.

Long term monitoring of a non skewed three span prestressed concrete girder IAB was performed by Lawver et al. (2000) in Minnesota. The abutment piles were oriented in weak axis bending to incorporate the bridge superstructure thermal movement due to temperature changes. Longitudinal abutment movement was primarily a translational movement that induced double curvature bending in the abutment piles. Tensile strains were measured in the winter as the superstructure pulled the abutment away from the backfill. Strain gages at the abutment piles were placed during the construction of the bridge and induced axial strains due to the self weight of the bridge superstructure were measured in selected abutment piles. The maximum axial compressive strain in an abutment pile was 392 micro strains for the combined loading due to self weight of superstructure and thermal movements of the bridge. As the temperature of the bridge deck increased, the axial strains increased in an interior pile and decreased in an exterior pile of the abutment. The maximum compressive strains in an abutment pile due to the combined loading of axial forces and bending moments were larger than the yield strain of the steel pile.

Behavior of a prestressed concrete IAB was studied by Huang et al. (2004) in Minnesota. Monitoring of abutment horizontal movements, abutment rotations, abutment pile strains, earth pressure, pier pile strains, prestressed girder strains, concrete deck strains, thermal gradients and weather were performed from 1996 to 2004. Two live load tests were also conducted. A three-dimensional finite element model of the bridge including

soil-structure interaction was calibrated to the live load tests and the seasonal temperature changes. The finite element model was used to investigate the long term behavior of IABs. It was noted that abutment substructure provided small rotation restraint to the end span girders and thermal loading effects were as large as or larger than the live load effects. The 131 ^{o}F measured temperature range was larger than the 80 ^{o}F temperature range specified in the AASHTO LRFD Specifications (2002). The measured thermal gradients were 9 ^{o}F to 10 ^{o}F smaller than the specified thermal gradients in the AASHTO LRFD Specifications (2002). It was indicated that average pile curvatures also steadily increased. Nearly two percent of the flange cross section had longitudinal strains that exceeded the steel yield strains. The measured coefficient of thermal expansion and contraction for the bridge, which was between 6.1 and 6.4 micro strains per ^{o}F, was greater than the AASHTO recommended value of 6.0 micro strains per ^{o}F.

Several recommendations were provided by Huang et al. (2004) for the construction of IABs. Recommendations included that a 130 ^{o}F temperature range should be used for prestressed concrete girder bridges. Four to six foot depth pre-drilled holes should be used for the abutment piles. The abutment piles should be oriented to bend about the weak axis during thermal expansion and contraction of the bridge superstructure. Pile can be designed for only vertical loads with an allowable stress of 9 ksi for the combined loading of axial force and bending moment. Furthermore, it was

reported that a hinged connection should be used between the abutment pile cap and abutment diaphragm in order to reduce the concrete stress and improve the pile behavior. Huang et al. (2004) also reported that the configuration of abutment wingwall has little effect on the behavior of the abutment piles.

An experimental monitoring program of a 210 feet long, three span IAB with a 10^{o} skew in Oklahoma was conducted by Hanlon (2010). The bridge was instrumented with pile strain gages, earth pressure cells, crack meters, tilt meters and thermistors in order to capture the behavior during thermal loading. More details of this instrumentation work are provided in Chapter 3. The behavior of this skewed IAB for daily temperature changes immediately after the construction of the bridge are reported in Hanlon (2010).

2.3 Numerical Modeling of IABs

The effects of pre-drilled holes on vertical load-carrying capacity of HP piles were investigated by Yang et al. (1985). A non-linear finite element algorithm for pile-soil interaction was developed and implemented in a computer program to study the effects of pre-drilled oversize holes and layered soils on the vertical load carrying capacity of piles in IABs. It was found that the vertical load carrying capacity of HP piles was significantly affected by pre-drilling for a very stiff soil condition and a pile-head movement of more than two inches. Without pre-drilled holes, at least 50% of the ultimate vertical load capacity was reduced due to the high stresses in

piles comparing to the vertical load capacity without lateral movements. With a 6-feet long predrilled hole, the reduction of the ultimate load capacity was less than 3%.

A two-dimensional frame model was developed by Girton et al. (1989) to predict the longitudinal displacements of abutments in IABs. The model incorporated the flexural stiffness of the piles and axial and flexural stiffness of the bridge superstructure. Displacement restraint of the soil backfill was neglected in the model. A bilinear temperature distribution through the depth of the superstructure was applied to the model. A two-dimensional frame model was also developed by Girton et al. (1989) to predict the induced pile strains due to the longitudinal thermal movements of the superstructure.

A parametric study of single-span jointless steel bridges was conducted by Thippeswamy et al. (1994) in order to investigate the effects of variation in span length, abutment height, gravity load, earth pressure and soil settlement. In this study, a finite element analysis program was used to generate moment and deformation data. The soil-structure interaction was neglected in the two-dimensional linear frame model used by Thippeswamy et al. (1994). The moment and deformation data were also generated for a simply supported jointed bridge to compare with the jointless bridge. It was reported that maximum mid-span moment caused by external loads in a jointless IAB was to be approximately 50% of the maximum mid-span moment found in a simply-supported jointed bridge. The lower mid-span

moment in the jointless bridge explained the superiority of the performance of a jointless bridge over a simply-supported jointed bridge.

Numerical studies of five in-service IABs were performed by Thippeswamy and GangaRao (1995). Analyses were performed using two-dimensional frame models with different rotational restraint conditions for the supports. The orientation of the abutment piles in these analytical models was also set to produce either weak axis or strong axis bending of the abutment piles for the thermal loading. The loading conditions involved gravity, soil pressure, concrete creep and shrinkage, differential support settlement, and temperature. Following conclusions were obtained from the study: (i) temperature loading produced significant stresses in the bridge; (ii) concrete creep reduced the induced bending stresses; (iii) concrete shrinkage relieved some of the effect of concrete creep; (iv) soil pressures induced negligible stresses in the bridge; and (v) support settlements induced significant stresses in multiple span IABs.

A numerical study to investigate the effects of thermal loading and soil-structure interaction on the performance of steel girder IABs was conducted by Siros (1995). A uniform temperature change was applied along the length of the bridge superstructure and a temperature gradient was applied across the depth of the concrete deck. Furthermore, stresses in the concrete deck and steel girders were calculated for various boundary conditions of the abutments. The bottom surface of the abutments were considered to be either fixed, pinned, or horizontally restrained by springs

with an equivalent horizontal stiffness based on either an upper bound or a lower bound soil stiffness. When the lateral stiffness of the abutment backfill was set equal to an upper bound soil stiffness, the predicted stresses in the bridge deck and girders were about 9 and 28 percent of the allowable stresses for the concrete and steel, respectively. When the lateral stiffness of the abutment backfill was set equal to a lower bound soil stiffness, the stresses became 8 and 22 percent of the allowable stress for the concrete deck and steel girders, respectively.

A nonlinear finite element analysis considering the interaction between the abutments and the soil backfill was performed by Oesterle et al. (1999). It was indicated that the Rankine passive soil pressure model provided an adequate estimation of soil pressures against the back of a bridge abutment when large abutment movements were caused by expansion of the bridge superstructure. It was noted that the Clough and Duncan (1991) soil stiffness design curve for soil pressure based on wall movement provided a reasonable upper bound value for the soil pressure against an abutment that experiences large displacements. Oesterle et al. (1999) noted that a decrease in the compaction of the soil backfill from 90 to 80 percent will decrease the resultant passive soil pressure force by a factor of about two and a half. It was determined that a decrease in the slope of the in-situ soil backfill from 45 to 30 degrees will decrease the resultant passive soil pressure force by a factor of about two.

A simplified elastic model was developed by Lehane et al. (1999) to predict the axial forces and bending moments induced in the abutment piles of a frame type IAB when thermal expansion occurs in the bridge superstructure. A simplified plane frame model that incorporated an equivalent abutment height and a translational linear spring at the deck level, was developed to represent the abutment and soil backfill system. The results from the simplified analytical model correlated well with the results predicted by a more detailed finite element model.

Interactions between abutment piles and foundation soils, between approach fills and foundation soils, between abutments and approach fills, and between abutments and abutment piles were investigated by Arsoy et al. (2002). Finite element models for isolated piles, and IABs were used in this study. Both integral abutments and semi integral abutments and three soil conditions (dense, medium dense, and loose sand) were incorporated in the study. Based on the parametric analyses, it was concluded that the presence of approach fills significantly reduces the forces in the abutment piles from that which would occur without an approach fill as the approach fill drags the foundation soil in the same direction as the movement of the pile head. It was concluded that semi integral abutments induce significantly smaller pile stresses than those induced by integral abutments when both types of abutments had the same amount of horizontal displacement at the top of the abutment piles.

The long-term response predictions of IABs were presented by Pugasap et al. (2009) in Pennsylvania. An analytical long term response prediction methodology using finite element models was presented and the results were compared with the field measured response of three different IABs in Pennsylvania. An evaluation of measured responses indicated that bridge movement progresses year by year with long term response being significant with respect to static predictions. Both two-dimensional and three-dimensional finite element models were developed using ANSYS to determine an efficient and accurate analysis level required for modeling. Seasonal cyclic ambient temperature and equivalent temperature derived from time dependent strains using the age adjusted effective modulus method were employed as major loads in all finite element models. The elastoplastic *p-y* curve method, classical earth pressure theory, and moment-rotation relationships with parallel unloading paths were used to model hysteretic behavior of soil-pile interaction, soil-abutment interaction, and abutment to backwall connection. Predicted soil pressures obtained from all finite element models were similar to the measured response. Predicted abutment displacements, and corresponding design forces and moments at the end of the analytically simulated 100 year period showed that the time dependent effects (creep and shrinkage) of superstructure dominate total long-term abutment displacements near the abutment top, while elastoplastic behavior of soil-pile system and time dependent effects of superstructure share a nearly equal contribution near the abutment base elevation. It was

indicated an increase in prestressed girder age at erection will significantly mitigate long-term abutment top displacements and reduce long-term abutment bottom displacements. It was concluded that the significance of long-term behavior should be considered in the design of IABs.

Finite element programs, TeraGrande (ANATECH 2005) and TeraDysac (Muraleetharan et al. 2003, Ravichandran 2005) were used by Krier (2009) to study the behavior of IABs for thermal loading. Results from the field instrumentation of an IAB in Minnesota were used for this study. A series of analyses of the Minnesota IAB superstructure were performed using TeraGrande. The advanced reinforced concrete analyses which model rebar accurately and use a smeared crack model to study nonlinear concrete behavior showed that for the deformations experienced during the thermal loading, the linear structural elements developed for TeraDysac are adequate. Significant concrete cracking was not observed in the superstructure and stresses and strains were low enough that the linear elastic assumptions embedded in beam and plate formulations available within TeraDysac were acceptable. Two thermal events were studied in TeraDysac, a heating event during the summer and a temperature drop during the winter. The IAB used for the validation had a zero skew angle. A series of two-dimensional analyses were used to study the bridge behavior. A three-dimensional analysis comparing the Minnesota IAB superstructure (no skew) and a skewed version of the same superstructure was also presented. A non-uniform abutment movement and stress distribution in the

backfill soils were observed in the skewed IAB. The deformation at the obtuse corner was greater than at the acute corner.

Chapter 3: Instrumentation of the Oklahoma IAB

3.1 Bridge Description

The IAB mentioned in this research is the North-bound I-44 Bridge over the Medicine Bluff Creek in Comanche County near Lawton, Oklahoma. The bridge under construction is shown in Figure 3.1. This is a 210 feet long, three span IAB with a 10^{o} skew. The exterior spans are 60 feet long, and the interior span is 90 feet long. The dimensions of the Oklahoma IAB are shown in Figure 3.2. The structure was designed for two lanes of traffic with a roadway of 24 feet. A 13 feet shoulder is provided along the east side of the bridge deck and a 4 feet sidewalk along the west side of the deck. The structure includes a concrete deck supported on four prestressed concrete girders. Each abutment wall is supported on seven HP 10x42 steel piles and the central piers are supported on two 60-inch diameter drilled shafts per pier. The abutment piles are embedded 2 feet into the bottom of the abutment wall. The abutment piles are oriented with their weak axis perpendicular to the longitudinal bridge axis to offer the least resistance to bending during thermal movements of the bridge.

Figure 3.1: North Bound I-44 Bridge over Medicine Bluff Creek under Construction

The soil underneath the south abutment is a 8-foot thick layer of stiff lean clay. This soil deposit is underlain by a 2-foot thick layer of dense silty sand, followed by a laminated sandstone rock interbedded with shale seams (very weak to weak rock). The soil underneath the north abutment is a 11-foot thick layer of stiff lean clay, followed by a 5-foot thick layer of dense silty sand. This layer is underlain by the laminated sandstone interbedded with shale seams (very weak to weak rock).

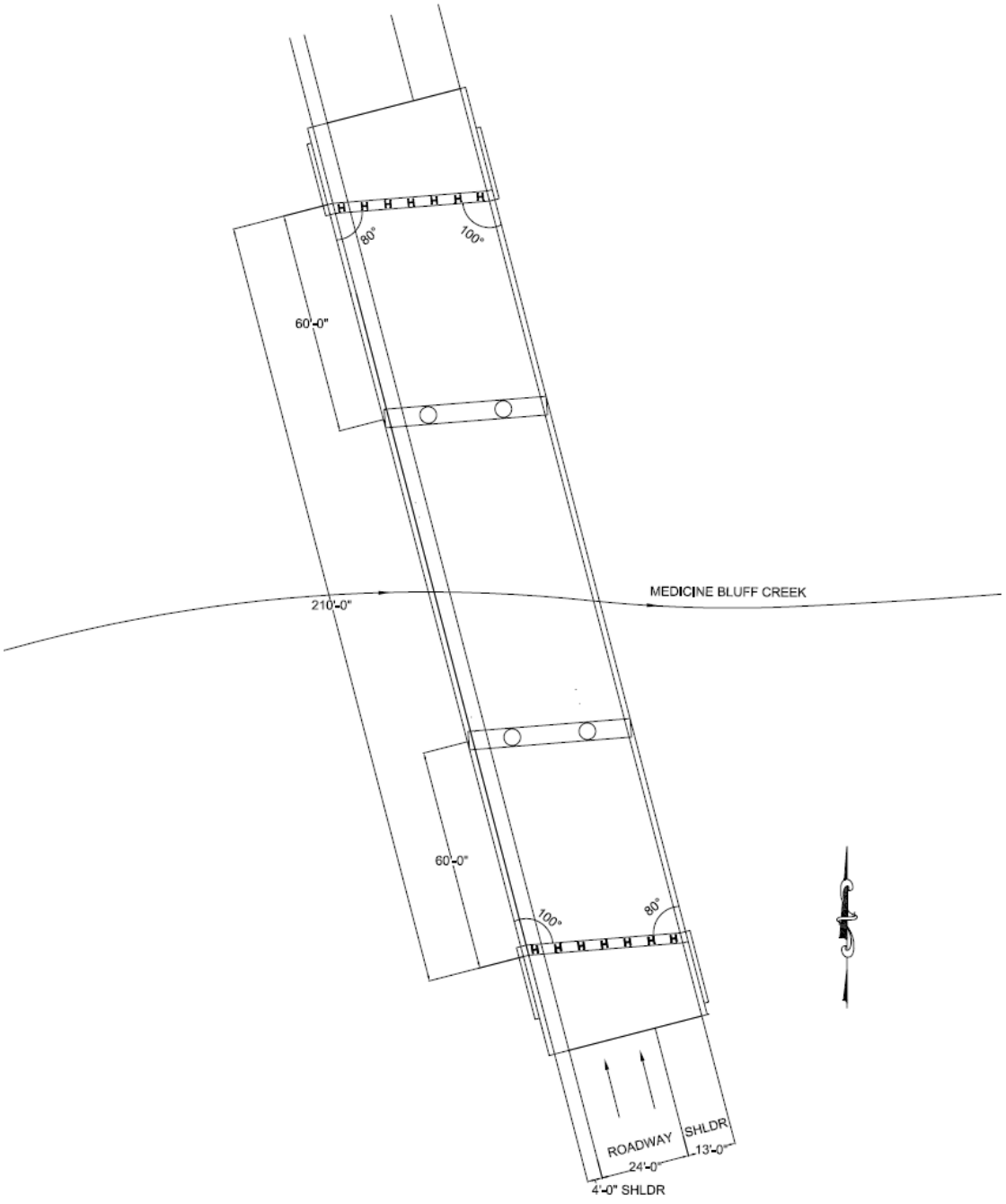

Figure 3.2: Dimensions of the Oklahoma IAB

3.2 Bridge Instrumentation

The bridge was instrumented with 46 separate instruments to capture the behavior during thermal loading. Detailed description of the bridge instrumentation was provided by Hanlon (2010). Key details of Hanlon's (2010) work are summarized here. Five different types of instruments (pile strain gages, earth pressure cells, crack meters, tilt meters, and thermistors) were employed in the bridge instrumentation. All of them were vibrating wire type instruments manufactured by Geokon, Inc.

3.2.1 Strain Gages

Abutment piles instrumented with vibrating wire strain gages (SG) are shown in Figure 3.3. The north east (NE) and south east (SE) piles were instrumented at three depths while the south west (SW) pile was instrumented at two depths. At each depth, two strain gages were placed on the web on the opposite sides (north and south sides) so that the bending strains can be separated from the axial strains. Therefore a total of sixteen strain gages were attached to the abutment piles. The piles were driven after the instrumentation. The locations of strain gages are presented in Figure 3.4. It was planned to instrument the north east abutment pile at a shallower depth, however, the pile was driven to a greater depth than the planed depth in order to achieve the required bearing capacity. Therefore the strain gages attached to the north east abutment piles were placed at a greater depth compared to the south abutment piles. Furthermore, the south west abutment pile reached the required bearing capacity at a shallower depth

than the planned depth and therefore only two strain gages were placed in the south west abutment pile. Pre-drilled holes were used to drive the south abutment piles as a stiff soil layer was available at shallower depths, however, pre-drilled holes were not used for the north abutment piles as there were no stiff soil layers at shallower depths.

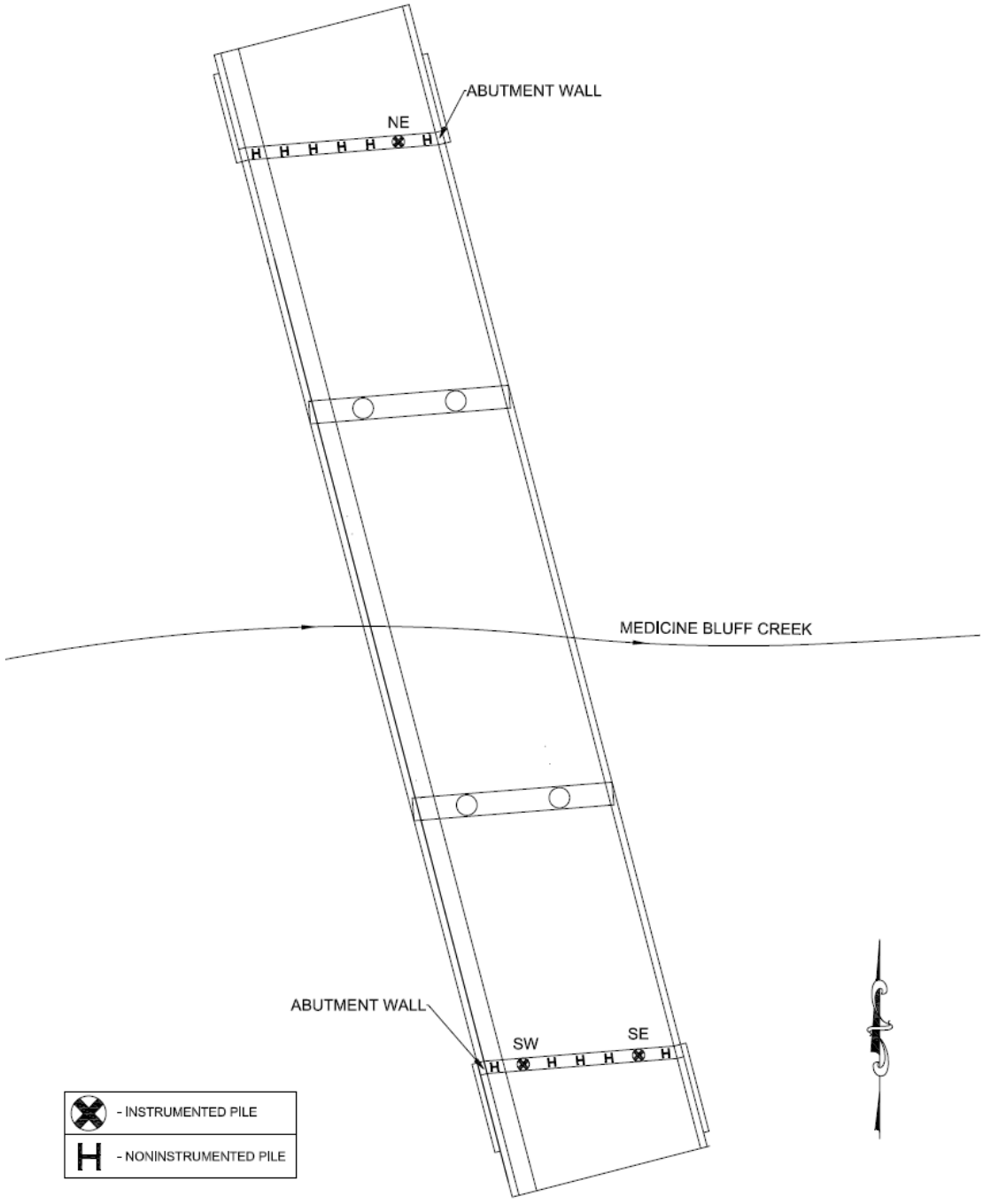

Figure 3.3: Locations of the Instrumented Piles (after Hanlon, 2010)

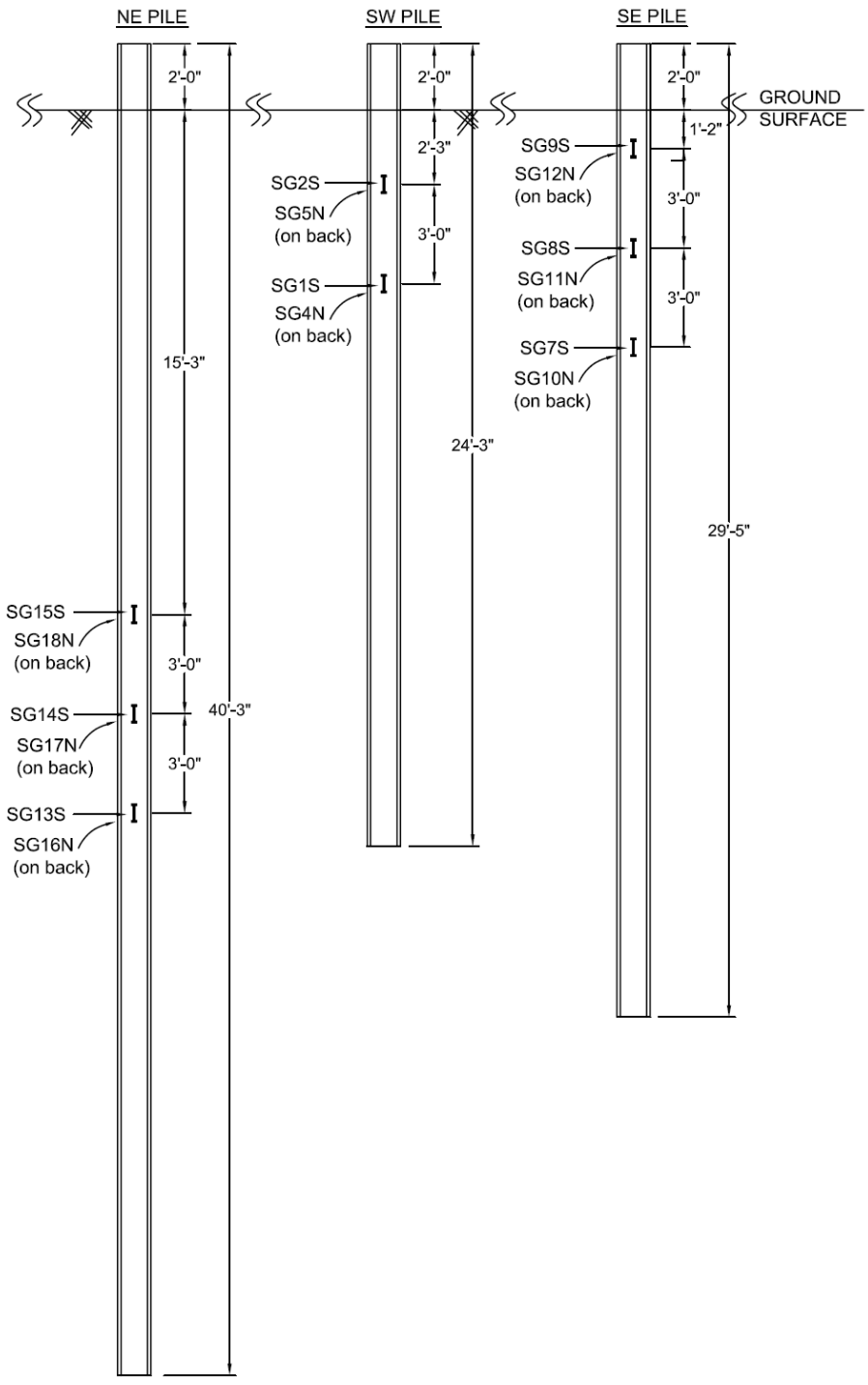

Figure 3.4: Strain Gage Depths for Instrumented Abutment Piles (after Hanlon, 2010)

3.2.2 Earth Pressure Cells

Earth pressure cells (EPC) were located behind the abutment walls at different locations to measure the distribution of stresses behind the abutment walls. Six earth pressure cells, four on the north abutment and two on the south abutment, were installed to measure the earth pressures changes during the expansion and contraction of the bridge. The locations of earth pressure cells on the bridge are shown in Figure 3.5. The locations of the earth pressure cells were chosen carefully to determine the variations of earth pressure on the abutment walls. On both the north and the south abutment walls, cells were positioned equidistant from each other at the same height on the wall to measure the variation in pressure along the length of the wall. On the north wall, a cell was placed directly below the middle cell to measure the variations in earth pressure with respect to depth along the abutment wall. Cross section of the south and north abutment walls showing the locations of the earth pressure cells are illustrated in Figures 3.6 and 3.7, respectively.

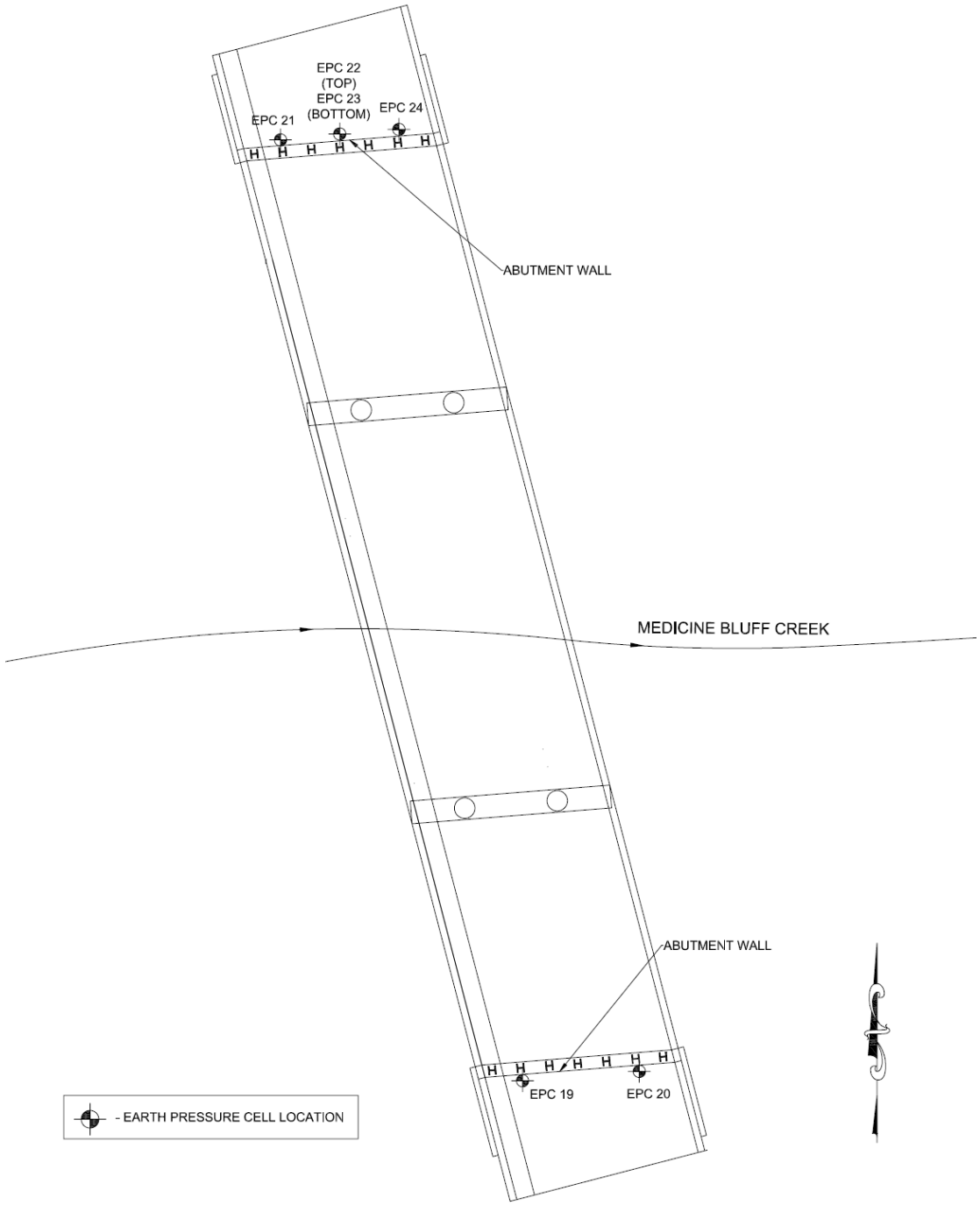

Figure 3.5: Locations of the Earth Pressure Cells (after Hanlon, 2010)

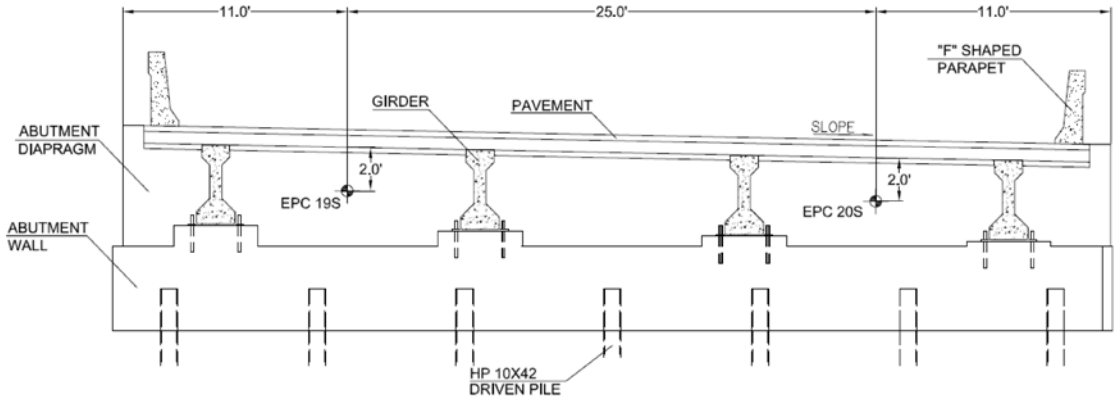

Figure 3.6: Locations of the Earth Pressure Cells on the South Abutment (after Hanlon, 2010)

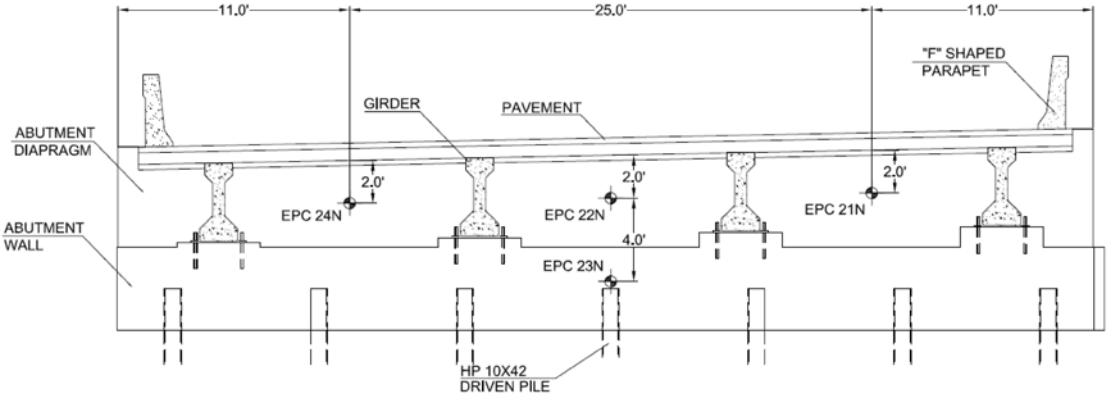

Figure 3.7: Locations of the Earth Pressure Cells on the North Abutment (after Hanlon, 2010)

3.2.3 Tiltmeters

At each abutment, two vibrating wire tiltmeters were attached to measure the rotation of the abutments about a horizontal axis. Tiltmeters were installed directly below the bridge deck after the completion of the bridge construction. Uniaxial mounting set up was used for the tiltmeters since the abutment rotations in longitudinal bridge direction was the focus of research. The locations of tiltmeters are shown in Figure 3.8. Cross section of the south and north abutment walls showing the locations of the tiltmeters are illustrated in Figures 3.9 and 3.10, respectively.

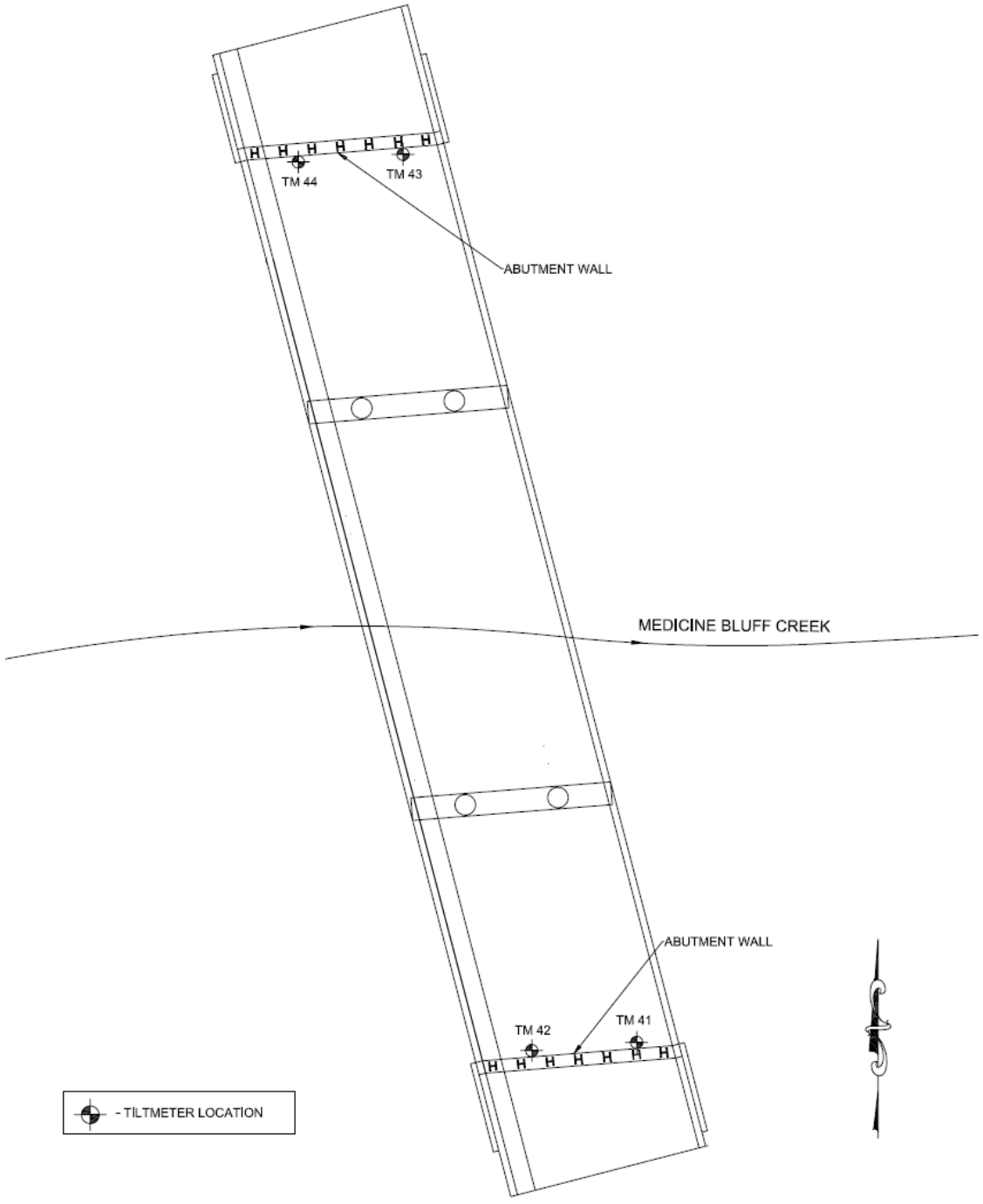

Figure 3.8: Locations of the Tiltmeters (after Hanlon, 2010)

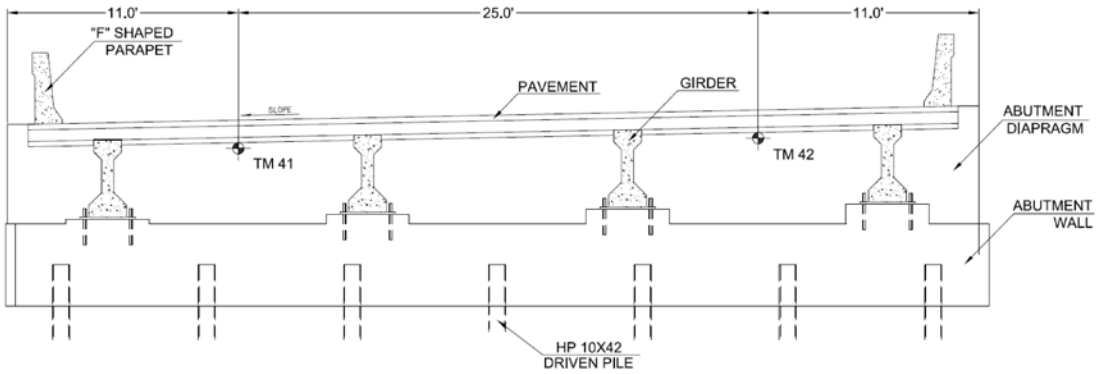

Figure 3.9: Locations of the Tiltmeters on the South Abutment (after Hanlon, 2010)

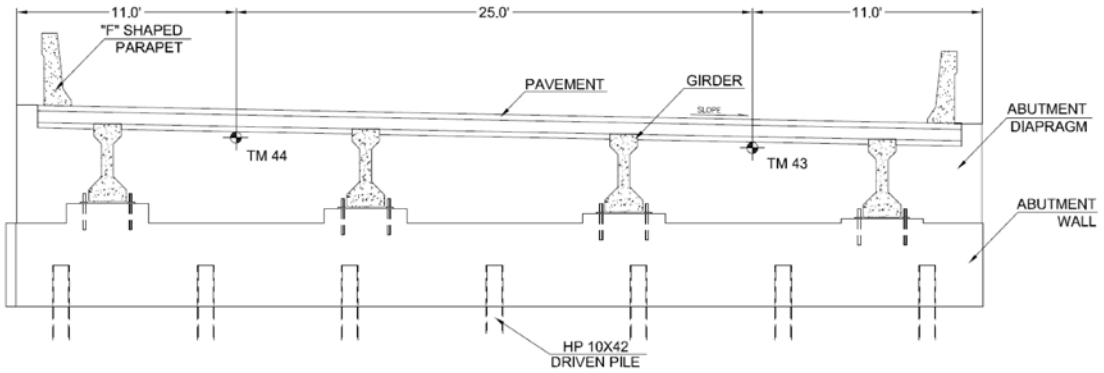

Figure 3.10: Locations of the Tiltmeters on the North Abutment (after Hanlon, 2010)

3.2.4 Crackmeters

A total of four crackmeters (CM) were attached between the pavement and the approach slabs of the bridge to measure the translation of the bridge during the expansion and contraction of the bridge superstructure. The locations of crackmeters are shown in Figure 3.11. Crackmeters were exposed to the direct sun light and to avoid the damage to instruments due to overheating, the crackmeters were covered by 2-inch diameter foam tubing. The foam was designed to protect the gage from direct sunlight, rain, and other outside elements. Crackmeter CM 145 experienced some problems during installation.

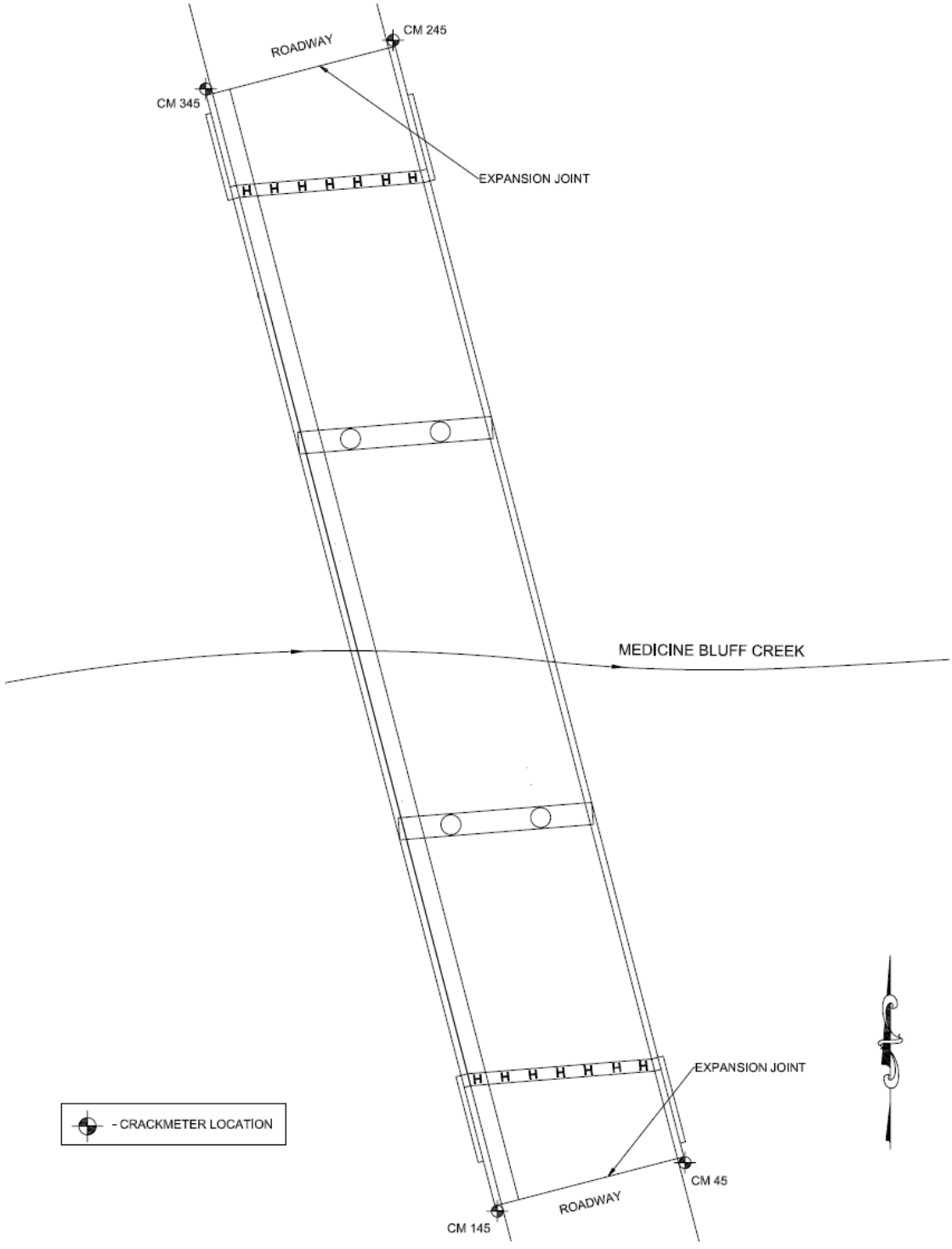

Figure 3.11: Locations of the Crackmeters (after Hanlon, 2010)

3.2.5 Thermistors

Finally, sixteen thermistors were attached to the girders and deck to measure the temperature changes. Thirteen thermistors were installed on the north side of the bridge, while only three were installed on the south side. North side locations nearly cover the entire profile of the bridge, so the south side locations were mainly used for comparison. To make sure the temperatures of the bridge were being measured at the thermistor locations and not the ambient temperatures, the thermistors were covered in 0.5-inch thick foam. Locations of thermistors are shown in Figures 3.12 and 3.13. Cross section of the south and north sides of the bridge showing the locations of the thermistors are illustrated in Figures 3.12 and 3.13, respectively.

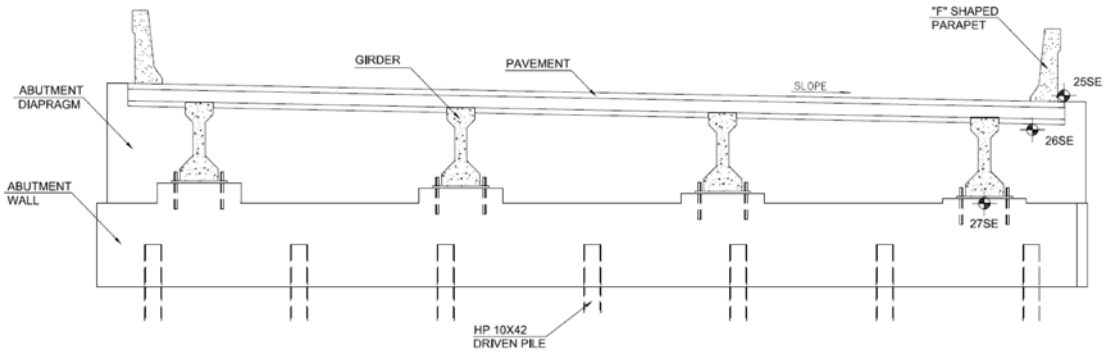

Figure 3.12: Locations of Thermistors on the South Side of the Bridge (after Hanlon, 2010)

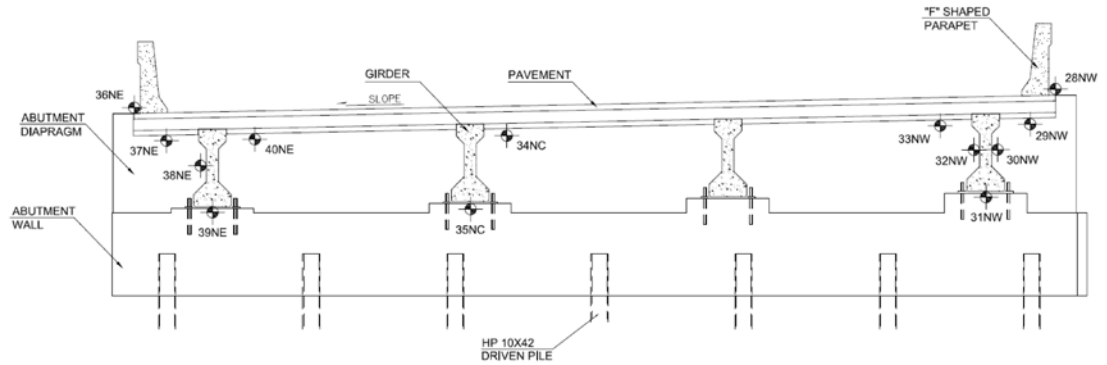

Figure 3.13: Locations of Thermistors on the North Side of the Bridge (after Hanlon, 2010)

3.2.6 Data Collection

All instruments were connected to a Geokon Micro-1000 data logging unit through the use of 16-channel multiplexer cards. The system is programmed to acquire and store data from all the instruments every hour. The stored data are downloaded every month and processed on a personal computer using a spreadsheet. Data collection from the instruments started in June 2009 and completed in October 2012.

Chapter 4: Subsurface Investigation for the Oklahoma IAB

4.1 Introduction

A subsurface exploration program was carried out for the Oklahoma IAB in order to assess the condition of abutment backfill and also measure geotechnical properties of the soil layers located at the abutments of the Oklahoma IAB. In addition, a series of in-situ and laboratory tests were carried out to measure the geotechnical properties of the soil layers. The subsoil exploration was performed from August 28, 2012 to September 11, 2012. The bridge was constructed in June 2009 and a limited subsurface exploration was conducted during the design phase of the bridge.

4.2 Subsoil Exploration and In-Situ Testing

The subsurface investigation at the Oklahoma IAB was performed on the approach slab of the north and south abutments. The approach slab was made of reinforced concrete and it had to be cored before initiating the subsoil exploration. The boring and Cone Penetration Test (CPT) locations are shown in Figure 4.1. Soil borings were drilled at three locations; two on the north approach slab and another one on the south approach slab. CPTs were performed at three locations; two on the north approach slab and another one on the south approach slab. During drilling, disturbed and undisturbed samples were collected for the laboratory testing. The coring of approach slab is shown in Figures 4.2 and 4.3. The approach slab was cored

at six locations and it was found that voids exist below the approach slab due to the settlement of abutment backfill material. The height of the void varied from 0.15 feet to 0.5 feet.

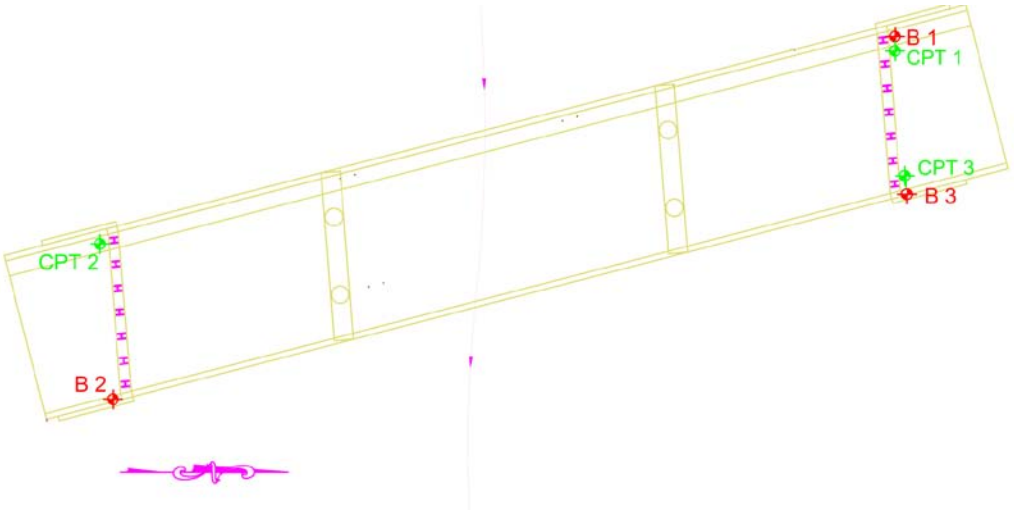

Figure 4.1: Locations for Borings

Figure 4.2: Coring of Approach Slab

Figure 4.3: Removing the Core

The subsurface exploration at the Oklahoma IAB was carried out using mechanically operated solid stem augers with air rotary drilling. SPT was performed in sand backfill at regular intervals and throughout the boring depths, soil samples were obtained with a 1.40 inch I.D., 2.00 O.D., split spoon sampler. The split spoon sampler is shown in Figure 4.4. A sample collected during the split spoon sampling is shown in Figure 4.5.

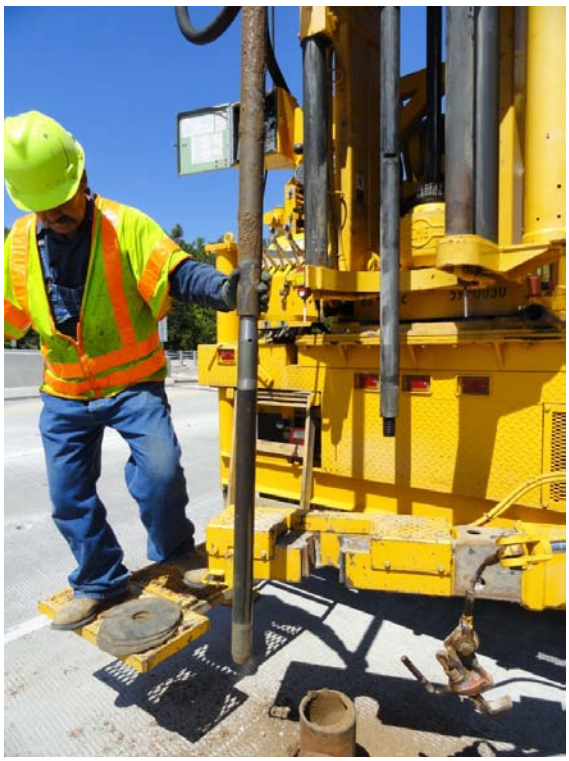

Figure 4.4: Split Spoon Sampler Used for Testing

Figure 4.5: A Sample Collected during Split Spoon Sampling

The split spoon sampling procedures used during this exploration are in basic accordance with ASTM Standard D1586. Split spoon samples are suitable for visual examination and classification tests, but generally are not sufficiently intact for quantitative laboratory testing. The penetration resistance, ‘N-value’, is designated as the number of hammer blows required to drive the sampler the final one foot and, when properly evaluated, is an index to cohesion for clays and relative densities for sands. Samples were collected to measure the moisture content of soil. Records of subsurface exploration containing soil description, stratification, penetration resistance, locations of split spoon sampling and ground water level are reported on the boring logs presented in Appendix A.

When clay layers were observed during drilling, undisturbed samples from the borehole were collected using thin walled Shelby tubes according to the ASTM Standard D1587. The Shelby tubes were of 2.5 feet long with an internal diameter of 3 inches. The Shelby tubes were pushed for two feet into the clay layers. The Shelby tubes were sealed immediately after removing from the borehole in order to preserve the in-situ moisture content. Care was taken to remove the air within the tube by using expandable plastic caps. The Shelby tube used for collecting undisturbed samples is shown in Figure 4.6. The collected undisturbed sample using Shelby tube and sealed Shelby tube are shown in Figures 4.7 and 4.8, respectively.

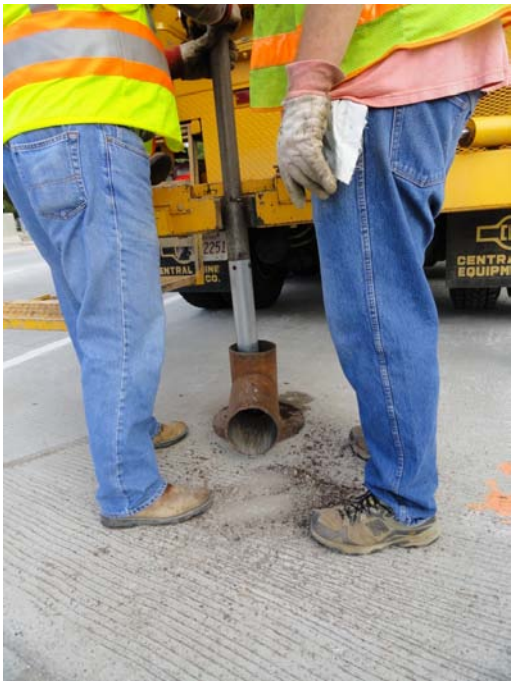

Figure 4.6: Shelby Tube Used for Sample Collection

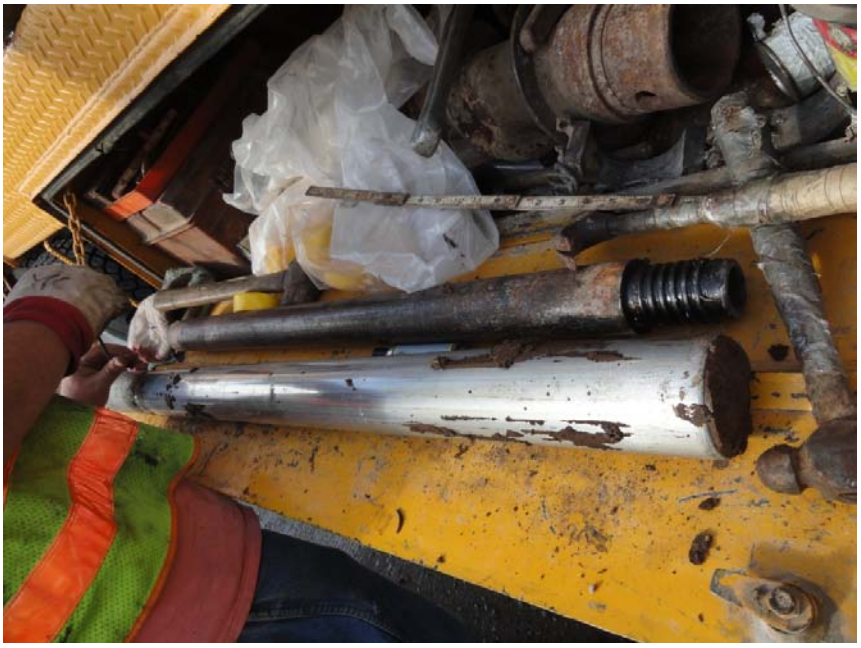

Figure 4.7: Collected Undisturbed Sample Using Shelby Tube

Figure 4.8: Sealed Shelby Tube

Samples were brought to the laboratory with care in order to avoid disturbance to the sample during transportation. The Shelby tubes are thin walled and cause less disturbance to the sample. Sample disturbance may alter the soil characteristics and care was taken to avoid disturbance. Also care was taken to preserve the in-situ moisture content of the samples.

In addition, CPT was performed to obtain the continuous profile of the soil layers and geotechnical properties of the different soils available at the site. CPT was performed in general accordance with ASTM Standard D3441. The test consisted of pushing a cylindrical cone tipped probe into the soil

deposit while simultaneously recording the penetration resistance. Electric friction cone probe was used in the testing. Recorded penetration resistance was automatically stored in the data acquisition system. The probe was attached to the end of a string of steel pile segments, each 1.0 m long, and pushed into the ground by means of heavy hydraulic rams mounted inside the rear compartment of the truck. Each downward stroke of the hydraulic rams pushes the string down one pipe length at a time, during which a constant penetration rate of 2 cm/s was maintained. Electric friction cone probe used in the testing is shown in Figure 4.9. Performance of a CPT is shown in Figure 4.10. Records of soil bearing resistance on the cone tip and soil friction resistance along the cylindrical friction sleeve are presented in Appendix B. Soil behavior type based on the bearing resistance on cone tip and soil friction resistance along cylindrical sleeve are also presented in Appendix B.

Figure 4.9: Electric Friction Cone Probe Used in the Test

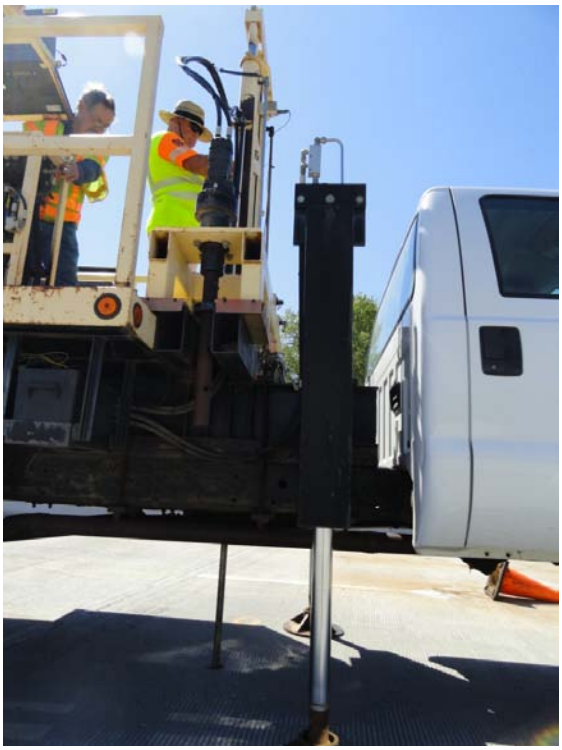

Figure 4.10: A CPT Being Conducted

Based on the SPT and CPT data, interpretation was done to obtain the stratigraphy at the south and north abutments of the Oklahoma IAB. Furthermore, SPT and CPT correlations were used to obtain the geotechnical parameters of the soil layers. The soil profile at the south and north abutments are shown in Figure 4.11 and 4.12, respectively.

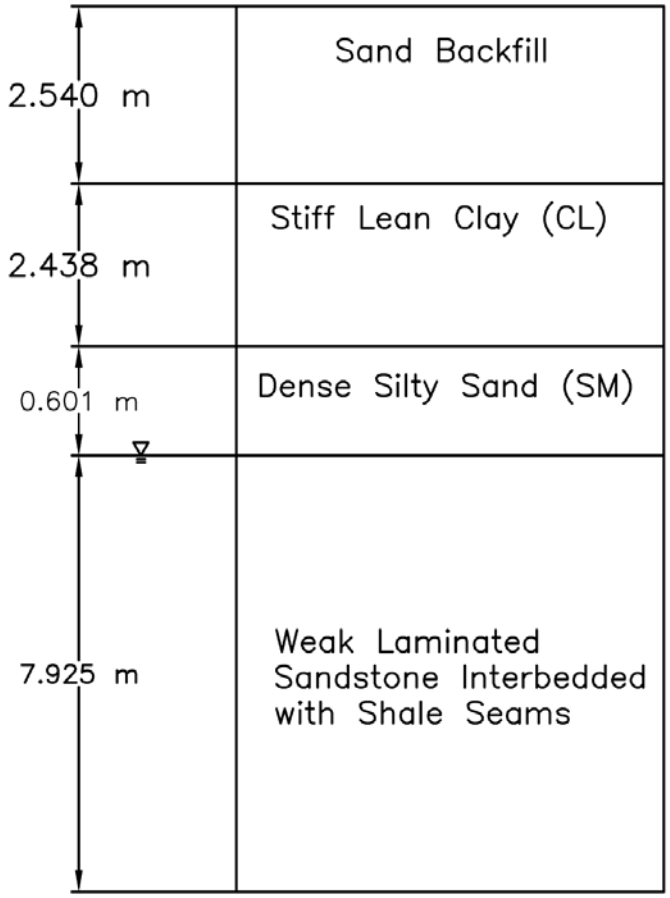

Figure 4.11: Soil Profile at South Abutment

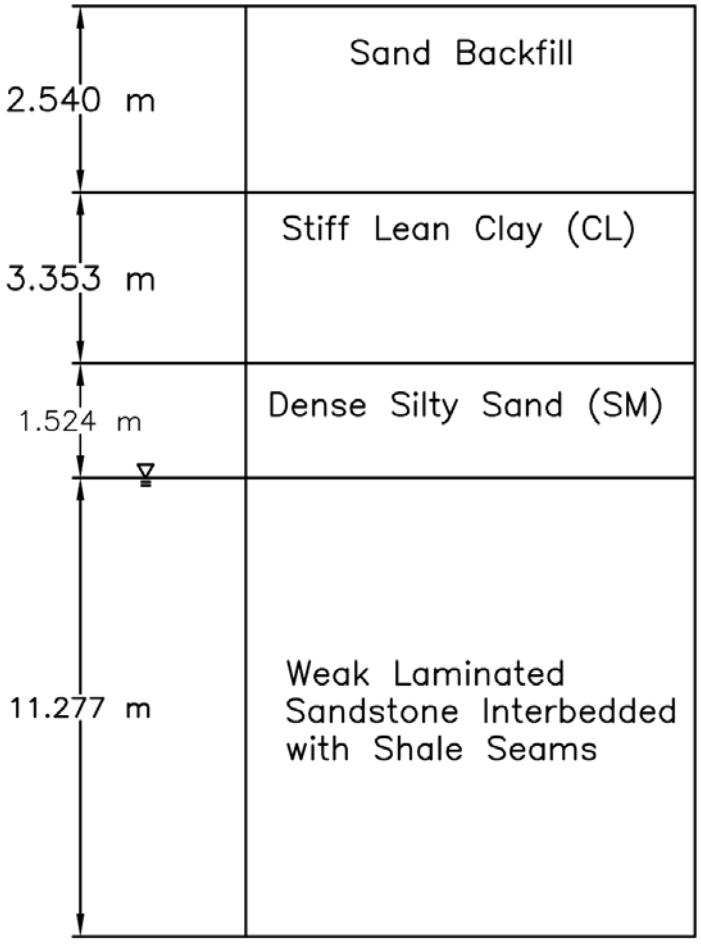

Figure 4.12: Soil Profile at North Abutment

4.3 Laboratory Testing

The soil samples obtained during the field exploration were transported to the laboratory and examined to measure the geotechnical properties of soils. Sample disturbance is an important criterion when an undisturbed sample is needed for the experiment and care was taken at all stages to avoid the disturbance. Samples were transported to the laboratory carefully avoiding serious disturbance to the samples in the tubes. Also when extrusion of sample from the tube is performed, serious disturbance was avoided. Then sample preparation for testing was done with much care. Samples were prepared without losing the in-situ moisture content and covered carefully to avoid loss of moisture.

Laboratory tests were performed on representative samples of the subsurface soils in accordance with the applicable ASTM Standards. The laboratory testing schedule included determination of the natural moisture condition of soils (ASTM D2216), Atterberg limit values (ASTM D4318), grain size distributions (ASTM D421 and ASTM D422), one-dimensional consolidation (ASTM D2435), and isotropically consolidated undrained triaxial compression (ASTM D4767). These test results are presented in Appendix C.

The geotechnical properties of the soil layers obtained from SPT and CPT corrections and laboratory testing are listed in Table 4.1. Unit weight of the soil layers are selected from Kamel et al. (1996), considering the stiffness of the soil.

Table 4.1: Properties of Different Soil Layers

Soil Layer	Total Unit Weight (kN/m^3)	Undrained Cohesion, c (kN/m^2)	Internal Friction Angle (^{o})	Dry Density, Dr (%)	Over Consolidation Ratio, (OCR)
Loose sand backfill	15.63	-	30	40	-
Stiff lean clay	21.50	65	-	-	2.2
Dense silty sand	20.72	-	35	80	-

Chapter 5: Behavior of the Oklahoma IAB for Daily Temperature Variations

5.1 Introduction

For traditional bridges, thermal expansion joints and sliding bearings are often placed between the superstructure and the supporting abutments. As a result, the thermal expansion and contraction of the superstructure are accommodated by the sliding of the bearings and the change in width of the expansion joints. Consequently, the effect of temperature on the internal forces and deformations of the substructure are negligible. Therefore the substructures are often designed without considering the effect of temperature. For IABs, due to their special structural characteristics (integral construction of superstructure and the abutment), the thermal effect becomes more complicated than that of traditional bridges. The temperature changes cause internal forces and deformations of the substructure. Therefore soil-structure interaction is involved when IABs undergo expansion and contraction. In this chapter, the effect of daily temperature changes on the Oklahoma IAB is the focus of discussion. A discussion of heat transfer, thermal gradients and temperature range are presented first. Then, the observed daily trends of the Oklahoma IAB are described considering abutment movements, rotation, and abutment pile bending moment.

Data collection from the north side abutment pile strain gages, earth pressure cells and tiltmeters started on June 23, 2009. Monitoring of the south side abutment pile strain gages, earth pressure cells and tiltmeters started on July 3, 2009. Data collection from the crackmeters started on July 9, 2009. Data collected during daily temperature variations were analyzed to study the effects of daily temperature changes on the behavior of Oklahoma IAB.

5.2 Heat Transfer and Thermal Gradients

For concrete IABs, the superstructure is exposed to the atmosphere. Heat transfer occurs between the concrete and the surrounding environment through solar radiation from the sun, and convection of heat between the concrete surface and its surrounding environment.

Solar radiation is an important part of heat transfer. During the day time, when the bridge is exposed to sun, especially on sunny summer days, a net gain of heat energy occurs through the depth of the superstructure due to solar radiation. A much higher temperature rise occurs at the top surface of the deck than the bottom flange of the girder. As a result, a positive thermal gradient ($\Delta T_{top} > \Delta T_{bottom}$) forms across the cross section. At night, the concrete loses stored heat energy to its surrounding environment. Thus, positive thermal gradient decreases. Negative thermal gradient ($\Delta T_{top} < \Delta T_{bottom}$) occurs during nights when more heat is lost from the bridge deck due to sudden temperature drops, strong wind or rain. In addition to

heat transferred by solar radiation, convection between the concrete surface and surrounding air also take place, which is affected by the wind velocity, ambient air temperature and surface temperature.

Due to the mechanisms of heat transfer, the temperature varies through the depth of the superstructure, resulting in thermal gradients which varies over time and is dependent on the following variables: (i) geometry and material properties of the superstructure (ii) orientation of the bridge axis, latitude and altitude of the location (iii) time of day and season (iv) change of ambient air temperature and wind speed and (v) degree of cloudiness of the atmosphere. The first two items are mostly determined by bridge design. After a bridge is constructed, they are approximately fixed. The other three items change with time and environmental conditions.

Two different days were chosen to investigate the thermal gradients in the Oklahoma IAB: a sunny summer day (August 05, 2011) and a cloudy winter day (February 10, 2011). For the summer day, the variation of temperature across the depth of superstructure is shown in Figure 5.1. According to Figure 5.1, the readings at the depth of 0.2 m are the thermistor readings at the top surface of superstructure. The variation of thermal gradient across the depth of superstructure for the summer day is shown in Figure 5.2. Thermal gradients were calculated relative to the temperatures at the bottom of superstructure. The variation of temperature across the depth of the superstructure for the winter day is shown in Figure 5.3. The variation

of thermal gradient across the depth of superstructure for the winter day is shown in Figure 5.4.

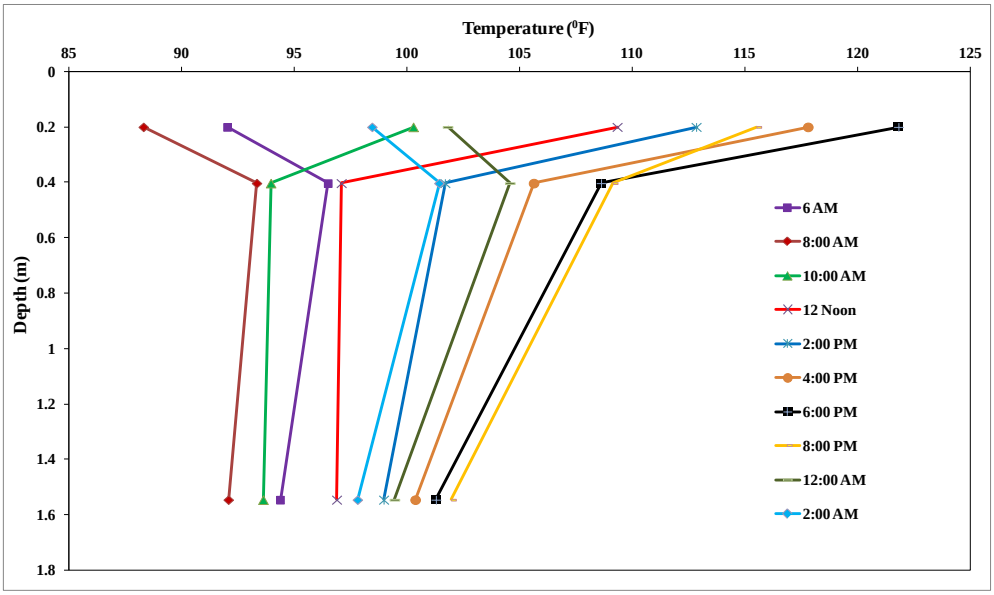

Figure 5.1: Variation of Temperature across Depth of Superstructure on a Summer Day

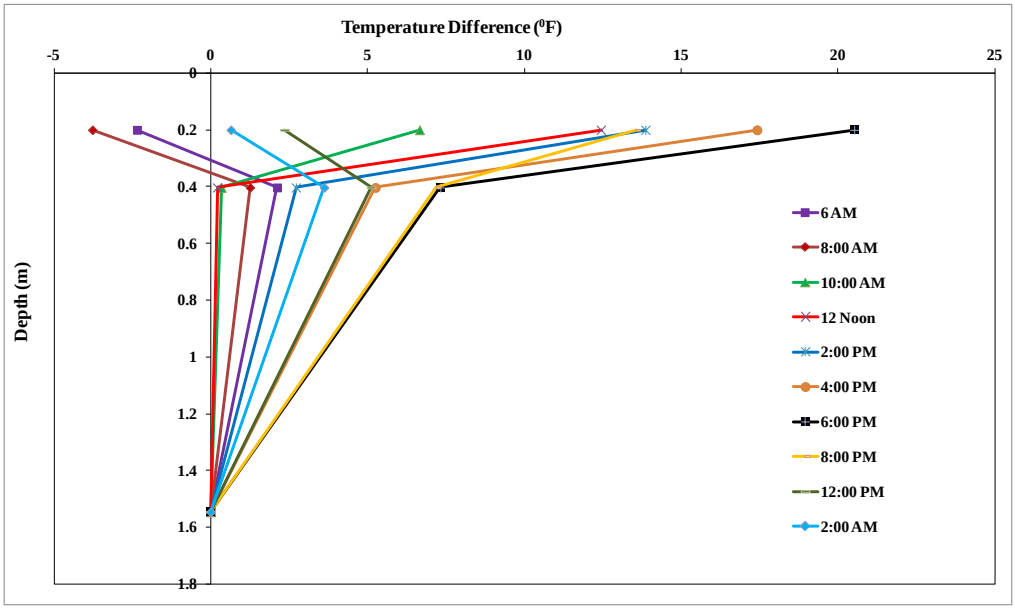

Figure 5.2: Variation of Thermal Gradient across Depth of Superstructure on a Summer Day

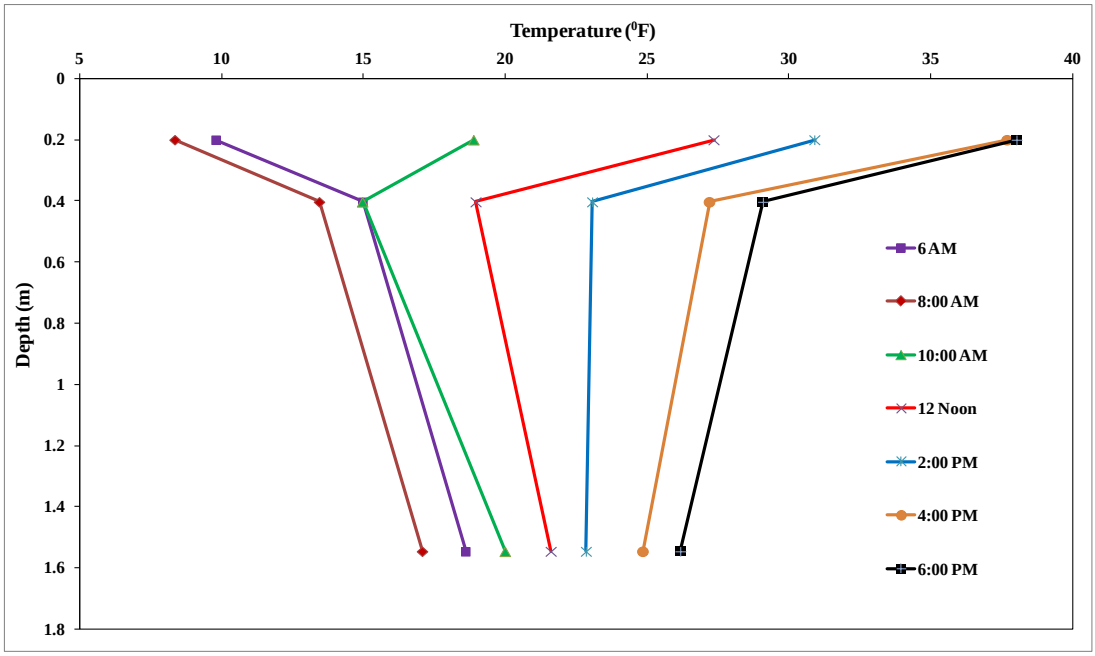

Figure 5.3: Variation of Temperature across Depth of Superstructure on a Winter Day

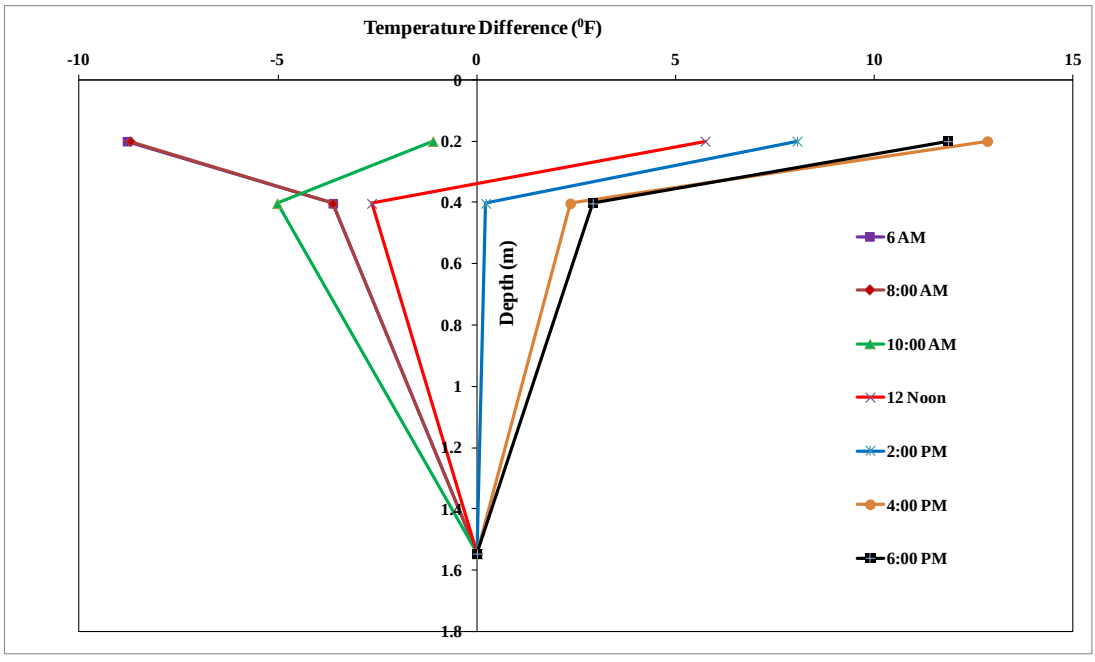

Figure 5.4: Variation of Thermal Gradient across Depth of Superstructure on a Winter Day

According to Figure 5.2, the largest positive thermal gradient was observed at 6.00 PM in the afternoon. It shows the largest solar radiation occurred during the afternoon of summer day. Then the positive thermal gradient decreases during night as the concrete loses stored heat energy to its surrounding environment. Later, negative thermal gradient occurred in the early morning when more heat was lost from the bridge deck. Thus, the largest negative thermal gradient occurred at 8.00 AM in the morning. According to Figure 5.4, a similar behavior was observed for a winter day; the largest positive thermal gradient occurred at 4.00 PM in the afternoon and the largest negative thermal gradient occurred at 6.00 AM in the morning. Figures 5.2 and 5.4 illustrate that the largest positive thermal gradient occurred during summer day and the largest negative thermal gradient occurred during winter day, however, positive thermal gradients are comparatively larger when compared to negative thermal gradients.

5.3 Temperature Variations

In order to study the behavior of the bridge for daily temperature variations, a five-day time period from September 26, 6.00 AM, 2009 to October 01, 6.00 AM, 2009 was selected. After long periods of Oklahoma summer heat and after 93 days from the installation of the instruments, this period had days where the temperature changed significantly when compared to the adjacent days. On September 27, 2009 the high and low temperatures at Oklahoma IAB were 91.3 ^{o}F and 65.4 ^{o}F respectively and on September 29, 2009, the high and low temperatures dropped to 79.6 ^{o}F and 59.3 ^{o}F, respectively.

The variation of temperature across the depth of the superstructure for the five-day time period is shown in Figure 5.5. The temperature readings from Thermistors 28NW and 36NE were averaged to obtain the temperature at the top surface of superstructure. Similarly, the temperature readings from Thermistors 29NW, 34NC and 37NE, and 31NW, 35NC and 39NE were averaged to obtain the temperatures at the middle and bottom of the superstructure, respectively. According to Figure 5.5, the largest positive thermal gradients were observed at 6.00 PM in the afternoon as the peak solar radiation occurred during the afternoons. The positive thermal gradients decrease during nights as the concrete loses stored heat energy to its surrounding environment. Negative thermal gradients occurred in the early mornings when more heat was lost from superstructure. Thus, the largest negative thermal gradients occurred at 7.00 AM in the mornings.

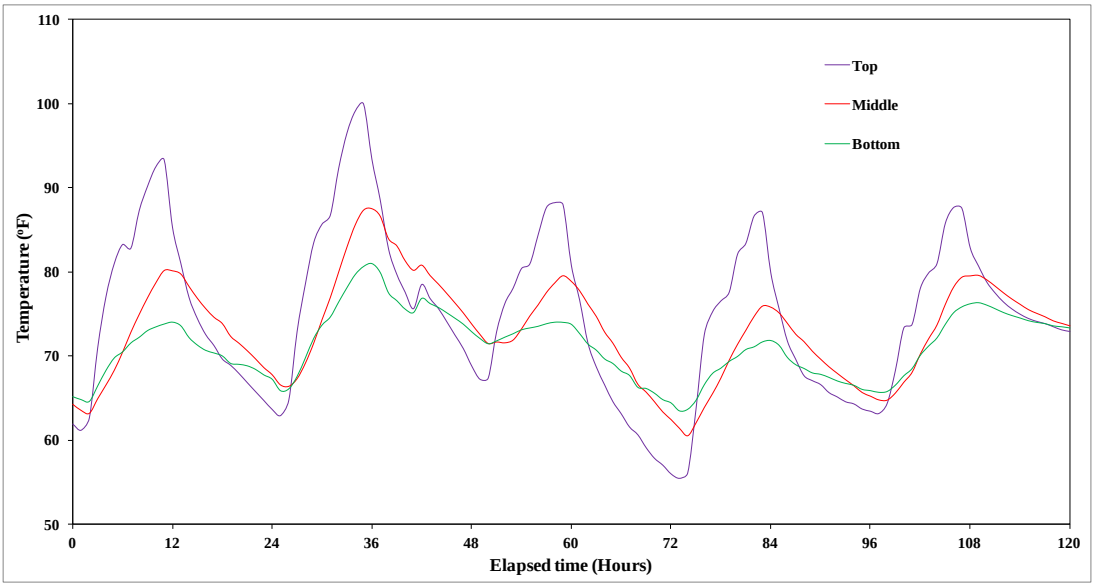

Figure 5.5: Variation of Temperature across Depth of Superstructure

The variation of temperature on East and West sides at the top surface of superstructure for the five-day time period is shown in Figure 5.6. While, Thermistor 36 NE shows the temperature variation on East side at the top surface of superstructure, Thermistor 28 NW shows the temperature variation on West side at the top surface of superstructure. According to Figure 5.6, East side reaches the maximum temperature around 12 PM where-as West side reaches the maximum temperature at 6.00 PM in the afternoon. Both sides have the same temperature around 7.00 AM in the morning. All these temperature profiles illustrate that non-uniform temperature changes are occurring in the superstructure of the Oklahoma IAB.

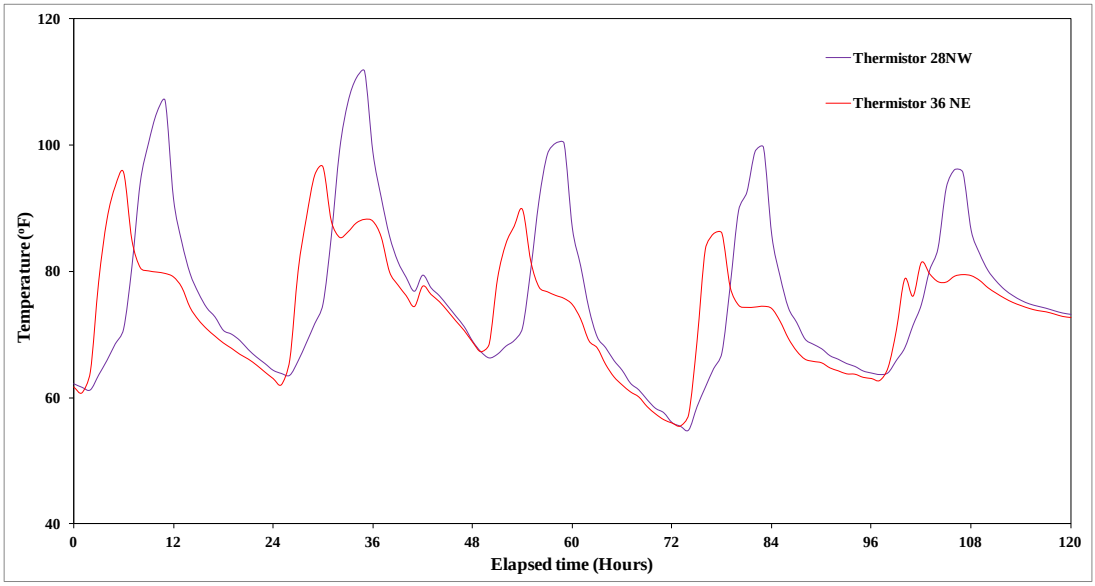

Figure 5.6: Variation of Temperature on East and West Sides at Top of Superstructure

The temperature loading of the bridge is very complex. The east side of the bridge is thermally loaded in the morning at a higher rate than the west side because it is directly exposed to the sun. During the middle of the day, both sides may be heated equally but the east side may retain some heat from the morning exposure that was not experienced on the west side, so even though both sides are being exposed to the same temperature, the loading on the east side is higher than the west side at that particular time. Once the sun starts moving westward, the heat on the east side of the bridge begins to dissipate while the west side is heated up. So the west side is exposed to more extreme heat when it is directly loaded around 6:00 PM, compared to when the east side was directly loaded in the morning.

In order to explain the behavior of Oklahoma IAB for daily temperature variations, an average temperature profile which represents the entire temperature variation at the superstructure is considered in the discussion. Average temperature variation for the bridge is shown in Figure 5.7. The temperature readings at six different thermistor locations (28NW, 29NW, 34NC, 36NE, 37NE and 40NE) are averaged to calculate a representative bridge temperature that is shown in Figure 5.7. These locations are spread across the bridge and can be used to develop the most representative average bridge temperature possible. The average temperature change that the bridge superstructure experienced over the five-day time period is 32 ^{0}F. As shown in Figure 5.7, the bridge temperature increases from 7.00 AM in the morning to 6.00 PM in the afternoon and then decreases from 6.00 PM in the afternoon to 7.00 AM in the next day morning. This cyclic behavior continued from day to day within the measurement time frame. As will be discussed below, these temperature variations are reflected in other instruments as well.

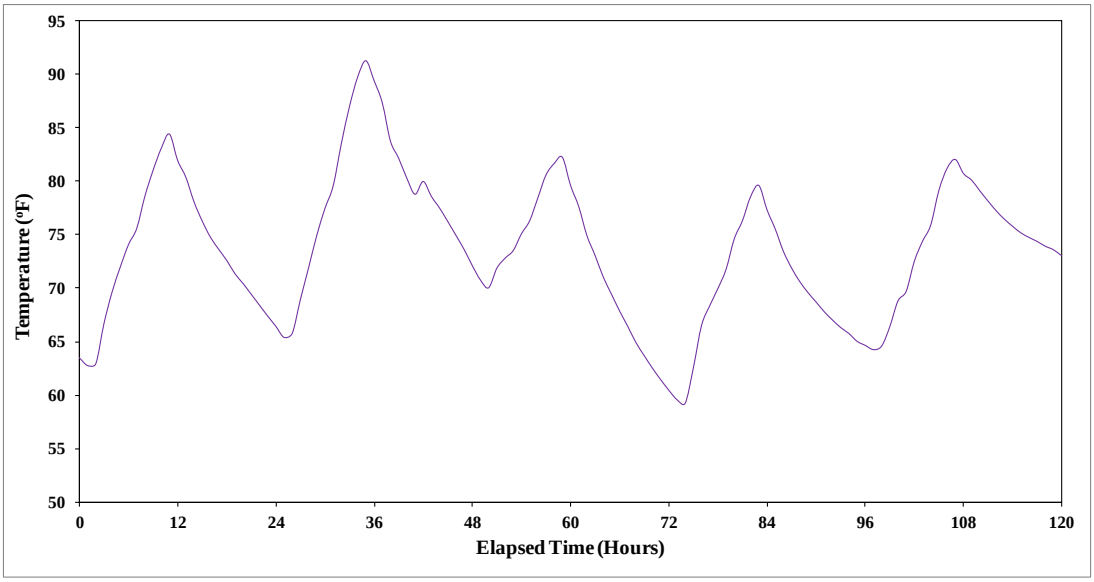

Figure 5.7: Variation of Average Bridge Temperature

5.4 Earth Pressures on the Abutments

The backfill soil pressure is measured with earth pressure cells behind the abutments. Changes in earth pressures recorded for the five-day time period are shown in Figure 5.8. Vertical variations in earth pressures can be seen in Figure 5.9, where the recorded readings for EPC 22 and 23 are presented. It can be observed that as the temperature decreases, earth pressures decrease and as the temperature increases, earth pressures increase. This is consistent with the expected behavior, as the temperature increases the bridge will expand and push the abutments outward resulting in positive change in earth pressures. Similarly, earth pressures will decrease as the temperature decreases. The maximum earth pressure changes were recorded on the obtuse corner of the north abutment (EPC 24). At this EPC

the maximum earth pressure change recorded in a single day was 4.0 psi (27.6 kPa). The reason for this behavior is that the perpendicular distance between the force vectors acting on the obtuse corners is smaller than that of the acute corners and hence the obtuse corners will carry larger loads for a given displacement of the abutments to keep the bridge in equilibrium. On the other hand, the measurements from EPCs on the south abutment did not agree with the expectations. The change in earth pressure for the two south abutment cells were similar for both acute and the obtuse corners. Both corners had less change in pressure than was observed at the obtuse corner of the north abutment wall. Why similar behavior is not seen in the obtuse corner of the south abutment (EPC 19) is not clear at this point. Moreover, as shown in Figure 5.9, larger changes in earth pressures were observed near the bridge deck (EPC 22) than at a greater depth (EPC 23). The abutments are expected to rotate and translate as a rigid body during heating and cooling of the bridge. Hence, the top of abutments will undergo larger lateral displacements resulting in larger changes in earth pressures. The observed earth pressures (Figure 5.9) confirm this expected behavior.

EPCs on the north abutment wall indicate the skew of the bridge plays a role in the pressures on the back wall of the abutments. The pressures on the obtuse corner were more than two time higher than the pressures on the acute corner due to 10° skew of the Oklahoma IAB, however, the south abutment EPC readings did not show the effect of skew angle. From Figure 5.8, it can be concluded that the changes in pressures between the backfill

and the abutment wall are higher on the obtuse corner of the wall when compared to the acute corner for the entire time period.

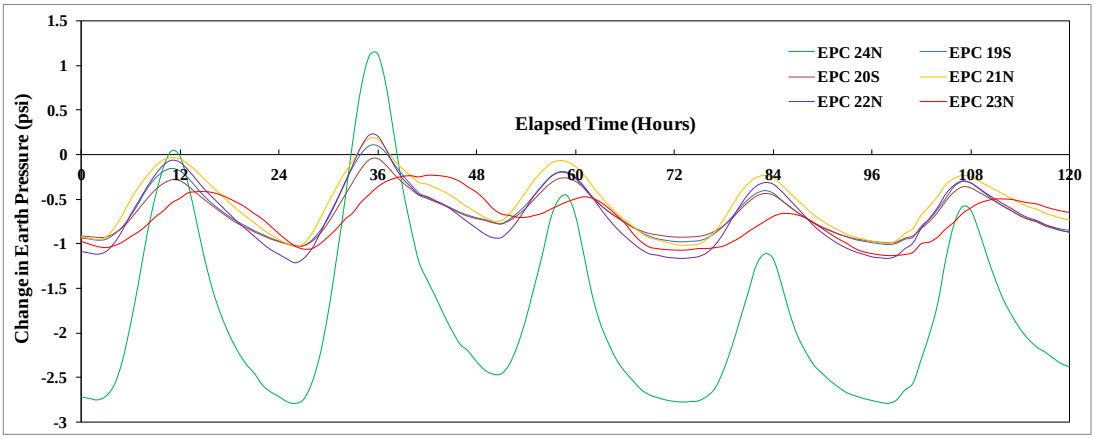

Figure 5.8: Changes in Earth Pressures behind the Abutments

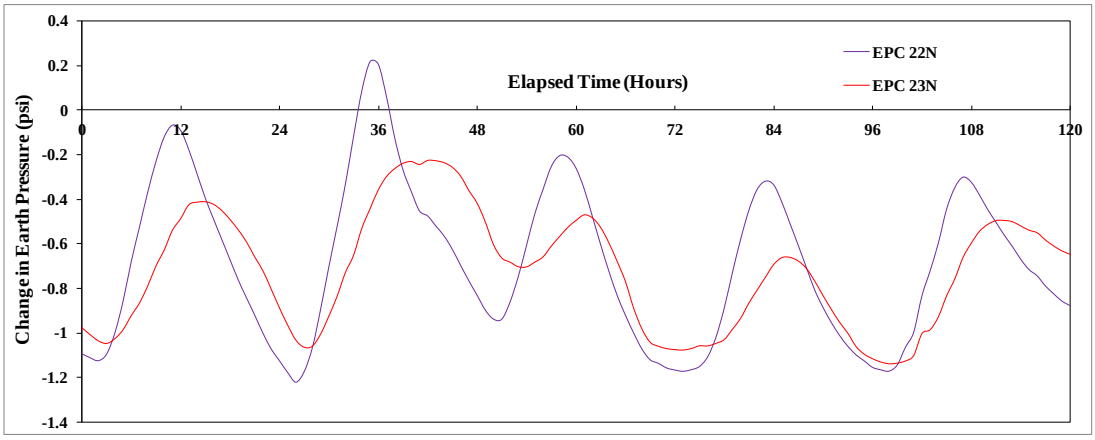

Figure 5.9: Changes in Earth Pressures with Depth on the North Abutment

5.5 Translation of the Bridge

Crackmeters (CM) were attached between the road pavement and the approach slab of the Oklahoma IAB to measure the translation of the bridge during heating and cooling. Crackmeters measure the relative movement in between the road pavement and the approach slab of IAB. For the temperature changes, the displacement of the road pavement is negligible when compared to the displacement of the superstructure due to flexibility of abutments in the Oklahoma IAB. Therefore, the changes in crackmeter readings are considered as the translation of the bridge. The measured approach slab movements are presented in Figure 5.10. According to Figure 5.10, the crackmeter readings are consistent from day to day and show a distinct pattern that follows the variation of temperature changes for the bridge. The results for CM 145 SW should be used with caution. A longer wire was used for this crackmeter since the original wire length was not sufficient to reach the multiplexer. To extend the wire, a splicing technique explained in Geokon manual was used. It appears the change in joint width measured by CM 145 SW is similar to the other crackmeters, but the results are flipped upside down. This may have been caused by the wires being crossed during the splicing process (Hanlon, 2010). The trend of the measurements for the other crackmeters goes down as the temperature goes up, which means the gap in the expansion joint is closing as the bridge is expanding due to thermal loading. This is consistent with the finding of the other instruments that show the bridge is expanding when heated and thus

pushing out on the top of the abutment walls and the approach slab causes the expansion joints to close. The bridge undergoes 2 to 4 mm translation during this period.

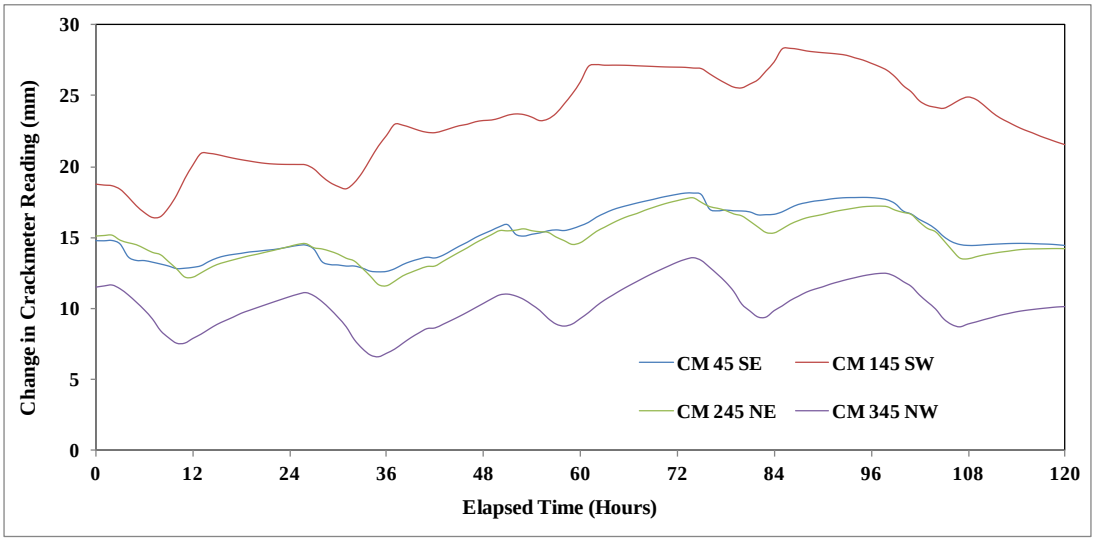

Figure 5.10: Crackmeter Measurements

5.6 Rotation of the Abutments

Tiltmeters (TM) were attached to the abutments to measure the rotation of the abutments about a horizontal axis. The measured rotations are shown in Figure 5.11. Sudden change in TM 43 NE readings around 20 days was suspicious and the measurement from this tiltmeter is not included in the discussion. According to Figure 5.11, the tiltmeter readings are consistent from day to day and show a distinct pattern that follows the variation of temperature changes for the bridge. The tiltmeters are very sensitive to movement, so whenever a heavy vehicle passes the bridge as the datalogger takes a tiltmeter reading, the reading may be affected. This could

be attributed to numerous spikes observed in the data. After eliminating the spikes, a basic trend of the data can be observed. It follows a curve that is similar to the shape of temperature variation. A positive change in tilt means the wall is rotating into the backfill and a negative change in tilt means the wall is rotating away from the backfill. It agrees with the behavior of EPCs and Crackmeters that the bridge is expanding when heated, pushing on the top of the abutment walls, and shortening when the bridge is cooled.

The rotation of the abutment can be considered as 0.05^{o} during this time period and it is equivalent to 2.4 mm translation at the top of abutment. So in general, the wall moves between 2 to 4 mm in a day. These results agree with the results from the crackmeters. Both the crackmeters and tiltmeters indicated between 2 to 4 mm of bridge movement during this period.

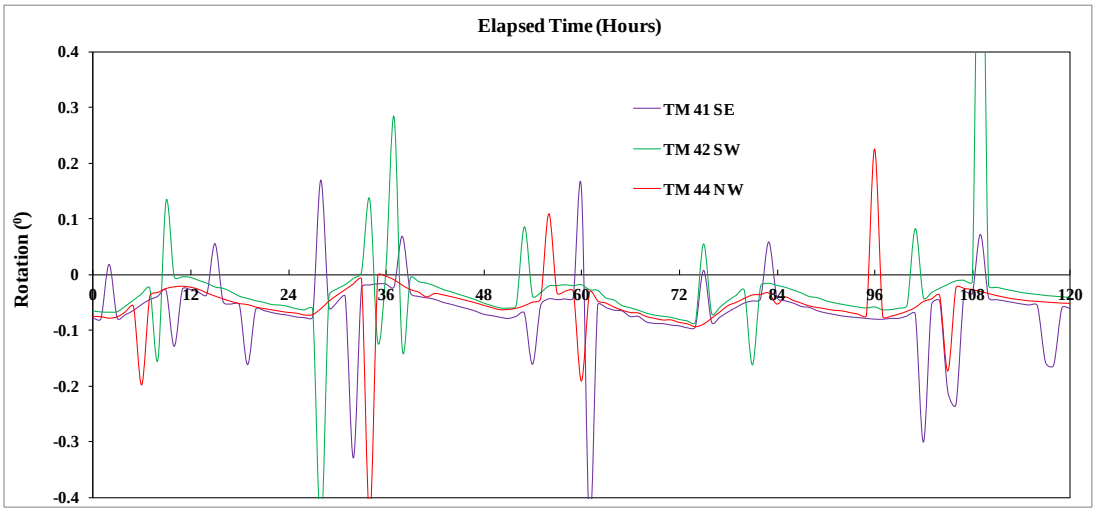

Figure 5.11: Rotations of Abutments

5.7 Abutment Pile Strains

Figures 5.12 – 5.14 show the change in axial strains for the three instrumented piles during the selected time period. The variations in axial strains within the South West (SW), South East (SE) and North East (NE) abutment piles are presented in Figures 5.12, 5.13 and 5.14, respectively. It should be noted that S or N located next to a strain gage number refers to what side of the pile that gage was installed on. S stands for South and N stands for North. Figure 3.4 should be used as a reference for the depth of installation for all the strain gages.

The axial strains can be interpreted as follows; if the axial strain is decreasing with time (i.e. sloping downward), this means the strain gage is being compressed, which also means the compressive axial strain is increasing. The opposite is true when the change in axial strain is increasing with time, which means the strain gage is elongating or the axial compressive strain is decreasing. It should be noted that the initial baseline reading of all the strain gages correspond to compressive strains caused by the axial loads on the piles. According to the strain measurements, it appears that as the temperature of the bridge increases, the axial strain on the piles decreases or becomes less compressive. On the other hand, when the temperature decreases, the gage readings decrease, thus the axial compressive strain on the pile is increasing with time. The results appear to show that as the bridge is expanding due to the increase in temperature, the downward strain on the piles decreases, which may be caused by the increased horizontal load

created by the expansion. The increased horizontal loads appear to decrease the axial loads on the piles. The effect of the depth of the strain gages can also be noticed in Figures 5.12 – 5.14

The axial strain tended to be higher for the gages located at shallow depth when compared to the ones located at a greater depth. It was expected that the gages located in shallow depth will experience more strain due to movement of the superstructure. Also, at the top of the pile, more bending moment should occur due to the bridge expanding or contracting when compared to a deeper location. The changes in axial strain were found to be higher in the two south piles that had strain gages closer to the surface when compared to the north east pile.

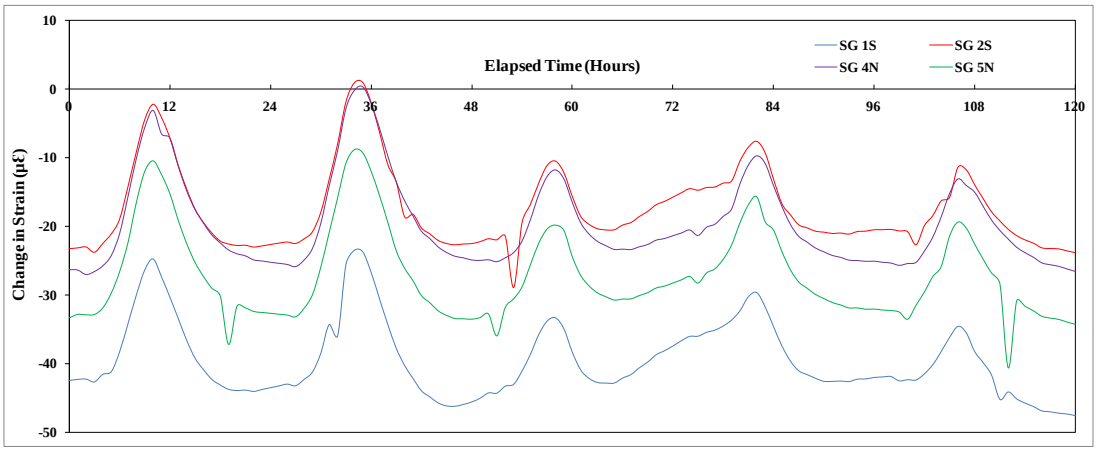

Figure 5.12: Changes in Axial Strains in the SW Abutment Pile

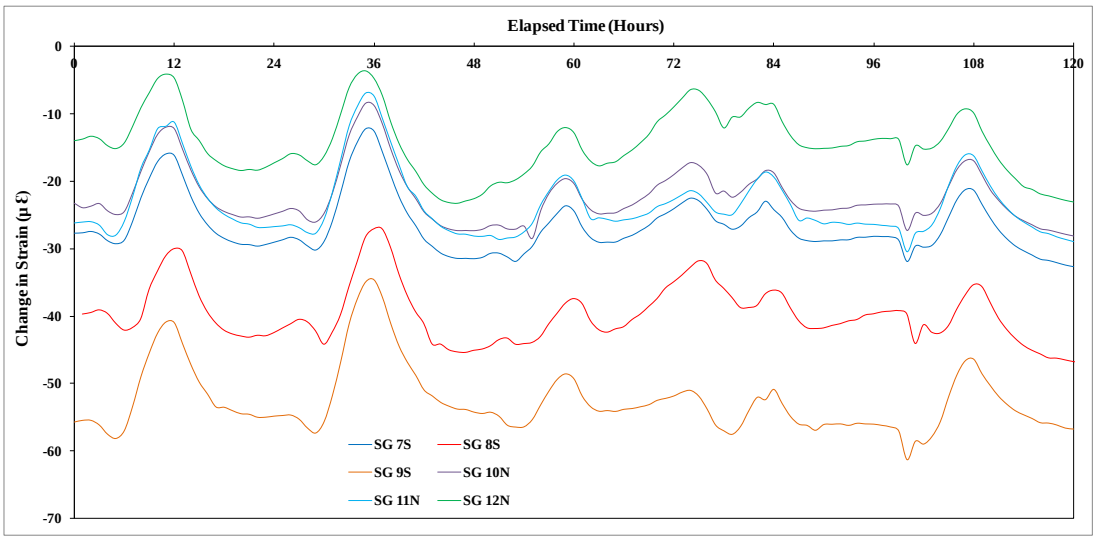

Figure 5.13: Changes in Axial Strains in the SE Abutment Pile

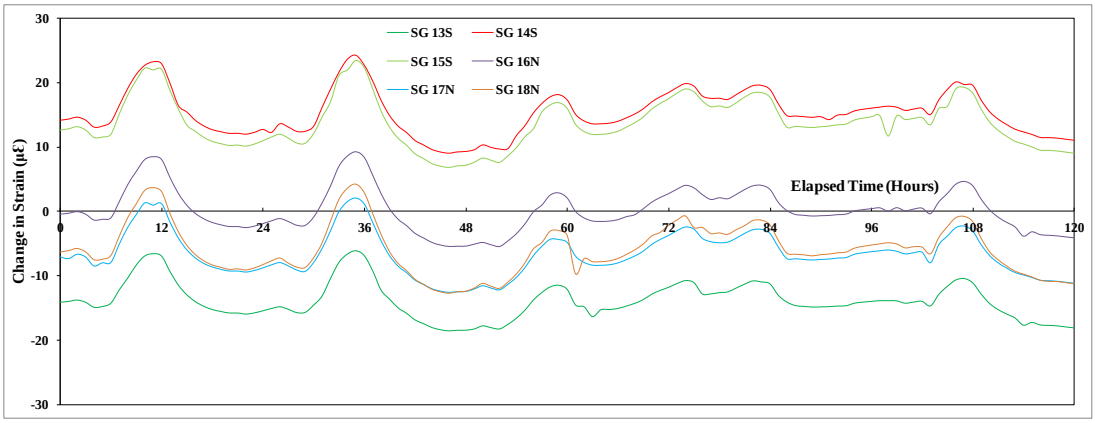

Figure 5.14: Changes in Axial Strains in the NE Abutment Pile

Chapter 6: Behavior of the Oklahoma IAB for Seasonal Temperature Variations

6.1 Introduction

The connections between the superstructure and abutments for IABs are rigid joints. As a result, the restrained displacements of the bridge superstructure caused by the integral construction, thermal expansion and contraction, and concrete creep and shrinkage of the bridge superstructure induce strains in the bridge members. Primary concern in IABs is related to the forces and displacements that are induced in the abutments and abutment piles during the seasonal thermal loading of the bridge superstructure and therefore the behavior of the Oklahoma IAB for seasonal temperature variations is presented in this chapter. Furthermore, seasonal behavior of bridge will indicate the long term performance of the bridge. The data collection started on June 23, 2009 and 40 months of high quality data from this bridge were collected, and presented in this discussion. This is the first time such a comprehensive set of data is being collected for an Oklahoma IAB.

Data collection from the north side abutment pile strain gages, earth pressure cells and tiltmeters started on June 23, 2009. Monitoring of the south side abutment pile strain gages, earth pressure cells and tiltmeters started on July 3, 2009. Data collection from the crackmeters started on July 9, 2009. The data from July 23-August 11, August 28-September 7, and

October 10-11 in 2009 is not available due to a malfunction in the data acquisition system. Earth pressure cells EPC 19S and EPC 21N, and abutment pile strain gages SG 1S, SG 4N, SG 7S and SG 10N stopped providing reliable readings after a certain time, however, sufficient data were already collected from these instruments. All other instruments continued to provide reliable and valuable data over 3 years. Furthermore, erroneous data were identified and eliminated before the field measured data are presented.

6.2 Temperature Variations

Average temperature variation for the bridge is shown in Figure 6.1. The temperature readings at six different thermistor locations (28NW, 29NW, 34NC, 36NE, 37NE and 40NE) are averaged to calculate a representative bridge temperature that is shown in Figure 6.1. The average temperature change that the bridge superstructure experienced over a six month period of time is 95 ^{o}F. As shown in Figure 6.1, the bridge temperature decreases for six month duration (from July to January) and then increases for the following six month duration (January to July). This repetitive pattern (cyclic behavior) continued from year to year within the measurement time frame. As will be discussed below, these temperature variations are reflected in other instruments and provide a valuable and complete set of data for the Oklahoma IAB for a 40-month time period.

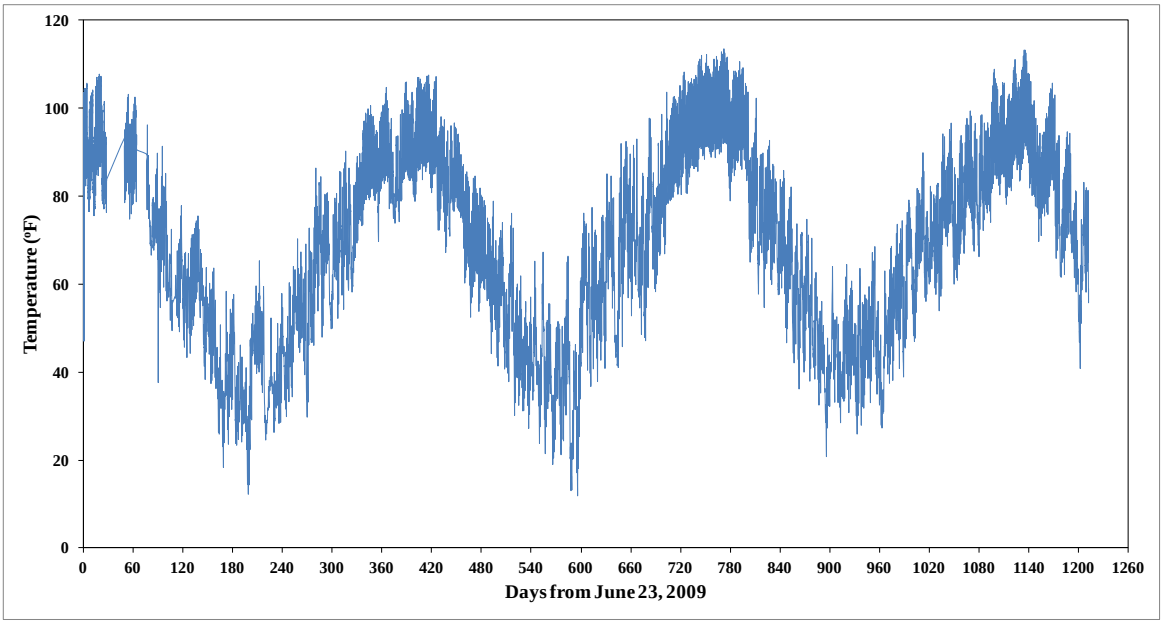

Figure 6.1: Variation of Average Bridge Temperature

The AASHTO LRFD Specifications (2007) has been widely used by the bridge-design agencies in the design of IABs. It describes two procedures in Section 3.12 for the selection of design temperature range for IABs with concrete girders and deck, and steel girders and concrete deck. Either Procedure A or Procedure B can be employed for concrete deck bridges having concrete or steel girders. According to Procedure A, the temperature range for IABs with concrete girders in moderate climate condition is 10 ^{o}F to 80 ^{o}F. Procedure A is considered as the historic method that has been used for bridge design and the specified minimum and maximum temperatures are considered as $T_{minDesign}$ and $T_{maxDesign}$ for the bridge design. Therefore the temperature change that should be considered for the design is 70 ^{o}F. Contour maps for maximum and minimum design temperatures for bridges located throughout the U.S. with two different bridge

superstructure conditions (concrete girders and deck, and steel girders and concrete deck) are presented in Procedure B. According to Procedure B, the temperature range ($T_{minDesign}$ and $T_{maxDesign}$) for IABs with concrete girders and deck located in Lawton, Oklahoma is 15 ^{o}F to 115 ^{o}F. Therefore the temperature change to be considered for the design is 100 ^{o}F. The field measured bridge temperatures for the Oklahoma IAB agree with the temperature range specified in Procedure B.

6.3 Earth Pressures on the Abutments

The backfill soil pressure is measured with earth pressure cells behind the abutments. Changes in earth pressures recorded are shown in Figure 6.2. Vertical variations in earth pressures can be seen in Figure 6.3, where the recorded readings for EPC 22 and 23 are presented. The baseline reading for EPC 24 (green curve in Figure 6.2) seems to have drifted after about 420 days and the data from this EPC should be used with caution. It can be observed that as the temperature decreases, earth pressures decrease and as the temperature increases, earth pressures increase. This is consistent with the expected behavior, as the temperature increases the bridge will expand and push the abutments outward resulting in positive changes in earth pressures. Similarly the earth pressures will decrease as the temperature decreases. The maximum earth pressure changes were recorded on the obtuse corner of the north abutment (EPC 24). At this EPC the maximum earth pressure change recorded in a single day was 7.4 psi (51.0 kPa). The reason for this difference is that the perpendicular distance

between the force vectors acting on the obtuse corners is smaller than that of the acute corners and hence the obtuse corners will carry larger loads for a given displacement of the abutments to keep the bridge in equilibrium. Why similar behavior is not seen in the obtuse corner of the south abutment (EPC 19) is not clear at this point. Moreover, as shown in Figure 6.3, larger changes in earth pressures were observed near the bridge deck (EPC 22) than at a greater depth (EPC 23). The abutments are expected to rotate and translate as a rigid body during heating and cooling of the bridge. Hence, the top of abutments will undergo larger lateral displacements resulting in larger changes in earth pressures. The observed earth pressures (Figure 6.3) confirm this expected behavior. Earth pressure measurements show that fairly significant amount of abutment back pressures during the first summer and these pressures continue to increase from summer to summer (see the peaks for EPC22). This phenomenon is discussed in detail in Section 6.8.

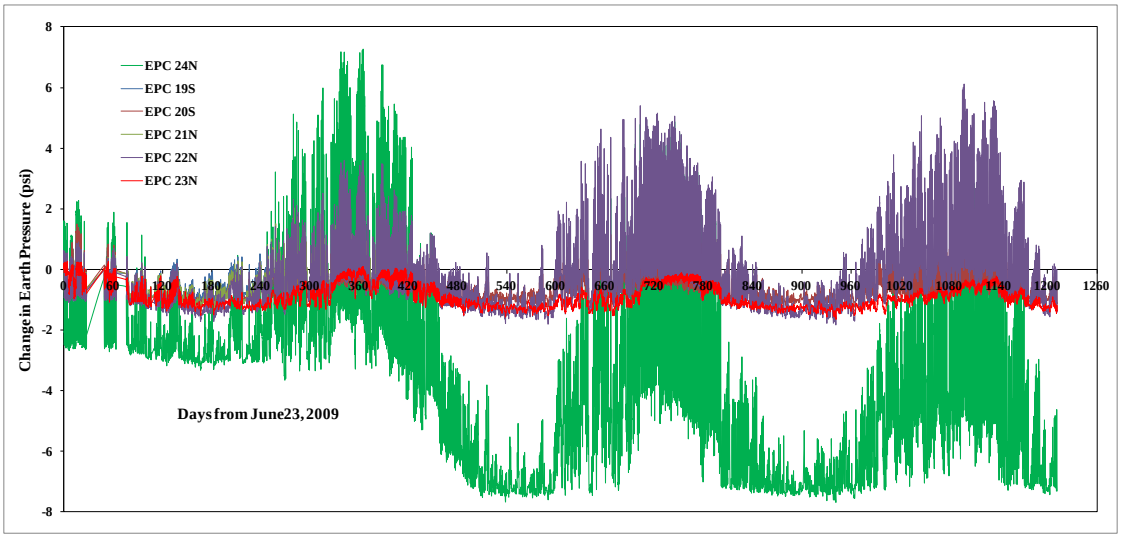

Figure 6.2: Changes in Earth Pressures behind the Abutments

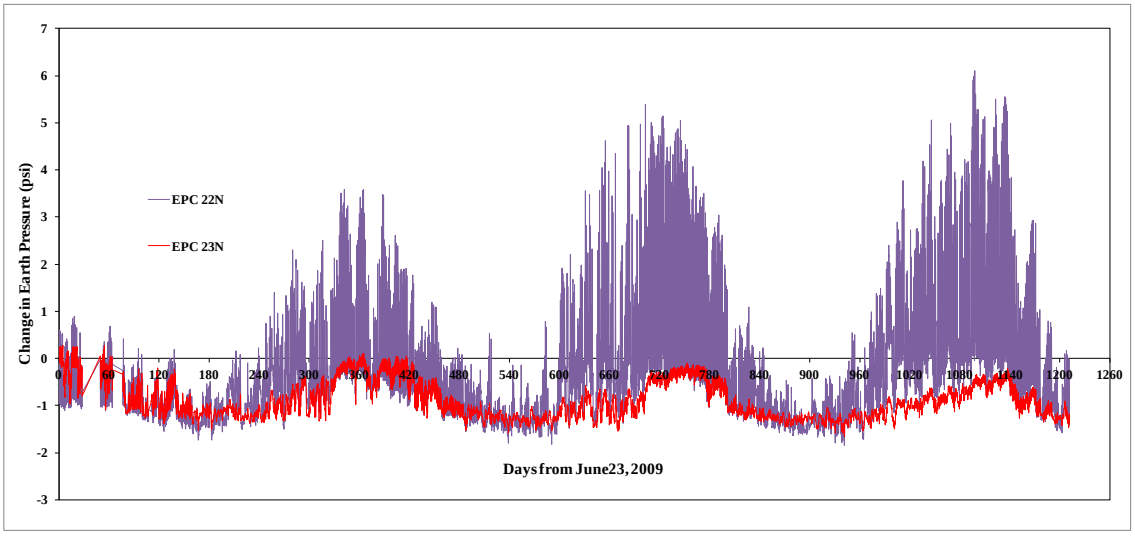

Figure 6.3: Changes in Earth Pressures with Depth on the North Abutment

6.4 Translation of the Bridge

Crackmeters (CM) were attached between the road pavement and the approach slabs to measure the translation of the bridge during heating and cooling. For the seasonal temperature changes, the displacement of the road pavement is negligible when compared to the displacement of the superstructure due to flexibility of abutments in the Oklahoma IAB. Therefore, the changes in crackmeter readings are considered as the translation of the bridge. The measured approach slab movements are presented in Figure 6.4. Crackmeter readings from June 23, 2009 through June 21, 2010 are presented in Figure 6.4 as the crackmeter readings indicate inconsistent behavior after June 21, 2010. As the temperature reduces from July 2009 through January 2010, the expansion joints open (a positive change in crackmeter reading) and as the temperature increases from January 2010 to July 2010, the expansion joints close (a negative change in crackmeter reading). The bridge undergoes 22 mm translation during this period. The crack width was physically measured and this independent field measurement confirms the reading from the crackmeter.

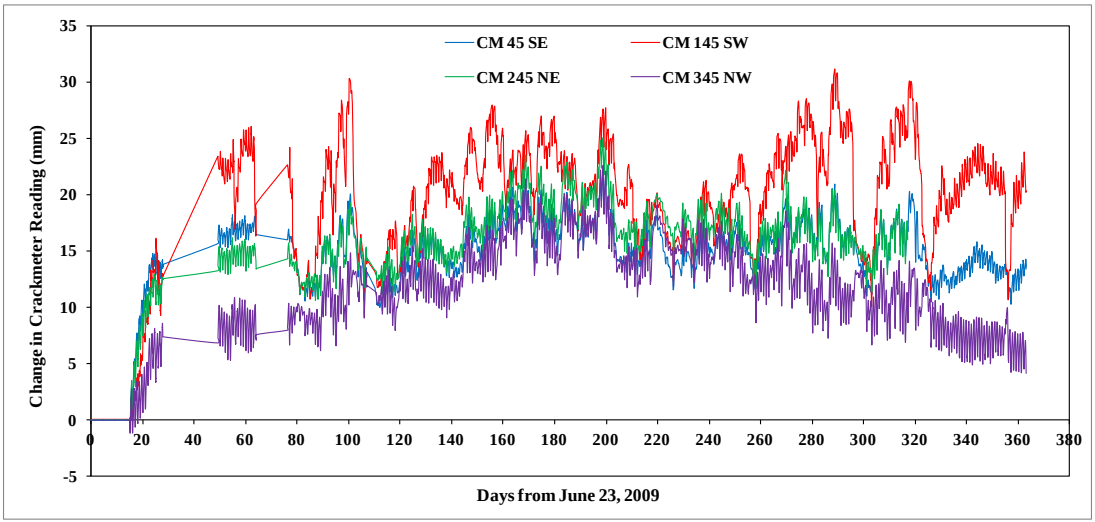

Figure 6.4: Crackmeter Measurements

6.5 Rotation of the Abutments

Tiltmeters (TM) were attached to the abutments to measure the rotation of the abutments about a horizontal axis. The measured rotations are shown in Figure 6.5. Tiltmeter readings from June 23, 2009 through June 21, 2010 are presented in Figure 6.5 as the tiltmeter readings indicate inconsistent behavior after June 21, 2010. Negative changes in rotations are measured during temperature decrease and positive changes in rotations are measured during temperature increase indicating that abutments rotate inward when the bridge cools and rotate outward when bridge is heated. Tiltmeter data had spikes due to traffic related vibrations and not due to actual rotations of the abutments. Therefore spikes are removed during the data processing and Figure 6.5 shows the actual rotations of the abutments. Sudden change in TM 43 NE around 20 days (blue curve in Figure 6.5) is

suspicious and the measurement from this tiltmeter should be viewed with caution. The abutment rotates 0.125^{o} during this period and it is equivalent to 6 mm translation at the top of abutment. Since the translation of bridge is 22 mm, rest of the translation (16 mm) is occurring at the top of abutment piles. It indicates that the majority of translation is accommodated by the abutment pile movements in IABs.

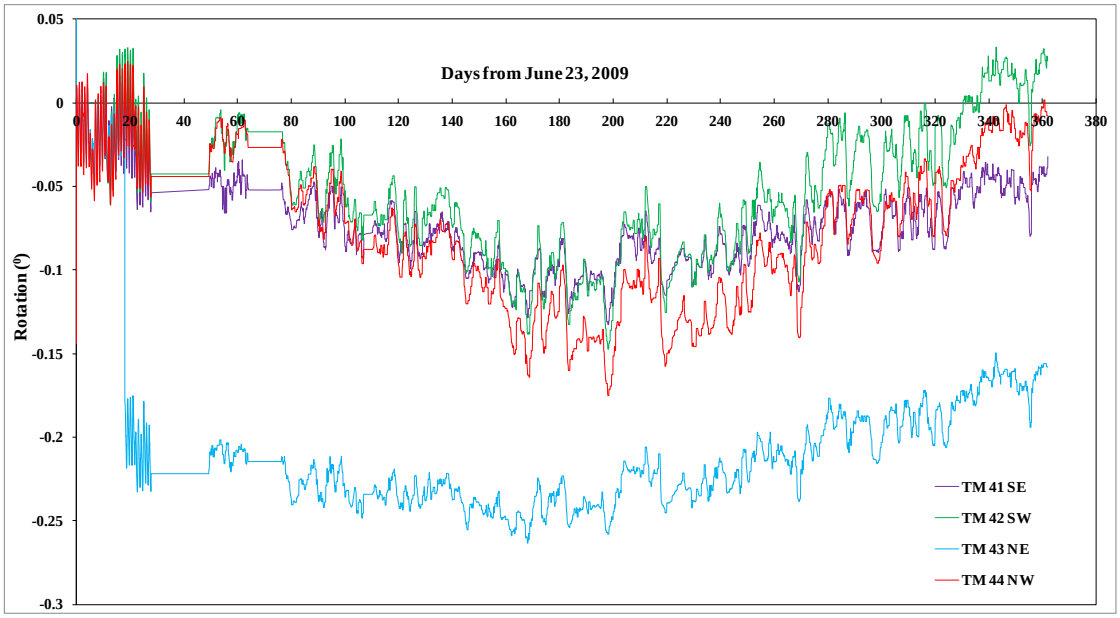

Figure 6.5: Rotations of Abutments

6.6 Abutment Pile Strains

The variations in axial strains within the South West (SW), South East (SE) and North East (NE) abutment piles are presented in Figures 6.6, 6.7 and 6.8, respectively. A positive change in strain means an increase in tension and a negative change in strain means an increase in compression at that location. Strain gages in the SW and SE abutment piles are located at shallower depths compared to the strain gages in the NE abutment pile. The abutment movements result in translation of the top of piles and hence larger strains are expected at the shallower depths.

It can be seen from Figure 6.8 that after some accumulation, strains in NE abutment pile are stabilizing except for SG17N. Since strain gages in NE abutment pile are located at a greater depth, they are not showing larger variations in strains over time. According to Figures 6.6 and 6.7, strains in the SW and SE abutment piles are continuing to accumulate. This observation is further investigated in the next section.

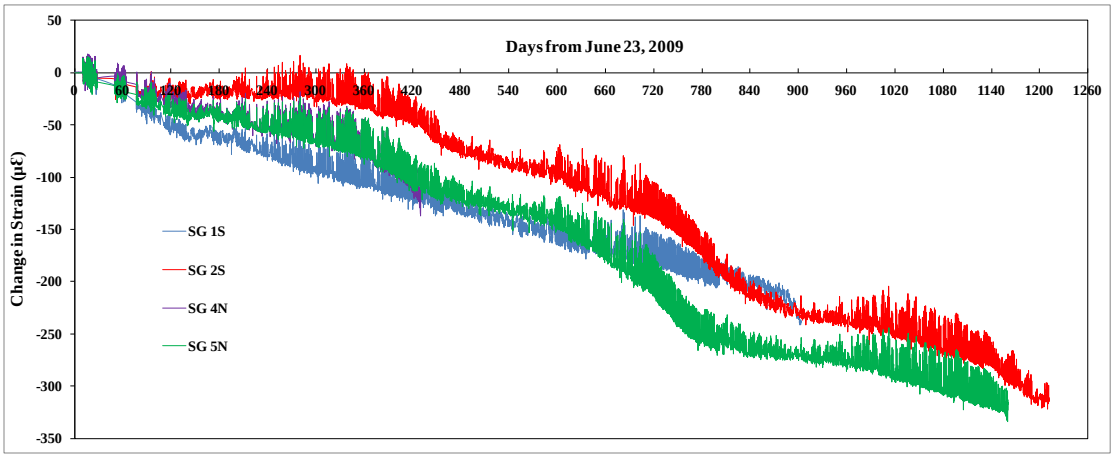

Figure 6.6: Changes in Axial Strains in the SW Abutment Pile

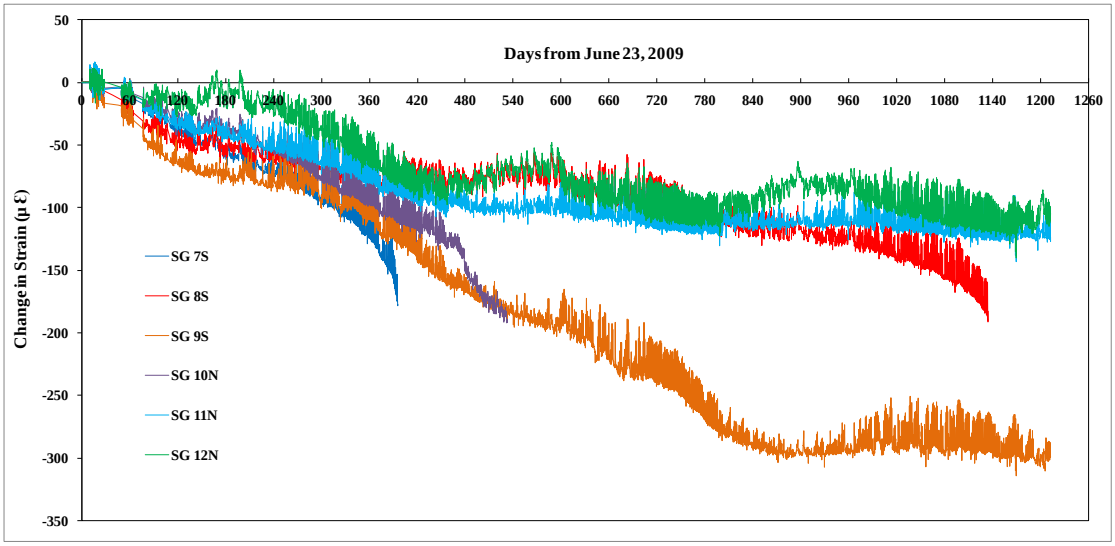

Figure 6.7: Changes in Axial Strains in the SE Abutment Pile

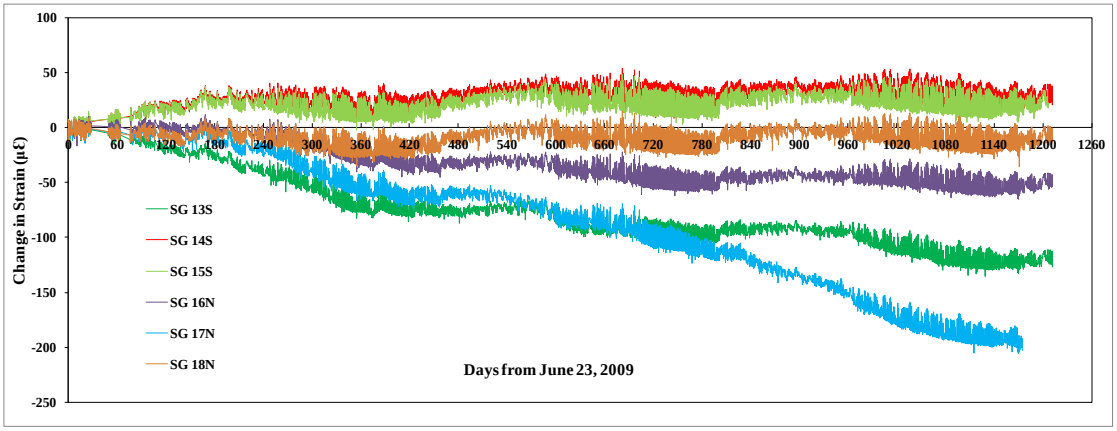

Figure 6.8: Changes in Axial Strains in the NE Abutment Pile

6.7 Behavior of the Abutment Piles

The long term behavior of abutment piles can be explained using the strain gage data. At each depth, two strain gages were placed on the web on the opposite sides (north and south sides) so that the bending strains can be calculated for that particular location. The cross-section of an HP pile with the locations of strain gages is shown in Figure 6.9.

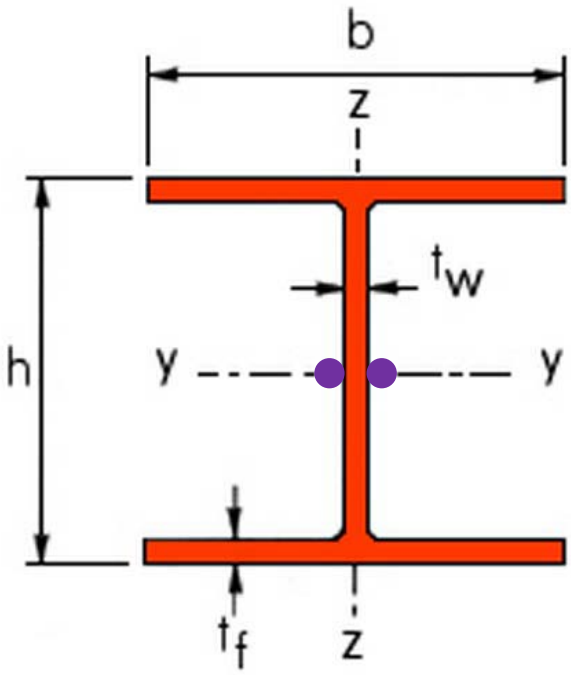

Figure 6.9: Cross-section of an HP Pile with the Locations of Strain Gages

The bending strain, $\Delta\varepsilon$ can be calculated from the difference between two opposite strain gage readings at a particular depth as shown in Equation 6.1. The bending moment, M can be calculated from Equation 6.2.

$$\Delta\varepsilon = \frac{\varepsilon_1 - \varepsilon_2}{2} \tag{6.1}$$

$$M = \frac{EI\Delta\varepsilon}{y} \tag{6.2}$$

where,

Young's modulus of steel, $E = 200\ GPa$

Moment of inertia, $I = 2.98x10^{-5}\ m^4$

Distance from neutral axis, $y = \frac{t_w}{2} = 5.27x10^{-3}\ m$

The seasonal variations in bending moment for the SE and SW abutment piles are shown in Figures 6.10 and 6.11, respectively. Variations in bending moment for the NE abutment pile are presented in Figure 6.12. It is interesting to notice that even though strain gages are located at a greater depth in NE abutment pile when compared to south abutment piles, they are also experiencing significant bending moment.

The yield bending moment, M_y and ultimate bending moment, M_{ult} of steel pile can be calculated from Equations 6.3 and 6.4, respectively (ENSOFT 2004).

$$M_y = f_y S \tag{6.3}$$

$$M_{ult} = fZ \tag{6.4}$$

Properties of steel HP 10x42 piles oriented in weak axis are listed below:

Elastic section modulus, $S = 2.33x10^{-4}\ m^3$

Plastic section modulus, $Z = 3.57x10^{-4}\ m^3$

Yield strength of steel, $f_y = 0.276\ GPa$

Ultimate strength of steel, $f = 0.414\ GPa$

The yield bending moment, M_y and ultimate bending moment, M_{ult} of steel HP 10x42 pile are 64.2 kN.m and 147.9 kN.m, respectively.

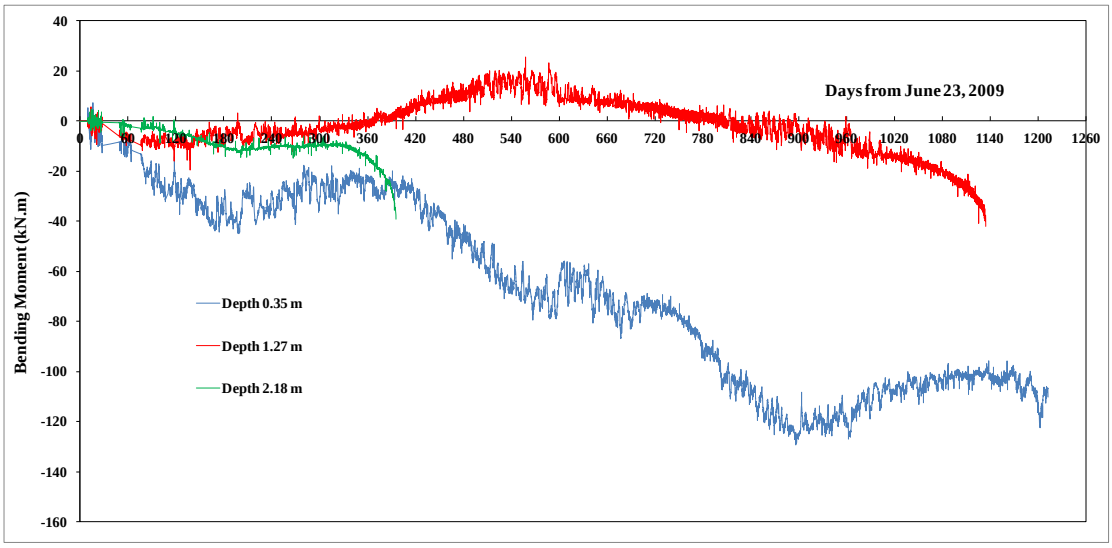

Figure 6.10: Bending Moment in the SE Abutment Pile

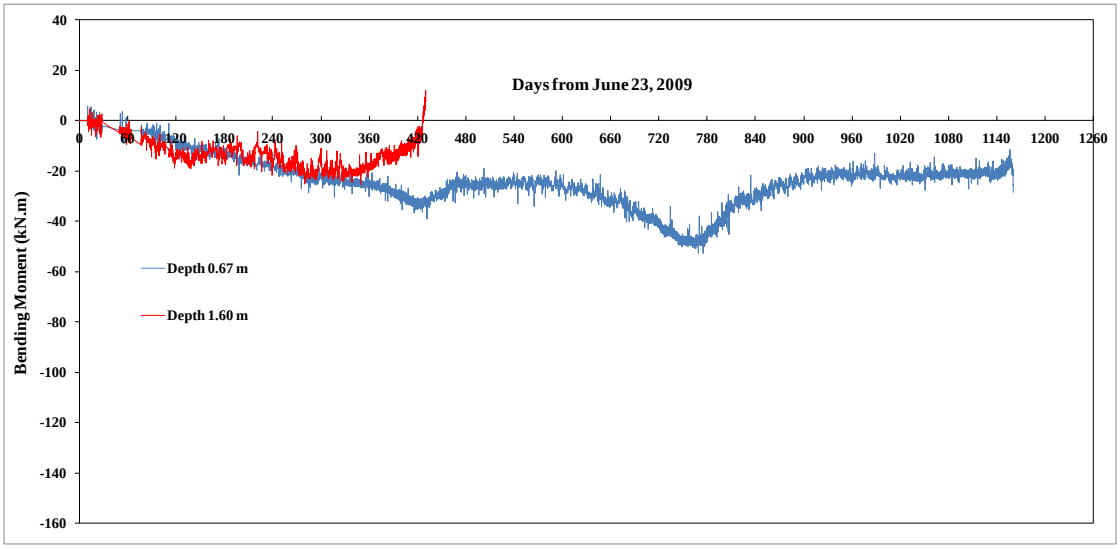

Figure 6.11: Bending Moment in the SW Abutment Pile

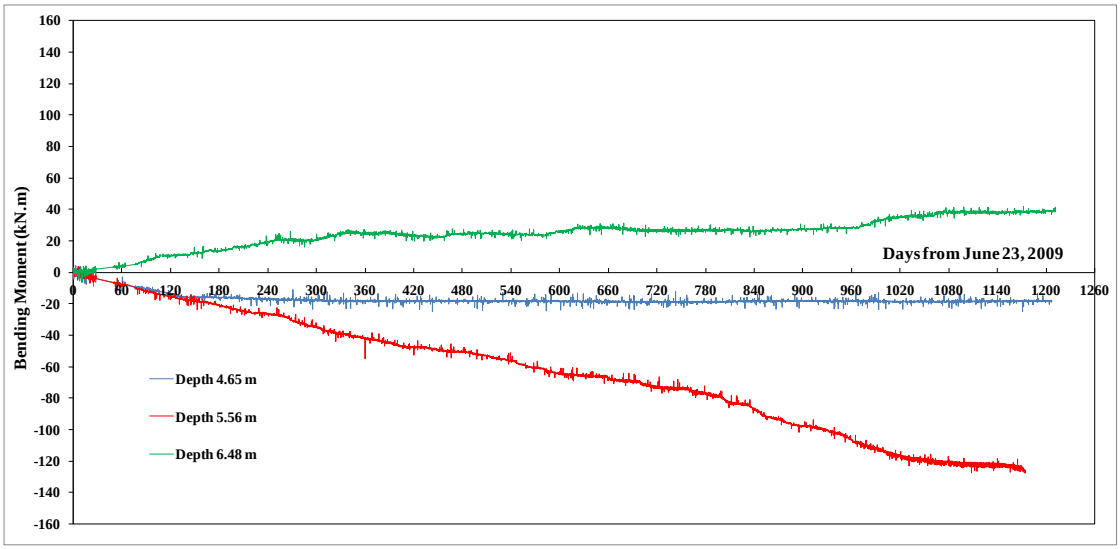

Figure 6.12: Bending Moment in the NE Abutment Pile

As shown in Figure 6.10, the shallowest instrumented depth is 0.35 m and bending moment at this particular location is showing continuous increment over time. It confirms the strains in abutment piles are accumulating. Furthermore, it shows the induced bending moment due to thermal loading in the abutment pile is larger than the yield bending moment, however, it has not reached the ultimate bending moment. Similarly, bending moment at the depth of 0.67 m is showing continuous increment over time as shown in Figure 6.11, however, the induced bending moment is below the yield bending moment. The bending moments in north east abutment pile have positive and negative values as shown in Figure 6.12 and they represent the change in curvature of the abutment pile. Furthermore, it shows the induced bending moment in the abutment pile is larger than the yield bending moment, however, it has not reached the ultimate bending moment at the depth of 5.56 m. The measured bending moments are on the webs and the bending moments on the tip of the flanges will be even higher. It can be concluded the abutment piles of IABs are experiencing bending moments beyond the yielding bending moment along a portion of a flange at the shallow depth for seasonal temperature changes in the bridge superstructure. To accommodate these large bending moments, pile ductility demands have to be increased. Ideally, the upper portion of the pile length should be in a pre-drilled hole that is filled with a material, which has a very low stiffness (such as bentonite slurry or loose sand). Numerical analyses

described in Chapter 7 provide further insight into bending of the abutment piles.

6.8 Geotechnical Problems with IABs

Although IABs have proven to be successful in eliminating expansion joints and bearing problems in addition to being economical in initial construction for a wide range of span lengths, it has problems related to maintenance in actual service life. It happens due to the shortcomings in addressing how the relative displacement between the moving superstructure and fixed ground is being accommodated. The tendency of a bridge superstructure to undergo seasonal temperature and length changes has to be properly accommodated in IABs.

As the bridge superstructure goes through its seasonal length changes, it causes the structurally connected abutments to move inward and away from the soil they retain during the winter, and outward and into the retained soil during the summer. The specific mode of abutment movement is primarily rigid-body rotation about the bottom of the abutments, however, there is a component of rigid-body translation of the abutments as well. Since rotation is dominant, the magnitude of the range of horizontal displacements is thus greatest at the top of each abutment.

At the end of each annual thermal cycle, there is often a net displacement of each abutment inward towards each other and thus away from the retained soil. Thermally induced displacement of the abutment in an

IAB is shown in Figure 6.13. The primary reason for this is that the inward winter displacement is typically of sufficient magnitude to cause an active earth pressure soil wedge to develop adjacent to each abutment and follow the abutment inward, with the soil slumping downward somewhat in the process. Due to the inelastic nature of soil behavior, this inward/downward soil displacement is not fully recovered during the outward summer cycle. It is relevant to note that this net inward/downward soil displacement will occur no matter what type of soil is used and how well it was compacted during original construction.

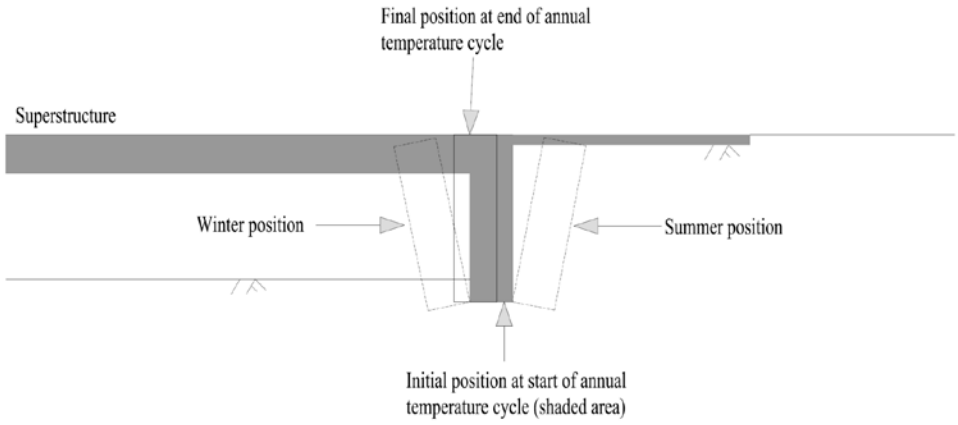

Figure 6.13: Thermally Induced Displacement of Abutment in an IAB

There are two significant problems in IABs due to the annual thermal cycle. The first one is the relatively large lateral earth pressures that develop on the abutments during the annual summer expansion of the superstructure. These pressures approach the theoretical passive state, especially along the upper portion of the abutments where horizontal displacements are largest.

These passive pressures are greater than the at-rest pressures for which bridge abutments are designed. This increase in lateral earth pressures can result in structural distress and even failure of abutments.

The seasonal increase in lateral earth pressures becomes a more significant and problematic issue since the summer seasonal increase in pressures is not necessarily constant and increases over time. The reason is during each winter the abutment moves inward slightly more than it did the preceding winter and each summer it moves outward slightly less than it did the preceding summer. As a result of this net soil displacement inward the abutments and the fact that the bridge superstructure still expands each summer the same amount as the preceding year, the summer lateral earth pressures increase over time as the soil immediately adjacent to each abutment becomes increasingly wedged in. Since the lateral earth pressures during summer are somewhat greater in magnitude than those from the preceding year, structural failure of the abutments may take a long time to develop.

The second significant problem in IABs which is due to the annual thermal cycle is also related to the net inward displacement of the abutments. The subsidence pattern that develops adjacent to each abutment is shown in Figure 6.14. This is the subsidence pattern that develops adjacent to each abutment and the result of the accumulated irreversible soil-wedge slumping behind each abutment. This subsidence develops and becomes problematic

relatively soon after an IAB is placed in service. According to a survey of 140 IABs with approach slab in South Dakota performed by Reid et al (1998), it was noted voids exist under virtually every slab and void depths ranged from 0.5 inches to 14 inches, and extended as much as 10 feet behind the abutment. Similar voids were observed in the Oklahoma IAB as discussed in Section 4.2.

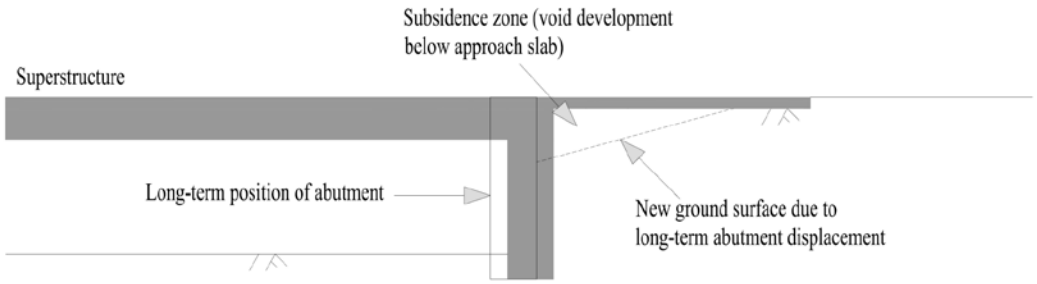

Figure 6.14: Ground Surface Subsidence behind Abutment of an IAB

Both issues, subsidence behind abutments and buildup of lateral earth pressures, have to be addressed to ensure the service life of IABs. Various types of relatively compressible materials such as expanded polystyrene (EPS) geofoam and tire shreds can be placed behind the IAB abutments. A compressible inclusion is intended to serve as a sacrificial cushion between a relatively rigid abutment and the adjacent ground with the overall goal of reducing lateral earth pressures. Although the use of a compressible inclusion can be highly effective in reducing the summer increase in lateral earth pressures, it is ineffective for controlling subsidence behind the

abutments. Even though the highly compressible nature of a compressible inclusion is desirable under summer expansion of an IAB, during winter as the superstructure contracts and pulls each abutment away from the retained soil, the relatively weak compressible inclusion between abutment and soil is unable to restrain the soil from slumping and displacing inward towards the abutment.

It is essential to come up with a solution which addresses both problems, i.e. the seasonal buildup of lateral earth pressures on the abutments and ground subsidence adjacent to abutments. Since the expansion and contraction of the bridge superstructure due to seasonal temperature changes is inevitable and unavoidable, the ground adjacent to IAB abutments have to be made inherently self-stable to prevent development of subsidence during the seasonal winter contraction of the IAB. In addition to the compressible inclusion, reinforcing the soil underlying approach slab with geosynthetics will create a mechanically stabilized earth mass within the retained soil adjacent to each abutment. Inclusion of EPS geofoam with geosynthetic reinforcement of backfill soil is shown in Figure 6.15. Geosynthetic reinforcement can also serve as drain for ground water. Otherwise, a self-stable wedge of some kind of geofoam or geocomposite blocks could be used as a solid light weighted fill material instead of geosynthetic reinforcement. Replacement of backfill soil with EPS geofoam block, adjacent to the integral abutment is shown in Figure 6.16. Use of a light weighted fill material would minimize settlements and enhance stability

of the ground adjacent to the bridge as well as greatly reduce the loads acting on the abutment and the abutment piles. Furthermore, the backfill soil can be replaced with the flowable fill material while deploying compressible EPS geofoam behind the abutment backwall. Controlled Low-Strength Material (CLSM) is a cementitious fill that is in a flowable state and has been widely used by DOTs as a backfill material. CLSM is effective in accommodating the displacement of abutments and also minimizes the settlement problem. Although these solutions will increase the construction cost of IABs, the in-service performance of IABs will reduce the future maintenance and repair costs.

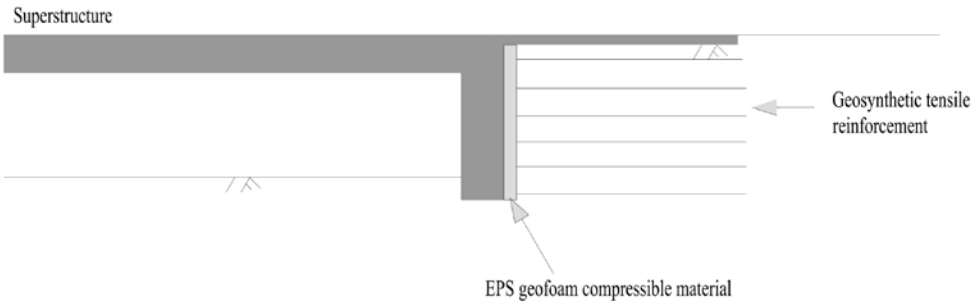

Figure 6.15: Inclusion of EPS Geofoam with Geosynthetics Reinforcement

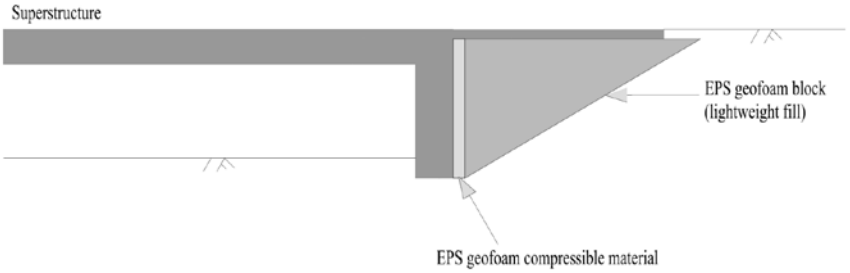

Figure 6.16: Inclusion of EPS Geofoam Block

Chapter 7: Numerical Modeling of the Oklahoma IAB

7.1 Introduction

Computer programs LPILE (ENSOFT 2007), GROUP (ENSOFT 2010), and TeraDysac (Muraleetharan et al. 2003, Ravichandran 2005) are used to study the long term behavior of the Oklahoma IAB. The thermal loading on abutment piles can be simulated using the above mentioned simulation tools considering the rigid connection between the abutment and superstructure. Numerically simulated results are compared with field measured results in order to validate the computer simulation tools, so they can be utilized for the parametric study.

It is important to note that wingwalls were positioned at the ends of the Oklahoma IAB to support the backfill. The Oklahoma IAB had wingwalls parallel to the bridge direction. The effect of wingwalls on the behavior of the Oklahoma IAB was not considered in the numerical modeling.

LPILE and GROUP consider the non-linear soil behavior by utilizing non-linear soil lateral resistance-displacement curves (p-y curves). These computer programs have built-in empirical curves to describe the soil behavior. Furthermore, user defined p-y curves can be specified to describe different soil behaviors. Pile behavior can be modeled as either elastic or plastic. The plastic behavior of the pile is modeled by either providing data for non-linear moment-curvature relations for specified sections or considering

user specified non-linear moment-curvature relations. LPILE models the behavior of single pile under lateral loading while GROUP models the behavior of a group of piles subjected to axial and lateral loading. Two-dimensional and three-dimensional modeling of abutment piles can be performed in GROUP, however, LPILE only considers two-dimensional modeling of a single pile.

The complete bridge structure can be modeled in TeraDysac. TeraDysac is a three-dimensional, fully coupled, parallel computer code and was developed using the TeraScale finite element framework (ANATECH, 2001). A framework is used for building different finite element codes. Framework based finite element approach is one of the powerful and efficient methods for developing extensible finite element applications. It is also useful in developing parallel computer codes that are essential for analyzing complex problems such as three-dimensional soil-structure interaction problems. TeraDysac solves the fully coupled dynamic governing equations for saturated soils presented by Muraleetharan et al. (1994) and unsaturated soils by Ravichandran (2005) within the TeraScale framework. Large deformation problems can be simulated in TeraDysac and both static and dynamic problems can be solved by using it. In TeraDysac, the soil can be modeled using four-node quadrilateral (2-D) and eight-node brick (3-D) isoparametric elements, and the girders and piles are modeled with Timoshenko beam elements. Plate elements can be used to model the bridge deck and abutments. The bounding surface elastoplastic constitutive

models developed by Dafalias and Herrmann (1982, 1986), and Yogachandran (1991) are used to simulate the soil behavior in TeraDysac. Solid and fluid displacements are the nodal unknowns for the soil elements, and displacements and rotations are the nodal unknowns for the pile elements. Therefore a pile element and a soil element will share the solid displacements when a pile element is connected to a soil element without an interface at a common node. The rotations will only belong to the pile element and the fluid displacements will only belong to the soil element, hence the fluid flow will not be impeded due to the presence of piles within the soil.

In literature, although soil was modeled using more advanced techniques, only simple nonlinear constitutive models were used to describe soil behavior in the modeling of soil-structure interactions in IABs (Duncan and Arsoy 2003). None of these studies considered the presence of water within the soils and the associated effects of pore water pressure in the analyses. TeraDysac can predict the effect of pore pressure in the soil-structure interaction taking place in IABs. Initial validation of TeraDysac for the analysis of IABs was presented in Krier (2009) by comparing its predictions with the field measurements from the Mn/DOT study reported by Huang et al. (2004).

7.2 LPILE Modeling of the Oklahoma IAB

The long term behavior of the Oklahoma IAB was studied with the use of the computer program LPILE. Since LPILE can only handle two-dimensional modeling of soil-pile interaction for a single pile, the tributary superstructure dimensions corresponding to single abutment pile is considered in the analyses. Furthermore, Oklahoma IAB has a skew angle of 10^{o} and it is not considered in LPILE analyses.

7.2.1 Input Material Properties

7.2.1.1 Properties of the Soil Layers

Soil profile at the bridge site is shown in Figure 7.1. The soil underneath the south abutment is a 2.438 m thick layer of stiff lean clay. This soil deposit is underlain by a 0.601 m thick layer of dense silty sand, followed by layer of laminated sandstone rock interbedded with shale seams (very weak to weak rock). The soil underneath the north abutment is a 3.353 m thick layer of stiff lean clay, followed by a 1.524 m thick layer of dense silty sand. This layer is underlain by layer laminated sandstone interbedded with shale seams (very weak to weak rock).

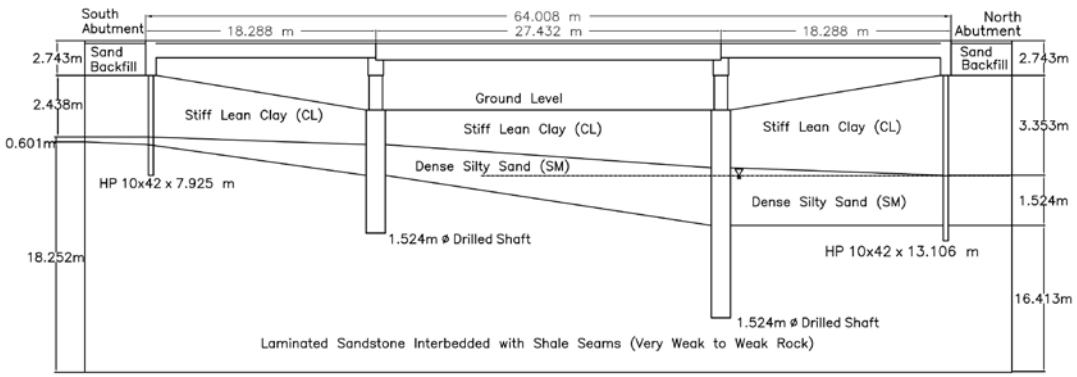

Figure 7.1: Soil Profile at the Bridge Site

The soil profiles at south and north abutments, considered for LPILE analyses are shown in Figures 7.2 and 7.3, respectively. Since the depth of the superstructure is 1.55 m, the middle point of the superstructure depth is considered as the load acting point in the LPILE analyses. The material properties of soil layers used for the analyses are shown in Table 7.1 (Reese et al. 1974, 1976; Detournay and Cheng 1993). Ground water level was 5.016 m below the ground surface as shown in Figures 7.2 and 7.3. Both abutment piles are anchored into the weak laminated sandstone interbedded with shale seams. Material properties of weak rock are listed below (Detournay and Cheng 1993, ENSOFT 2007):

Young's modulus of rock, $E_r = 15\ GPa$

Uniaxial compressive strength, $\sigma_c = 5000\ kPa$

Rock quality designation, $RQD = 50\ \%$

Dimensionless constant, $k_{ir} = 0.0005$

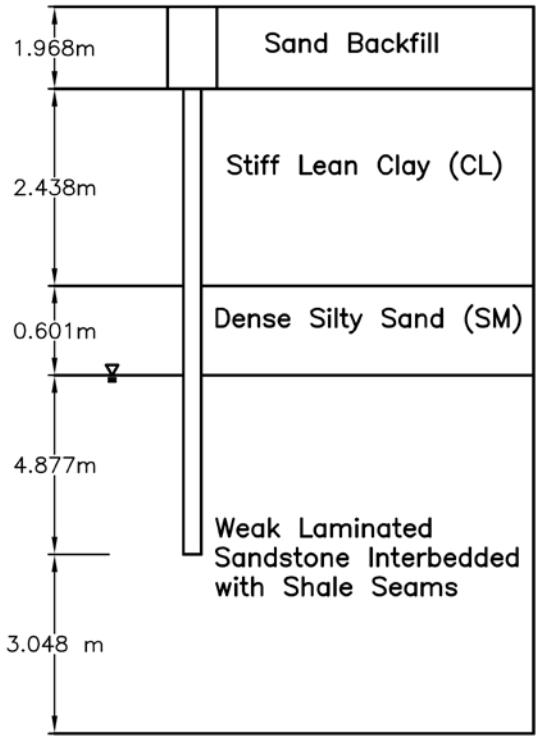

Figure 7.2: Soil Profile at the South Abutment

Table 7.1: Properties of the Soil Layers

Soil Layer	Total Unit Weight (kN/m^3)	Soil Lateral Stiffness, k (kN/m^3)	Undrained Cohesion, c (kN/m^2)	Internal Friction Angle (^{o})	Strain Factor, ε_{50}
Loose sand backfill	15.63	6 790	-	30	-
Stiff lean clay	21.50	136 000	65	-	0.007
Dense silty sand	20.72	61 000	-	35	-
Weak laminated sandstone interbedded with shale seams	24.35	-	-	-	-

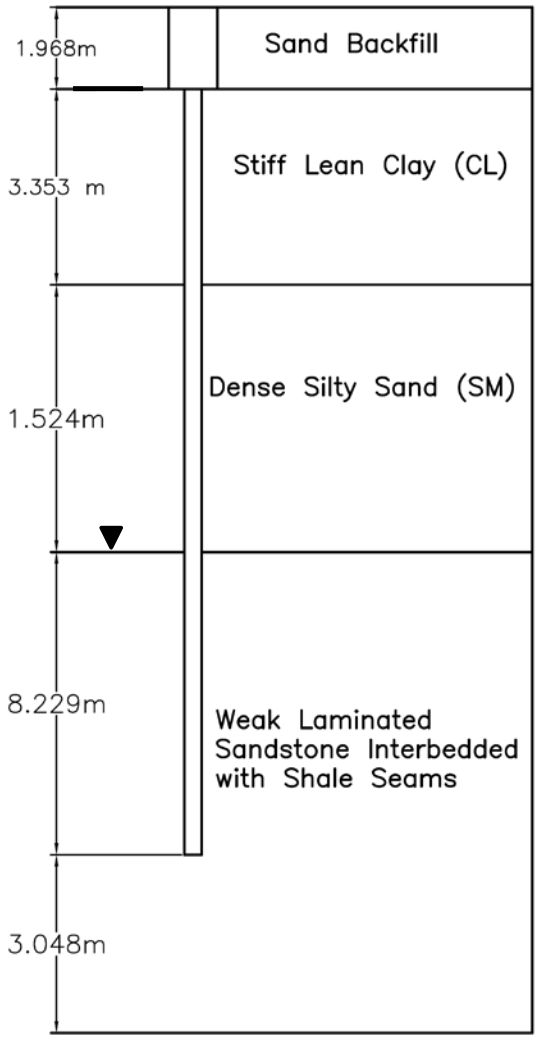

Figure 7.3: Soil Profile at the North Abutment

7.2.1.2 Properties of the Abutment Piles

The abutment pile considered in LPILE analysis has two sections (see Figures 7.2 and 7.3). Top section has reinforced concrete representing the abutment backwall and the bottom section is HP 10x42 steel pile oriented in weak axis bending. Average lengths of steel piles at south and north abutments are 7.925 m and 13.106 m, respectively.

Properties of reinforced concrete section are listed below:

Young's modulus of reinforced concrete, $E_c = 33.7 \ GPa$

Moment of inertia, $I = 0.1032 \ m^4$

Cross-sectional area, $A = 1.764 \ m^2$

Properties of HP 10x 42 steel piles are listed below:

Young's modulus of steel, $E_s = 200 \ GPa$

Moment of inertia, $I = 2.98x10^{-5} \ m^4$

Cross-sectional area, $A = 0.008 \ m^2$

7.2.2 Loading Condition

The superstructure of bridge undergoes an average temperature variation of 95 ^{o}F over a six month period (see Section 6.2). Assuming the thermal deformation of the bridge is symmetric to the center of the bridge, the thermally induced deformation of the superstructure at the abutment due to the change in temperature of superstructure can be evaluated by Equation 7.1.

$$\Delta L = \alpha \Delta T L / 2 \quad (7.1)$$

where, α is the coefficient of thermal expansion, ΔT is the change in temperature and L is the total length of the bridge. Thermal expansion coefficient of the reinforced concrete superstructure, α is considered as $6.23x10^{-6}/^{0}F$ in the thermal movement calculation. Thermally induced deformation of the superstructure at the abutment is 0.019 m. Furthermore, crackmeters are deployed at the expansion joints between road pavement and approach slab. The average movement of superstructure based on crackmeter reading is 0.022 m. Since the calculated superstructure movement is in the range of the measured reading from crackmeter, thermally induced deformation at the abutment is considered as 0.022 m. The displacement of the abutment is directly applied as the boundary condition in LPILE modeling. The axial load on the pile due to the superstructure is 136.6 kN.

7.2.3 Behavior of Abutment Piles

The behaviors of steel HP piles for the south and north abutments due to the thermally induced abutment deformation are shown in Figures 7.4 and 7.5, respectively. Even though north abutment piles are longer than the south abutment piles, the LPILE calculated bending moment are similar for both north and south abutment piles.

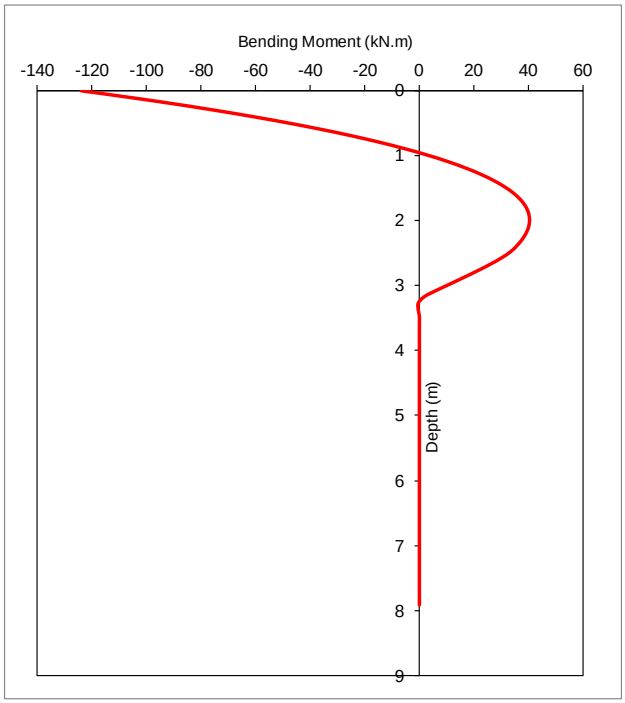

Figure 7.4: Bending Moment in the South Abutment Pile

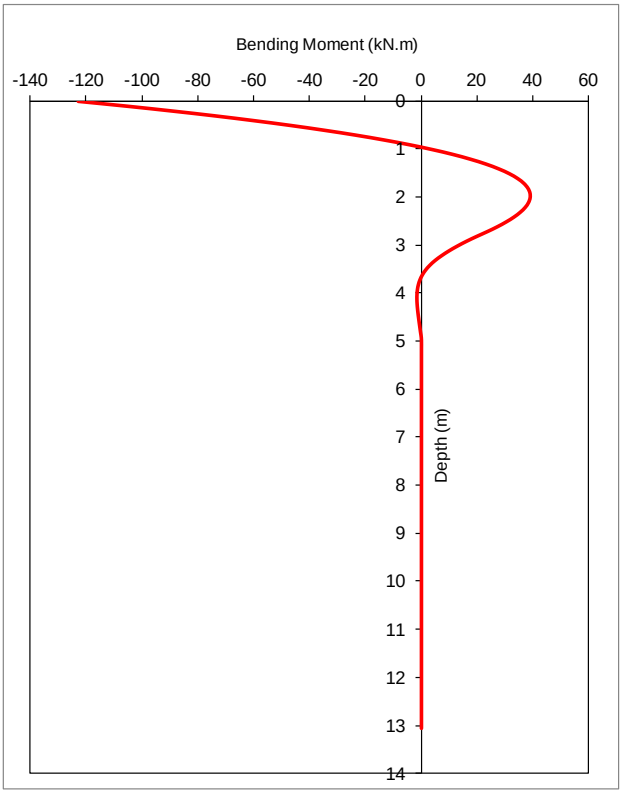

Figure 7.5: Bending Moment in the North Abutment Pile

The yield bending moment, M_y and ultimate bending moment, M_{ult} of steel HP 10x42 pile are 64.2 kN.m and 147.9 kN.m, respectively. The computed LPILE bending moment for abutment piles shows that the pile has yielded at shallow depths, however, it has not reached the ultimate bending moment.

7.2.4 Comparison of the Field Measurements and LPILE Modeling for Oklahoma IAB

The steel HP piles of the Oklahoma IAB were instrumented with strain gages at different depths. Strain gages were placed at shallow depths in south abutment piles and they were placed at greater depths in north abutment pile. The bending strain, $\Delta\varepsilon$ can be calculated from the difference between two opposite strain gage readings at a particular depth as shown in Equation 6.1. The bending moment, M can be calculated from Equation 6.2 as expressed in Section 6.7.

The comparison of field measured bending moment and computed LPILE bending moment based on thermal-induced abutment deformation for south and north abutment piles are shown in Figures 7.6 and 7.7, respectively.

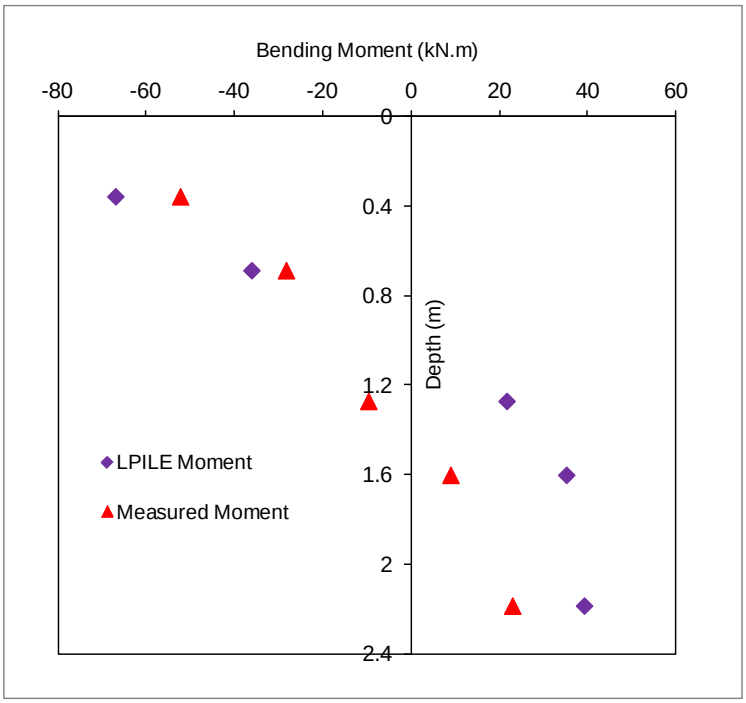

Figure 7.6: Measured and Calculated Bending Moments for the South Abutment Pile

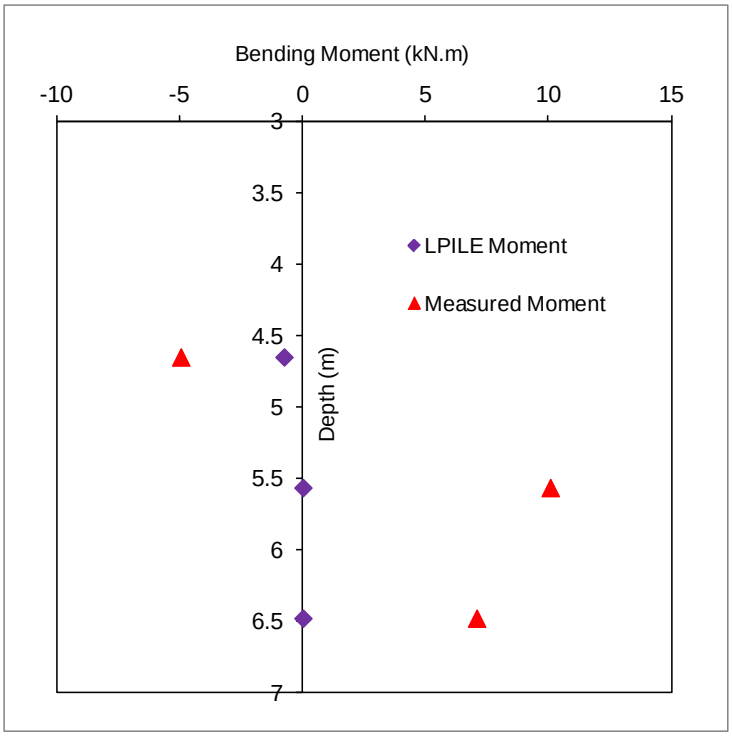

Figure 7.7: Measured and Calculated Bending Moments for the North Abutment Pile

The field measured bending moment for south abutment pile shows lower values than the computed LPILE bending moment. The field measured bending moment for north abutment pile, however, shows higher values than the computed LPILE bending moment. However, the variations in bending moment for north abutment pile are not important in this discussion as strain gages are located at a greater depth in north abutment pile and they do not experience significant bending moment.

The following reasons may have attributed for the difference between the field measured and computed values of bending moment. LIPLE considers simple two dimensional modeling of single pile and skew of the Oklahoma IAB is not considered in the analysis. Furthermore, thermal movement of the bridge was calculated based on the average temperature variation within the superstructure, however, the temperature variation of superstructure is not uniform across the depth of superstructure. Pre-drilled holes were used to drive south abutment piles, however, this particular condition was not modeled in LIPLE and it would play a significant role in the computed bending moments being higher than the measured values.

7.3 GROUP Modeling of the Oklahoma IAB

The long term behavior of the Oklahoma IAB was also studied with the use of the computer program GROUP. Since GROUP can handle both two-dimensional and three-dimensional modeling of abutment piles subjected to axial and lateral loading, the entire abutment structure comprised of seven abutment piles was considered in the analyses. Furthermore, Oklahoma IAB has a skew angle of 10^{o} and by incorporating three-dimensional modeling, the skew of the Oklahoma IAB is considered in GROUP analyses.

The embedded pile cap option available in GROUP was used to model the entire abutment structure. Since the passive soil resistance against the abutment backwall plays a vital role in the modeling of abutment subjected to lateral loading, the passive soil resistance against the pile cap was considered in the GROUP modeling of the Oklahoma IAB. The soil-structure interaction for the pile cap under translational movement is similar to the soil resistance (p-y curves) on piles under lateral loading. The approach adopted in the computer program GROUP is to derive the soil resistance for the pile cap using the same p-y criteria for piles, but with the diameter equal to the width of the front side of the concrete cap. The movements at the top and bottom of the pile cap are computed based on the translation and rotation of the cap.

7.3.1 Input Material Properties

The soil properties considered for the GROUP analyses remain the same as described in Section 7.2.1. The abutment piles considered in GROUP analysis have only one section. Single row of seven HP 10x42 steel piles oriented in weak axis bending are placed along the abutment with a spacing of 2.134 m. The width of the abutment is 14.289 m. The cross-section of the abutment considered for GROUP analyses is shown in Figure 7.8. Average lengths of steel piles at south and north abutments are 7.925 m and 13.106 m, respectively. Properties of abutment pile remain the same as described in Section 7.2.1.

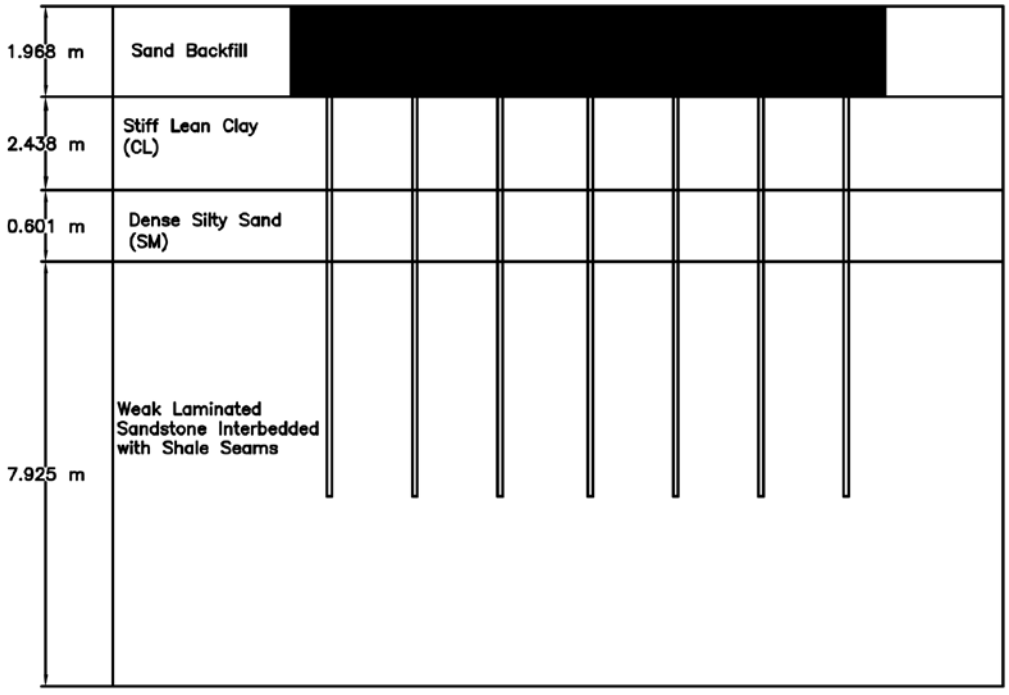

Figure 7.8: Cross-section of the Abutment

7.3.2 Loading Condition

Thermally induced deformation at the abutment is considered as 0.022 m as described in Section 7.2.2. Since only forces and moments can be applied as loading in GROUP, the displacement of the abutment cannot be directly applied as a boundary condition in GROUP. An alternative procedure was used to calculate the forces and moments acting on the abutment for the thermally induced deformation. The forces and moments at the top of the abutment, reported in LPILE analysis were used to calculate the forces and moments required for GROUP analysis. The forces and moments at the top of the abutment, reported in LPILE analysis were based on the tributary superstructure dimensions corresponding to a single abutment pile. Thus, total forces and moments acting on the entire abutment were calculated based on the number of piles and their corresponding superstructure dimensions. Since the skew of the bridge is considered in GROUP analysis, the longitudinal and transverse components of forces and moments were calculated based on the skew of the bridge. The axial load on the piles due to the superstructure is 871.8 kN. During the analysis, the displacement of the abutment for the above loading condition was verified with the actual deformation of the abutment and further adjustments were not required in the loads applied at the top of abutment.

7.3.3 Behavior of Abutment Piles

Since the thermal loading of the superstructure is not symmetric in a skewed IAB, biaxial bending (bending in longitudinal and transverse directions) of abutment piles occur in the Oklahoma IAB. There was not a significant difference among the calculated GROUP bending moment for each abutment pile (interior and exterior piles) even though the exterior piles have a reduced corresponding superstructure dimension than the interior piles, and this is attributed to the rigidity of the abutment during deformation.

The behaviors of steel HP piles for the south abutment due to the thermally induced abutment deformation are shown in Figures 7.9 and 7.10. The bending moments in longitudinal and transverse directions are shown in Figures 7.9 and 7.10, respectively. Similarly, the behaviors of steel HP piles for the north abutment due to the thermally induced abutment deformation are shown in Figures 7.11 and 7.12. The longitudinal bending moment in the north abutment pile is shown in Figure 7.11 and the bending moment in transverse direction is shown in Figure 7.12. Computed longitudinal GROUP bending moment distributions are similar to LPILE bending moment distributions, however, magnitudes are higher than LPILE bending moment. The soil-structure interaction for skewed IABs includes soil-abutment pile interaction and abutment-backfill soil interaction. The friction between the abutment and backfill material becomes very important in the skewed IAB in addition to the normal pressure acting against the surface of the abutments. The longitudinal component of the passive backfill soil pressure in a skewed

IAB was smaller than that in a straight IAB. Therefore, for a skewed IAB, the total force due to the backfill soil pressure was smaller than that of a straight IAB. Thus, in a skewed IAB, the reduction in backfill soil pressure increases the amount of abutment pile bending and larger longitudinal bending moments were observed in GROUP when compared to LPILE bending moment.

Furthermore, even though north abutment piles are longer than the south abutment piles, the GROUP calculated bending moments are similar for both north and south abutment piles.

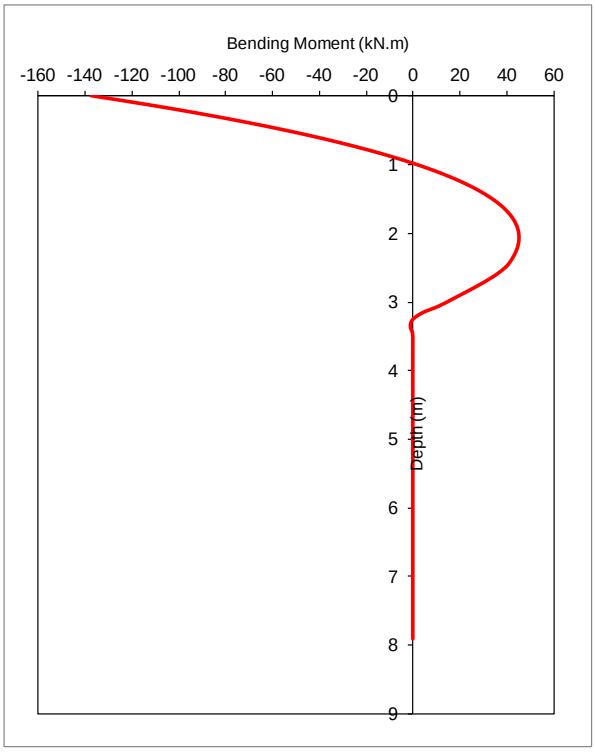

Figure 7.9: Bending Moment in Longitudinal Direction for the South Abutment Pile

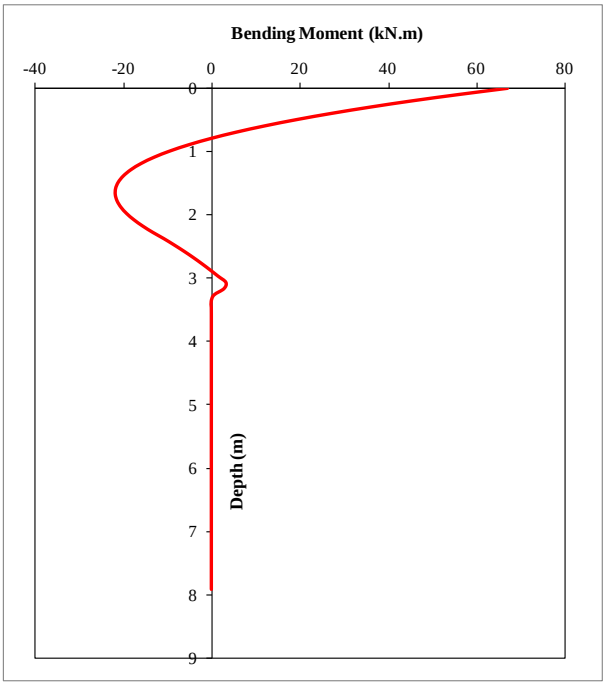

Figure 7.10: Bending Moment in Transverse Direction for the South Abutment Pile

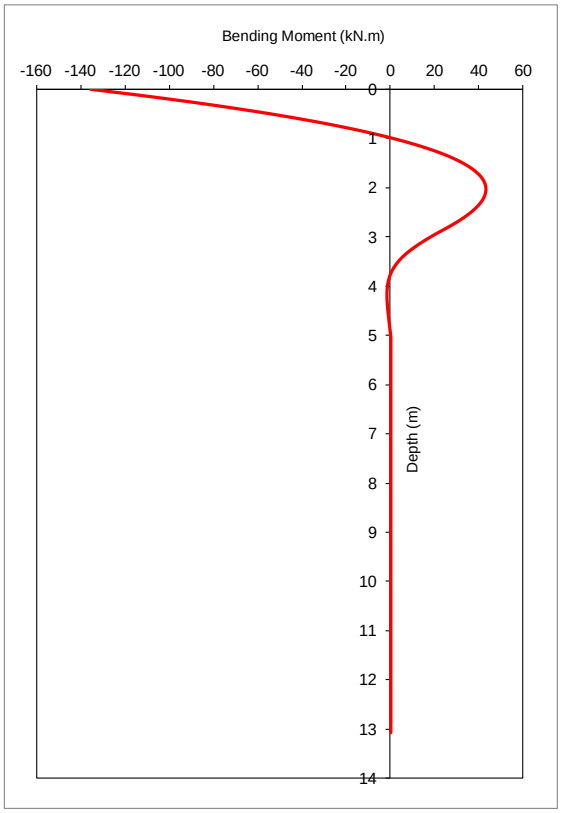

Figure 7.11: Bending Moment in Longitudinal Direction for the North Abutment Pile

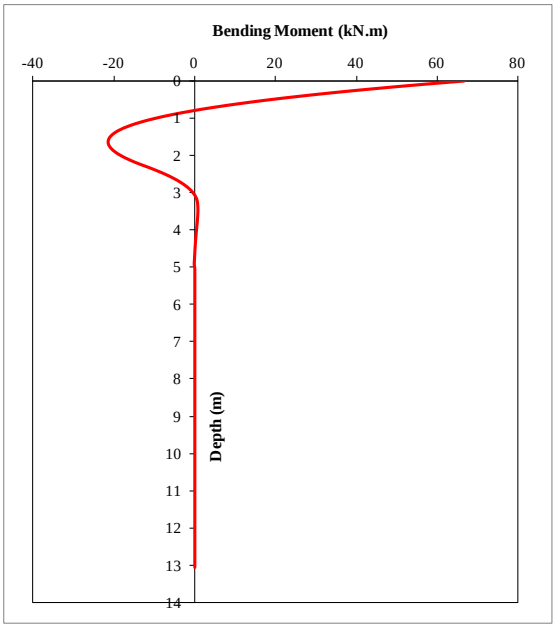

Figure 7.12: Bending Moment in Transverse Direction for the North Abutment Pile

The yield bending moment, M_y and ultimate bending moment, M_{ult} of steel HP 10x42 pile for weak axis bending are 64.2 kN.m and 147.9 kN.m, respectively. The computed longitudinal GROUP bending moment for abutment piles also shows that the pile has yielded at shallow depths, however, it has not reached the ultimate bending moment. Furthermore, abutment piles are oriented in strong axis bending in the transverse direction and therefore abutment piles will not have difficulty in accommodating the bending in transverse direction due to the asymmetric thermal loading of the Oklahoma IAB.

7.3.4 Comparison of the Field Measurements and GROUP Modeling for Oklahoma IAB

The comparison of field measured bending moments and computed longitudinal GROUP bending moments based on thermally induced abutment deformation for south and north abutment piles are shown in Figures 7.13 and 7.14, respectively.

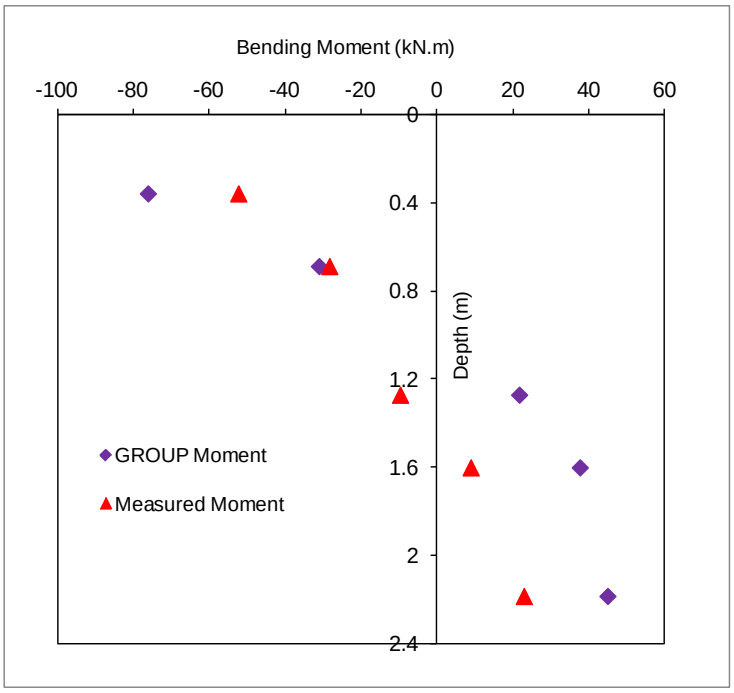

Figure 7.13: Measured and Calculated Bending Moments for the South Abutment Pile

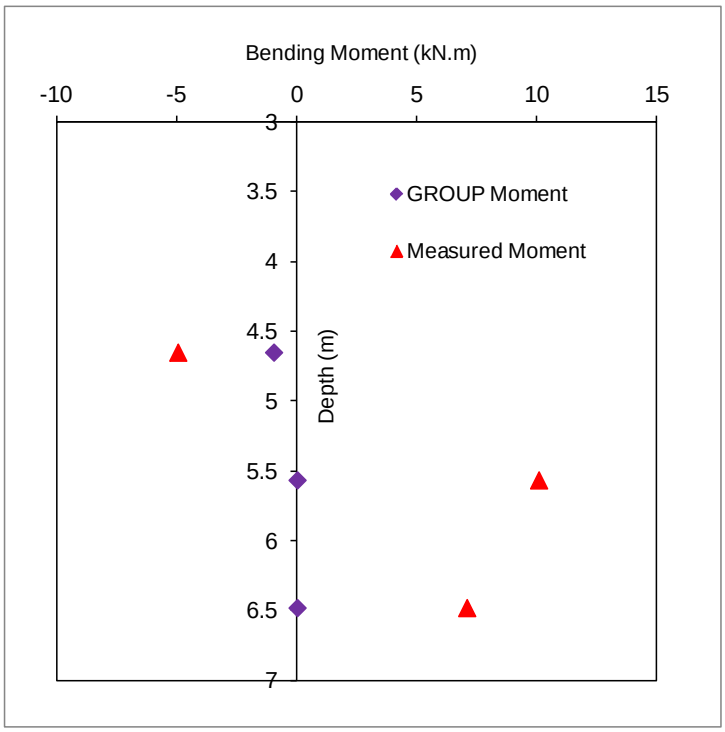

Figure 7.14: Measured and Calculated Bending Moments for the North Abutment Pile

The field measured bending moments for south abutment pile shows lower values than the computed GROUP bending moments. The field measured bending moments for north abutment pile, however, shows higher values than the computed GROUP bending moments. The variations in bending moment for north abutment pile are not important in this discussion as strain gages are located at a greater depth in north abutment pile and they do not experience significant bending moment.

Even though the skew of the bridge is incorporated in GROUP modeling, differences are observed in between the field measured and computed values of bending moments. The reasons that may be attributed to the difference between the field measured and computed values of bending moments are explained in Section 7.2.4.

7.4 TeraDysac Modeling of the Oklahoma IAB

A fully coupled finite element computer code, TeraDysac, was used to study the behavior of the Oklahoma IAB for thermal loading. TeraDysac considers the coupled differential equations governing the behavior of the solid skeleton, pore water, and structural elements. Bounding surface elastoplastic constitutive models are used to simulate the stress-strain behavior of soils in TeraDysac. The entire bridge structure can be modeled in TeraDysac considering the non-uniform thermal gradient that occurs in the superstructure of the bridge. The thermal loading feature implemented in TeraDysac allows a temperature change at the top and bottom of the superstructure with a linear distribution between the top and bottom surfaces. The difference between the top and bottom temperature changes controls the superstructure curvature. The curvature of the superstructure corresponding to the temperature increase (positive thermal gradient) and the temperature decrease (negative thermal gradient) are shown in Figures 7.15 and 7.16, respectively. The dotted lines represent the deformed shape due to the thermal effects.

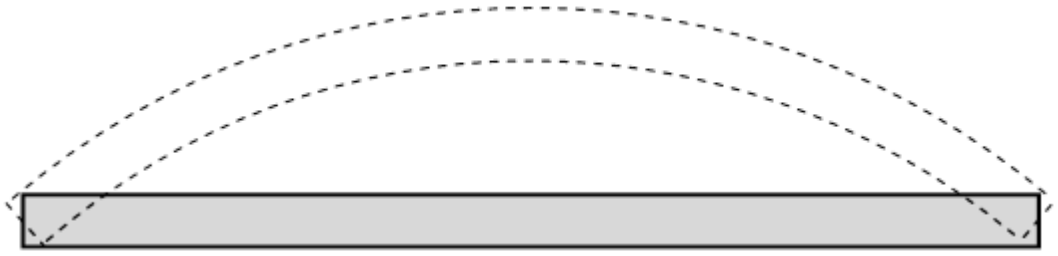

Figure 7.15: Curvature of Superstructure for Temperature Increase

Figure 7.16: Curvature of Superstructure for Temperature Decrease

The ability to track pore water pressure generation is a desirable feature of TeraDysac and the results provide insight into what soil regions may experience gains or losses in pore water pressure during the simulation. Two different analyses for the seasonal temperature increase and decrease were performed in TeraDysac. The obtained abutment displacement and bending moment in abutment piles from the TeraDysac analysis were compared with the field measurements.

7.4.1 Input Material Properties

The entire soil profile described in Section 7.2.1 was modeled in TeraDysac. Even though the ground water level is 5.016 m below the ground surface, the soil is assumed to be fully saturated for TeraDysac modeling.

7.4.1.1 Properties of the Soil Layers

In TeraDysac, the behavior of soil elements can be modeled as linear elastic or bounding surface elastoplastic clay and sand models can be used to model the behavior of soil elements. Bounding surface elastoplastic modeling of soil gives better prediction when compared to the linear elastic modeling of soils. The bounding surface model parameters used for stiff lean

clay and weak porous rock in the analysis are listed in Tables 7.2 and 7.3 (Muraleetharan 1994, Kirupakaran 2011). The model parameters listed in Table 7.2 can be measured in the laboratory. The other model parameters listed in Table 7.3 are calibrated using a single element computer code. The bounding surface model parameters used for loose sand backfill and dense silty sand are listed in Tables 7.4 and 7.5 (Muraleetharan et al. 2004). The sand at the bridge site was assumed to be Nevada Sand and the bounding surface properties for the sand layers were set based on the relative densities of the sand layers available at the bridge site. The soil stratum with the obtained relative density for sands and over consolidation ratio (OCR) values for clay and porous rock is shown in Figure 7.17. The OCR sets the initial bounding surface size which controls the soil response. Pore pressure effects were captured by setting the combined bulk modulus of pore fluid and solid grains, Γ as $2.2x10^6$ kPa for clays and sands. Combined bulk modulus of pore fluid and solid grains, Γ for the porous rock was considered as $7.2x10^9$ kPa (Kirupakaran 2011).

Table 7.2: Bounding Surface Parameters for Stiff Lean Clay and Weak Porous Rock

Parameter	Stiff Clay	Porous Rock
Slope of the isotropic consolidation line on $e - \ell n\ p'$ plot (λ)	0.17	0.25
Slope of an elastic rebound line on $e - \ell n\ p'$ plot (κ)	0.03	0.05
Slope of the critical state line in $q - p'$ space (compression) (M_c)	0.88	0.88
Initial void ratio (e_o)	0.98	0.772
Specific gravity	2.7	2.62
Permeability (m/s)	9.26×10^{-10}	7.7×10^{-12}

Table 7.3: Bounding Surface Parameters for Stiff Lean Clay and Weak Porous Rock

Parameter	Stiff Clay	Porous Rock
Traditional Model Parameters		
Poisson's ratio (ν)	0.3	0.16
Ratio of extension to compression value of M (M_e / M_c)	1.0	1.0
Bounding Surface Configuration Parameters		
Value of parameter defining the ellipse1 in compression (R_C)	2.4	2.4
Value of parameter defining the hyperbola in compression (A_C)	0.1	0.01
Parameter defining the ellipse 2 (tension zone) (T)	0.01	0.01
Projection center parameter (C)	0.0	0.0
Elastic nucleus parameter (S)	1.1	1.0
Ratio of triaxial extension to compression value of R (R_e / R_c)	0.92	0.92
Ratio of triaxial extension to compression value of A (A_e / A_c)	1.2	1.2
Hardening Parameters		
Hardening parameter (m)	0.02	0.02
Shape hardening parameter in triaxial compression (h_c)	3.0	3.0
Ratio of triaxial extension to compression value of h (h_e/h_c)	1.0	1.0
Hardening parameter on I-Axis (h_o)	2.0	2.0

Table 7.4: Bounding Surface Parameters for Loose Sand Backfill and Dense Silty Sand

Parameter	Loose sand	Dense sand
Slope of the isotropic consolidation line on $e - \ell n\ p'$ plot (λ)	0.017	0.007
Slope of an elastic rebound line on $e - \ell n\ p'$ plot (κ)	0.003	0.0014
Slope of the critical state line in $q - p'$ space (compression) (M_c)	0.89	0.89
Initial void ratio (e_o)	1.23	0.62
Specific gravity	2.65	2.67
Permeability (m/s)	5.71×10^{-4}	5.60×10^{-6}

Table 7.5: Bounding Surface Parameters for Loose Sand Backfill and Dense Silty Sand

Parameter	Loose Sand	Dense Sand
Traditional Model Parameters		
Poisson's ratio (ν)	0.3	0.3
Ratio of extension to compression value of M (M_e / M_c)	0.61	0.61
Bounding Surface Configuration Parameters		
Value of parameter defining the ellipse1 in compression (R_C)	1.5	1.5
Parameter related to gradient of ellipse 2 on I-Axis (α)	5.0	5.0
Parameter defining the ellipse 2 (tension zone) (T)	0.005	0.005
Projection center parameter (C)	0.0	0.0
Elastic nucleus parameter (S)	1.0	1.0
Ratio of triaxial extension to compression value of R (R_e / R_c)	1.0	1.0
Ratio of slope of critical state line to line OA in compression ($(M_u)_c / M_c$)	1.494	1.742
Hardening Parameters		
Hardening parameter (m)	0.02	0.02
Hardening parameter (a)	4.0	4.0
Hardening parameter (b)	1.0	1.0
Shape hardening parameter in triaxial compression (h_c)	2.0	2.0
Ratio of triaxial extension to compression value of h (h_e/h_c)	0.05	0.05
Hardening parameter on I-Axis (ho)	1.05	1.05
Unloading hardening parameter (hu)	0.2	0.2
Unloading hardening parameter (γu)	0.9	0.9
Deviatoric hardening parameter (β_0)	1.0	1.0
Deviatoric hardening parameter (β_1)	0.5	0.4

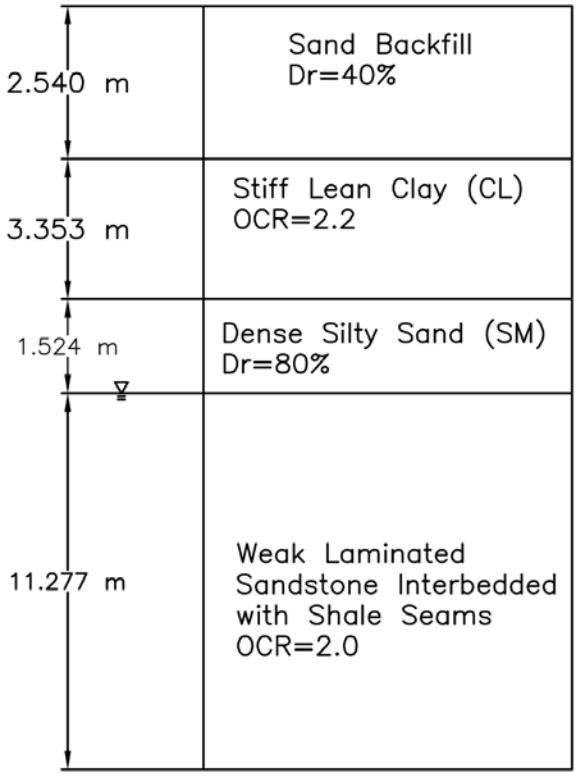

Figure 7.17: Soil Stratum Composition

The initial stress state of the soil is essential when using the bounding surface models. The initial stress state provides the starting location inside the bounding surface. Assuming a saturated soil stratum and using the soil unit weights, the initial stress state was calculated for all the soil elements. After the mesh was created, the mid-element depths were used to find the vertical effective stresses. A K_0 value of 0.69 was assumed to calculate the horizontal effective stresses. Initial effective stresses in the vertical direction for the rock layer are shown in Figure 7.18.

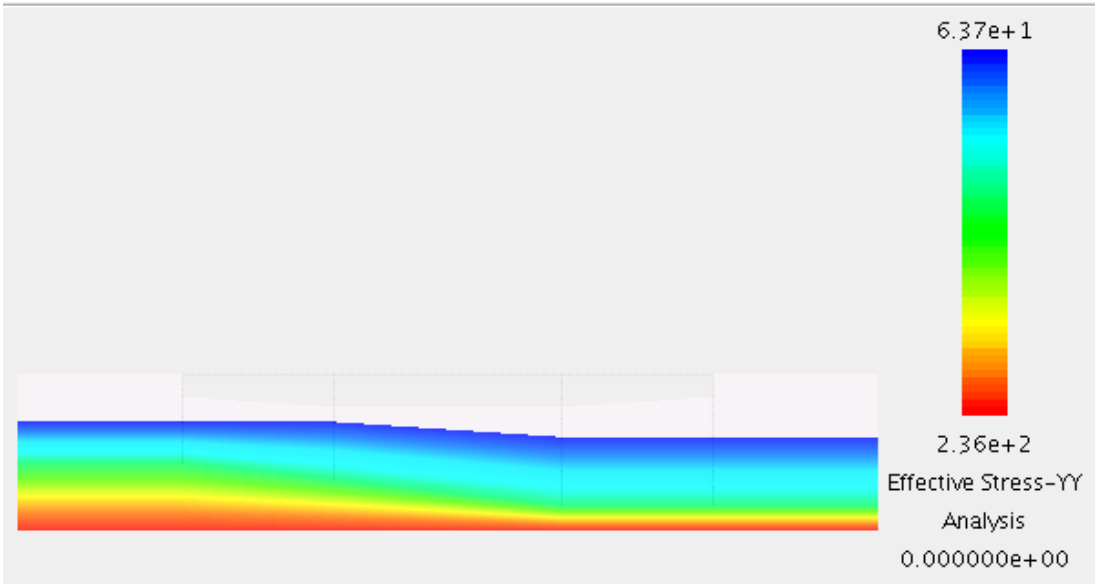

Figure 7.18: Initial Effective Stresses (kPa) for Rock Layer

7.4.1.2 Properties of the Structural Elements

The bridge deck, bridge girders, abutments, pier cap, and pier piles (drilled shafts) are all combinations of concrete and steel. The bridge deck, girders, abutments, and pier cap are made of reinforced concrete. Since these components consist of two materials, a weighted average approach was used to obtain the material properties required for the beam and plate elements.

The required beam element properties for the TeraDysac input include Young's modulus (E), Poisson's ratio (ν), area (A), strong axis moment of inertia (I_x), weak axis moment of inertia (I_y), and the coefficient of thermal expansion (α). The composite beam density (ρ) was also found using the

weighted average approach. The properties of various structural elements used in the analysis are listed below.

Properties of HP 10x 42 steel piles:

Young's modulus of steel, $E_s = 200\ GPa$

Moment of inertia, $I = 2.98x10^{-5}\ m^4$

Cross-sectional area, $A = 0.008\ m^2$

Coefficient of thermal expansion, $\alpha_s = 6.7x10^{-6}/^0 F$

Poisson's ratio, $\nu = 0.3$

Density, $\rho = 7.85\ Mg/m^3$

Properties of abutment section for a unit width:

Young's modulus of reinforced concrete, $E_c = 33.7\ GPa$

Moment of inertia, $I = 0.049\ m^4$

Cross-sectional area, $A = 0.838\ m^2$

Coefficient of thermal expansion, $\alpha = 6.23x10^{-6}/^0 F$

Poisson's ratio, $\nu = 0.2$

Density, $\rho = 2.51\ Mg/m^3$

Properties of pier cap:

Young's modulus of reinforced concrete, $E_c = 33.7\ GPa$

Moment of inertia, $I = 0.0636\ m^4$

Cross-sectional area, $A = 0.447\ m^2$

Coefficient of thermal expansion, $\alpha = 6.23x10^{-6}/^{0}F$

Poisson's ratio, $\nu = 0.2$

Density, $\rho = 2.51\ Mg/m^3$

Properties of superstructure:

Young's modulus of reinforced concrete, $E_c = 33.7\ GPa$

Moment of inertia, $I = 0.80\ m^4$

Cross-sectional area, $A = 4.046\ m^2$

Coefficient of thermal expansion, $\alpha = 6.23x10^{-6}/^{0}F$

Poisson's ratio, $\nu = 0.2$

Density, $\rho = 2.51\ Mg/m^3$

7.4.2 Loading Condition

In TeraDysac, the non-uniform thermal loading that is applied across the depth of the superstructure can be directly modeled by specifying temperature at the top surface of deck and the bottom of superstructure. The superstructure of bridge undergoes an average temperature variation of 95 ^{o}F over a six month period. The difference between the temperatures at top and bottom of superstructure was 12 ^{o}F for the temperature increase. Therefore, the temperatures at the top surface and bottom of the superstructure were considered as 101 ^{o}F and 89 ^{o}F for the temperature increase analysis, and the temperature varies linearly across the depth of the superstructure. The difference between the temperatures at top and bottom

of superstructure was 8 ^{o}F for the temperature decrease. The temperatures at the top and bottom of the superstructure were considered as 91 ^{o}F and 99 ^{o}F for the temperature decrease analysis.

7.4.3 Plane Strain Analysis

Two-dimensional plane strain analyses were performed in TeraDysac due to the computational complexity involved in three-dimensional analysis. The material properties described in Section 7.4.2 are used for the beams and plates in three-dimensional analyses. In two-dimensional analyses, an additional calculation is needed. The two-dimensional version of TeraDysac uses plane strain theory for the soil elements. Across the width of the bridge, there are four girders and seven piles at each abutment. Since the soil is represented by a unit width, the section properties for the girders and piles are spread over the bridge width. To find an approximate value of this moment of inertia over a unit width, the value is divided by the bridge width. In the two-dimensional model, the superstructure is a weighted average combination of the deck and the four girders which support the deck. Since the abutments are uniform across the bridge width, the abutment section properties are directly calculated for a unit width.

7.4.4 Finite Element Model

Finite element model considered for the Oklahoma IAB is shown in Figure 7.19. Several analyses were used to ensure the mesh has a minimum size (spatially) with minimal effect from the soil boundaries. The finite element mesh shown in Figure 7.19 has 1227 nodes and 1165 elements.

There are 109 beam elements and 1056 quadrilateral soil elements in the mesh. A close-up view of the structural elements is shown in Figure 7.20.

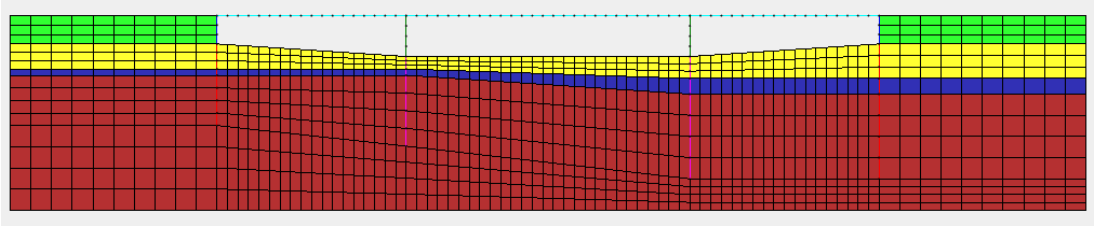

Figure 7.19: Finite Element Model

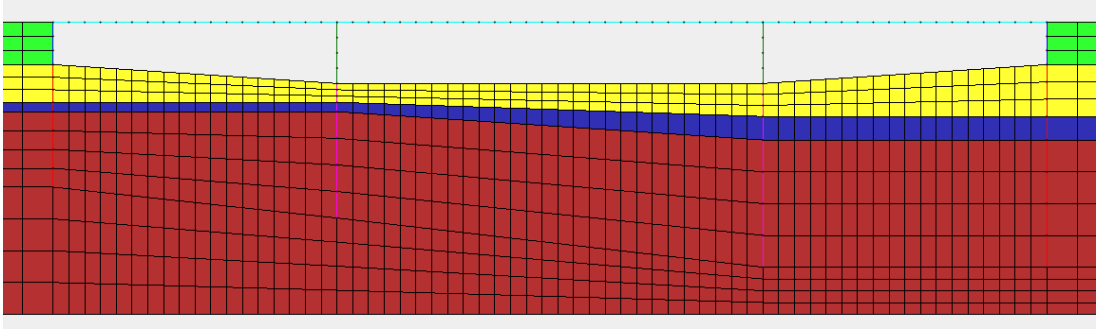

Figure 7.20: Close-up View of Finite Element Mesh

7.4.5 Analysis for Temperature Increase

Analysis was performed considering the seasonal temperature increase that takes place in the Oklahoma IAB. The temperatures at the top and bottom of the superstructure were considered as 101 ^{0}F and 89 ^{0}F for the temperature increase analysis, and the temperature varies linearly across the depth of the superstructure. The deformed mesh for the temperature increase is shown in Figure 7.21 (displacements magnified by a factor of 20).

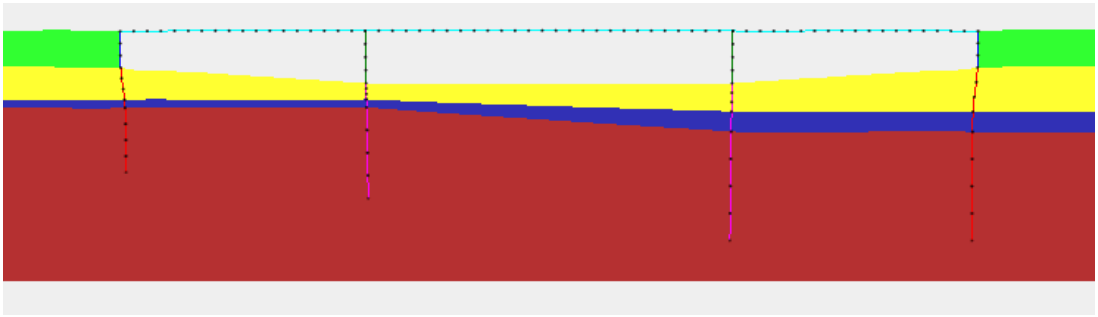

Figure 7.21: Deformed Mesh for Temperature Increase

Abutment and abutment pile deformation for both south and north abutments are presented in Figures 7.22 and 7.23, respectively. The transition from the abutment to the abutment pile occurs at a depth of 2.74 m. During the seasonal temperature increase, the crackmeters revealed an abutment movement of 22 mm. According to Figures 7.22 and 7.23, computed TeraDysac displacements are in good agreement with the field measured values.

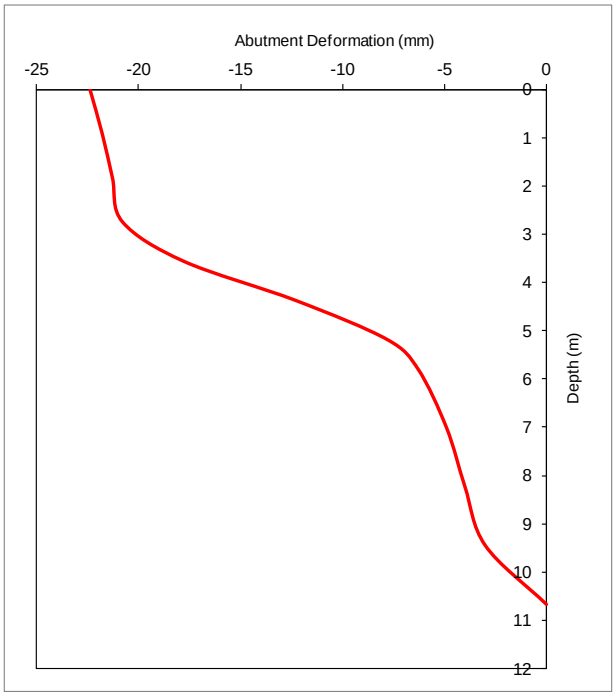

Figure 7.22: South Abutment and Abutment Pile Deformation for Temperature Increase

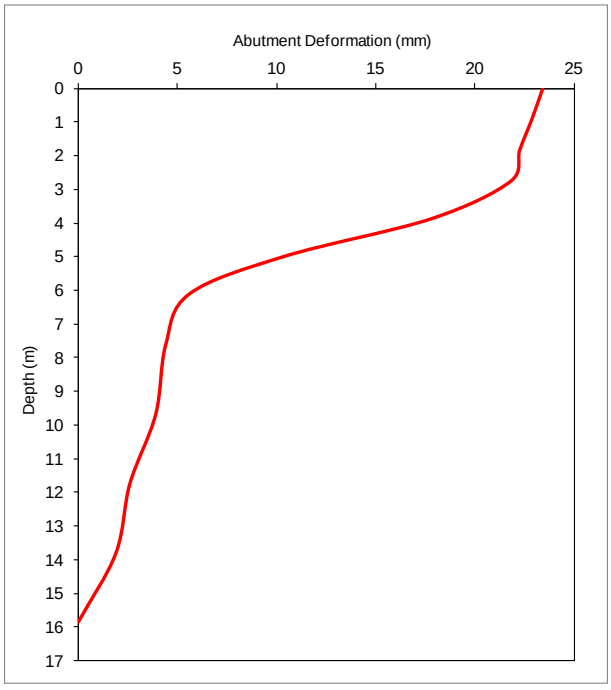

Figure 7.23: North Abutment and Abutment Pile Deformation for Temperature Increase

The computed TeraDysac bending moment for the abutment piles were compared with the field measurements. The comparison of field measured bending moment and computed TeraDysac bending moment based on temperature increase for south and north abutment piles are shown in Figures 7.24 and 7.25, respectively. According to Figures 7.24 and 7.25, computed TeraDysac bending moments agree well with the field measured bending moment.

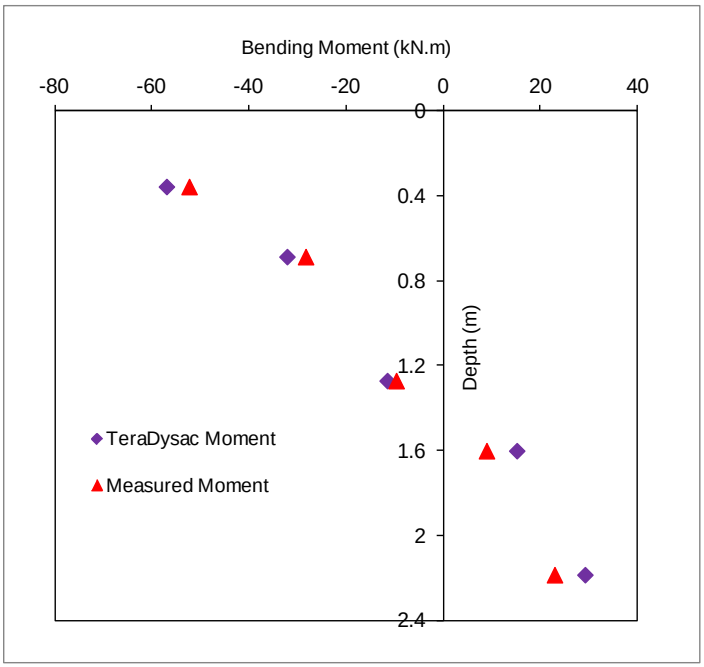

Figure 7.24: Measured and Calculated Bending Moments for the South Abutment Pile

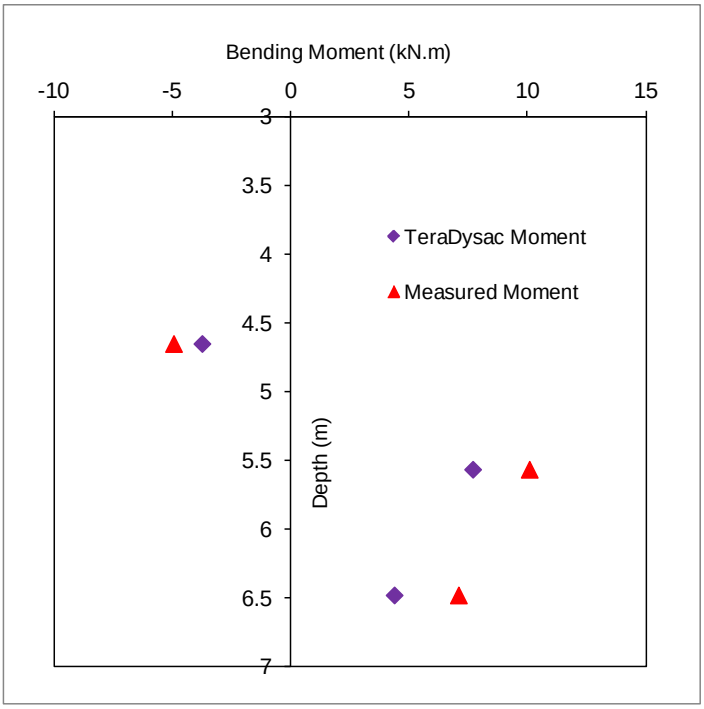

Figure 7.25: Measured and Calculated Bending Moments for the North Abutment Pile

Furthermore, the measured changes in earth pressure at the abutment backwall were compared with computed TeraDysac pressure changes. The TeraDysac pressure changes were calculated based on the initial horizontal effective stresses and final horizontal effective stresses after the simulation for soil elements adjacent to the abutment backwall. The comparison of field measured changes in earth pressure and computed TeraDysac pressure changes based on temperature increase for the north abutment is shown in Figure 7.26. The earth pressure changes measured along the centerline of the abutment for the seasonal temperature increase during first year of data collection are shown in Figure 7.26. According to Figure 7.26, computed earth pressure changes are higher than the measured values. The skew of the Oklahoma IAB is not considered in two-dimensional model developed in TeraDysac. The earth pressure changes will be higher for a straight IAB than that for a skewed IAB.

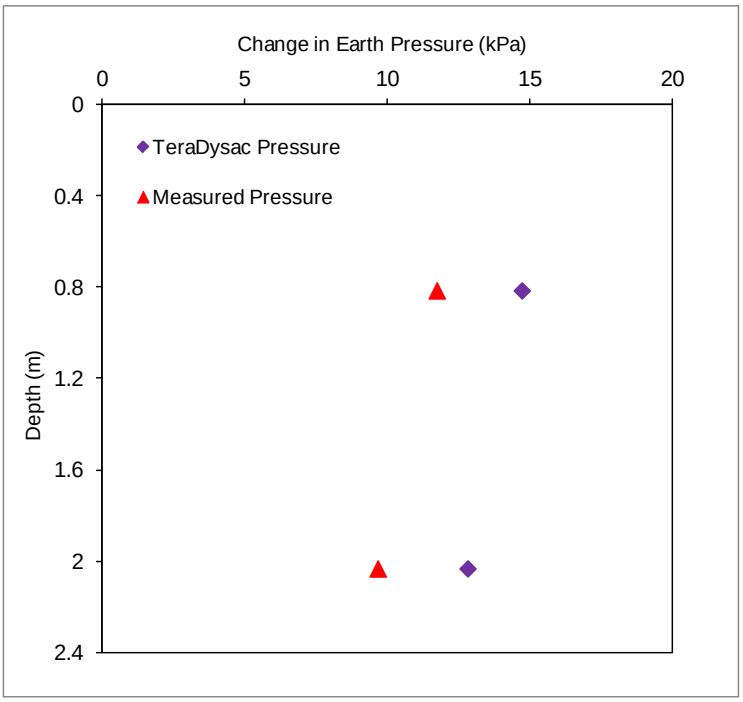

Figure 7.26: Measured and Calculated Earth Pressure Changes for the North Abutment

In addition to the results discussed above, one of the main advantages of using TeraDysac is the prediction of pore water pressure development during thermal loading. Pore pressure measurements are important when the soil becomes saturated. Pore pressure contours for the clay layer at the end of the analysis are shown in Figure 7.27. As the bridge deck is heated, it expands pushing the abutments into the backfill soil. This loading creates a positive pore pressure buildup in the backfill soils. On the interior sides of the abutments, negative pore pressure has developed. This phenomenon is related to the tied contact between the soil and structural elements. A positive pore pressure of 9.6 kPa and a negative pore pressure

of -1.8 kPa were generated in the clay layer. The developed pore pressure values are not significant in this case.

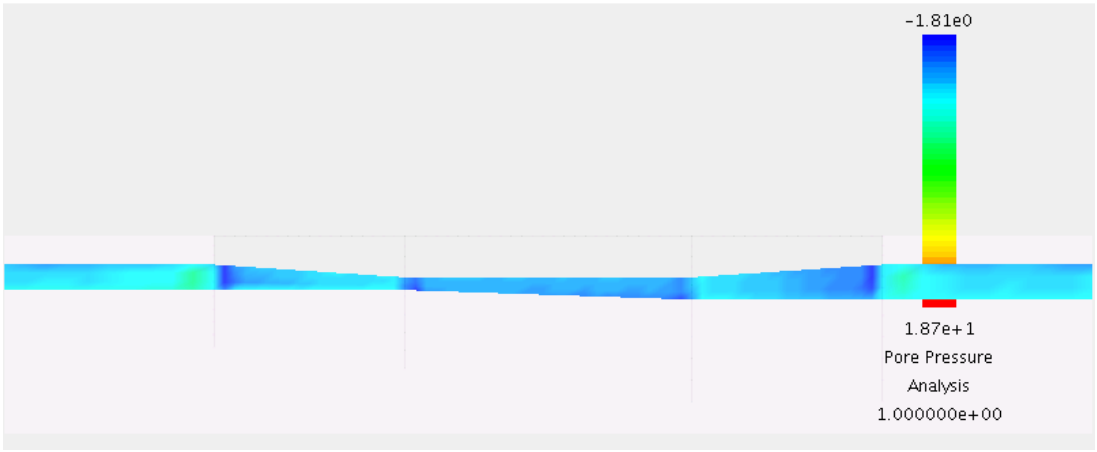

Figure 7.27: Developed Pore Water Pressure (kPa) in Clay Layer during Temperature Increase

7.4.6 Analysis for Temperature Decrease

Analysis considering the seasonal temperature decrease that takes place in the Oklahoma IAB was also performed. The temperatures at the top and bottom of the superstructure were considered as 91 ^{o}F and 99 ^{o}F for the temperature decrease analysis. The deformed mesh for the temperature decrease is shown in Figure 7.28 (displacements magnified by a factor of 20).

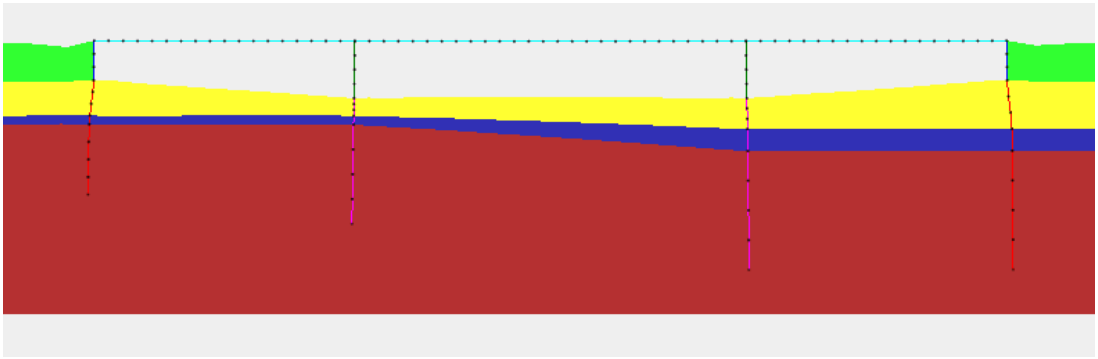

Figure 7.28: Deformed Mesh for Temperature Decrease

Abutment and abutment pile deformation for both north south and north abutments are presented in Figures 7.29 and 7.30, respectively. The transition from the abutment to the abutment pile occurs at a depth of 2.74 m. During the seasonal temperature decrease, the crackmeters revealed an abutment movement of 22 mm. According to Figures 7.29 and 7.30, computed TeraDysac displacements are in good agreement with the field measured values.

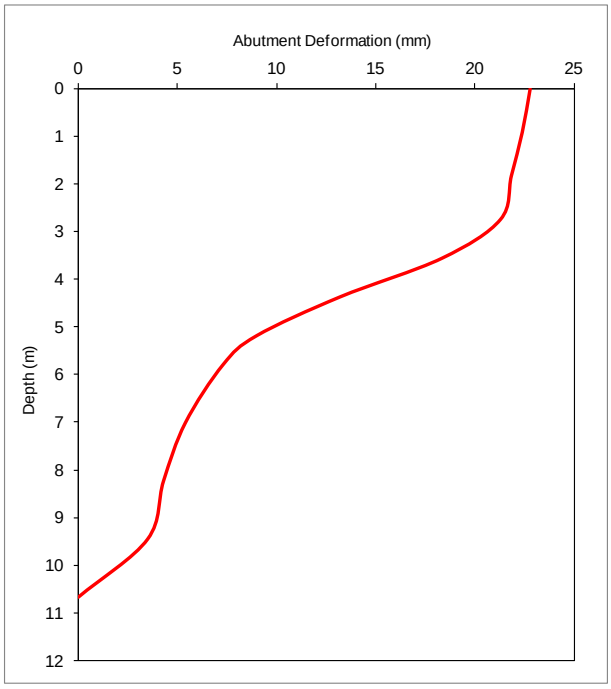

Figure 7.29: South Abutment and Abutment Pile Deformation for Temperature Decrease

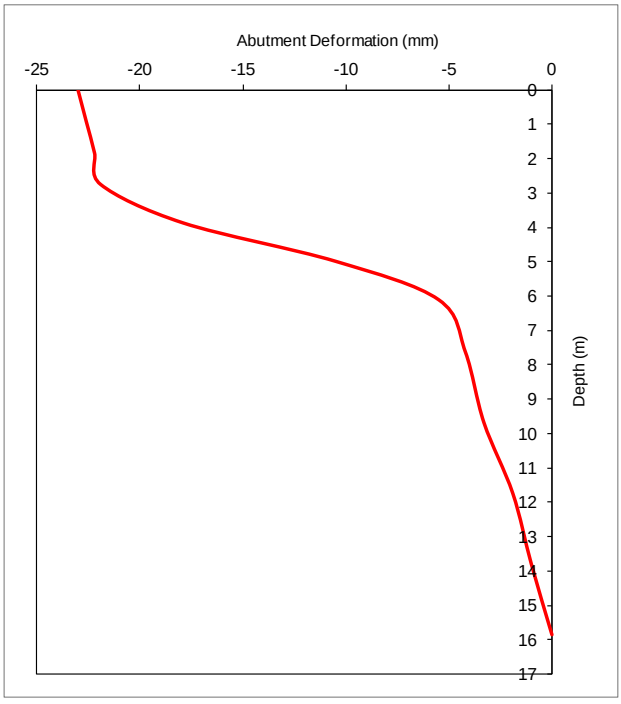

Figure 7.30: North Abutment and Abutment Pile Deformation for Temperature Decrease

Pore pressure contours for the clay layer at the end of the analysis are shown in Figure 7.31. As the bridge deck is cooled, it contracts pulling the abutments towards the river. This loading creates a negative pore pressure buildup in the backfill soils and positive pore pressure on the interior sides of the abutments. A positive pore pressure of 6.7 kPa and a negative pore pressure of -2.5 kPa were generated in the clay layer.

Figure 7.31: Developed Pore water Pressure (kPa) in Clay Layer during Temperature Decrease

The analyses performed in TeraDysac for the temperature increase and temperature decrease show the behavior of Oklahoma IAB for seasonal variations can be effectively modeled in TeraDysac. Since the non-uniform temperature changes occurring across the depth of the superstructure is considered in the model developed in TeraDysac, the bending stresses due to the curvature of the superstructure are incorporated in TeraDysac modeling. The curvature due to the gradient effect induces bending moments in the superstructure, and due to the rigid connection in between the

superstructure and the abutment structure, these bending moments are transferred to the abutment and abutment piles. Thus, TeraDysac gives a better prediction of the behavior of Oklahoma IAB when compared to the computer programs LPILE and GROUP.

Chapter 8: Parametric Study of IABs

8.1 Introduction

Only limited studies have been found in the literature regarding the parametric studies of IABs. One of the objectives of this research was to extend the results of the Oklahoma IAB to general IABs and propose design guidelines to build new IABs with longer lengths and larger skew angles. The validated simulation tools GROUP and TeraDysac were used to understand the long-term behavior of IABs in the parametric study. The base case was taken as the numerical models developed for the Oklahoma IAB in the computer programs GROUP and TeraDysac.

In this research, a parametric study was conducted to extend the results of the Oklahoma IAB to general IABs. Thermally induced deformation of the abutment and the bending moment in the abutment piles were studied to understand the long-term behavior of IABs.

8.2 Variables Considered in the Parametric Study

Abutment pile type, size and orientation, type of soil surrounding the abutment piles, pre-drilled holes around the abutment piles, bridge length and girder depth, and bridge skew angle are the variables considered in the parametric study to simulate various conditions of IABs. The variables are selected based on the literature review and the behavior of the Oklahoma IAB.

8.3 Abutment Pile Type, Size, and Orientation

In the literature, a range of discussions have been presented regarding the type of abutment piles designed for IABs. Steel HP piles were most frequently used in the design of IABs, however, cast-in-place (CIP), prestressed and pipe piles had also been used by the design agencies. HP piles have been used in a wide range of bridge spans and soil conditions with two types of pile orientations: weak axis bending and strong axis bending. CIP piles utilize driven steel pipes which are later filled with concrete, and steel reinforcement is placed in the top section of the piles. Prestressed concrete and pipe piles are sometimes used for short span IABs.

In this parametric study, the behavior of HP 10x42 steel piles, HP 12x53 steel piles and 12-inch diameter CIP piles are investigated for seasonal temperature changes. HP 10x42 piles were oriented in both weak axis bending and strong axis bending, however, HP 12x53 piles were oriented only in weak axis bending. Furthermore, the behavior of CIP piles with a 12-inch diameter was also investigated and compared to that of HP piles. A 210 feet long, three-span straight IAB (Bridge A) was considered in this parametric study. Variables considered in this parametric study are summarized in Table 8.1.

Table 8.1: Different Types of Abutment Piles

Description	Abutment Pile Type	Bending Axis	Number of Piles	Pile Spacing (ft)
Case 1	HP 10x42	Weak	7	7
Case 2	HP 10x42	Strong	7	7
Case 3	HP 12x53	Weak	7	7
Case 4	12-inch CIP	-	7	7

The sectional properties of the considered piles are given below:

Properties of HP 10x 42 steel piles in weak axis bending:

Young's modulus of steel, $E_s = 200\ GPa$

Moment of inertia, $I = 2.98x10^{-5}\ m^4$

Cross-sectional area, $A = 0.008\ m^2$

Properties of HP 10x 42 steel piles in strong axis bending:

Young's modulus of reinforced concrete, $E_s = 200\ GPa$

Moment of inertia, $I = 8.741x10^{-5}\ m^4$

Cross-sectional area, $A = 0.008\ m^2$

Properties of HP 12x 53 steel piles in weak axis bending:

Young's modulus of steel, $E_s = 200\ GPa$

Moment of inertia, $I = 5.286x10^{-5}\ m^4$

Cross-sectional area, $A = 0.01\ m^2$

Properties of 12-inch diameter CIP piles:

Young's modulus of reinforced concrete, $E_c = 31.3\ GPa$

Moment of inertia, $I = 0.0025\ m^4$

Cross-sectional area, $A = 0.0845\ m^2$

The number of piles under the abutments was selected based on the vertical load carrying capacity of the abutment piles. The axial load due to the superstructure was considered in calculating the number of piles required for the abutments. The computed GROUP pile bending moment with different pile types and sizes are shown in Figure 8.1. According to Figure 8.1, the largest bending moment occurred when CIP piles were used. From the computed results, CIP piles may be used only in short IABs. Except for CIP piles, HP 10x42 piles oriented in strong axis bending caused larger bending moments in the abutment piles than the other pile configurations considered in the modeling. The computed bending moment for HP 12x53 piles oriented in weak axis bending were larger than the bending moments for HP 10x42 piles oriented in weak axis bending.

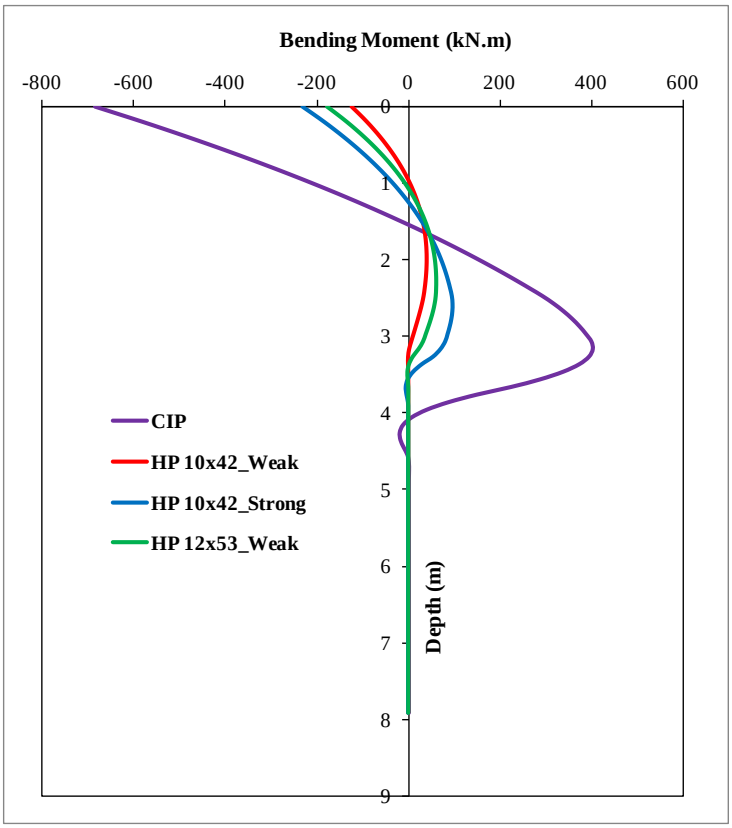

Figure 8.1: Variation in Pile Bending Moments for Different Pile Configurations

The orientation of HP piles with reference to the bridge longitudinal axis affected the thermally induced deformation in the abutment piles since the stiffness of the HP piles varies according to the bending axis. The orientation of weak axis bending helped to reduce the bending moment that occurs in the abutment piles. The orientation of weak axis bending will also help to reduce the thermally induced concrete stresses in the superstructure. The length of the bridge and the type of soil surrounding the abutment piles also play an important role in the behavior of abutment piles.

According to this parametric study, steel HP piles are most suitable to support abutments in IABs. The inherent flexibility of steel HP piles allows them to endure constant flexure induced by the cyclic thermal strains of the superstructure. Using a smaller HP pile section sufficient to carry vertical loads and orienting HP piles in weak axis bending will ensure the effective performance of IABs for seasonal temperature changes.

8.4 Bridge Length and Girder Depth

In practice, the length of an IAB is often limited. Girder depth and bridge length are often related and in general, deeper girders are used for longer bridges. For multi-span bridges, to reach the same bridge length, the bridges may consist of more short-span shallow girders or fewer long-span deep girders. Numerous span combinations exist for the considered bridge length and depth ranges.

In this study, three combinations illustrated as Bridge A, Bridge B and Bridge C were investigated. Bridge A and Bridge B had the same girder depths (Type III PCB) and different bridge lengths. Bridge B (420 feet, 6 spans) was twice as long as Bridge A (210 feet, 3 spans). Bridge B (6 spans) and Bridge C (3 spans) had the same total bridge length (420 feet) and different girder depths. Bridge C had Type IV PCB girders, which was deeper than that of Type III PCB girders used in Bridge B. To reach the same total length, six spans of girders were required in Bridge B and three spans in Bridge C. Bridges considered in this parametric study were straight IABs.

Abutment piles were oriented in week axis bending. Different types of bridge configurations considered in this parametric study are summarized in Table 8.2. Except for the varied parameters described above, other bridge parameters and soil conditions were kept constant.

Table 8.2: Different Types of Bridge Configurations

Description	Bridge A	Bridge B	Bridge C
Total Bridge Length (ft)	210	420	420
Number of Spans	3	6	3
Girder Type	Type III PCB	Type III PCB	Type IV PCB
Girder Length (ft)	60	60	120
Abutment Pile Type	HP 10x42	HP 10x42	HP 10x42
Number of Piles	7	7	12
Pile Spacing (ft)	7	7	3.9

The computed GROUP pile bending moment for different bridge and superstructure configurations are shown in Figure 8.2.

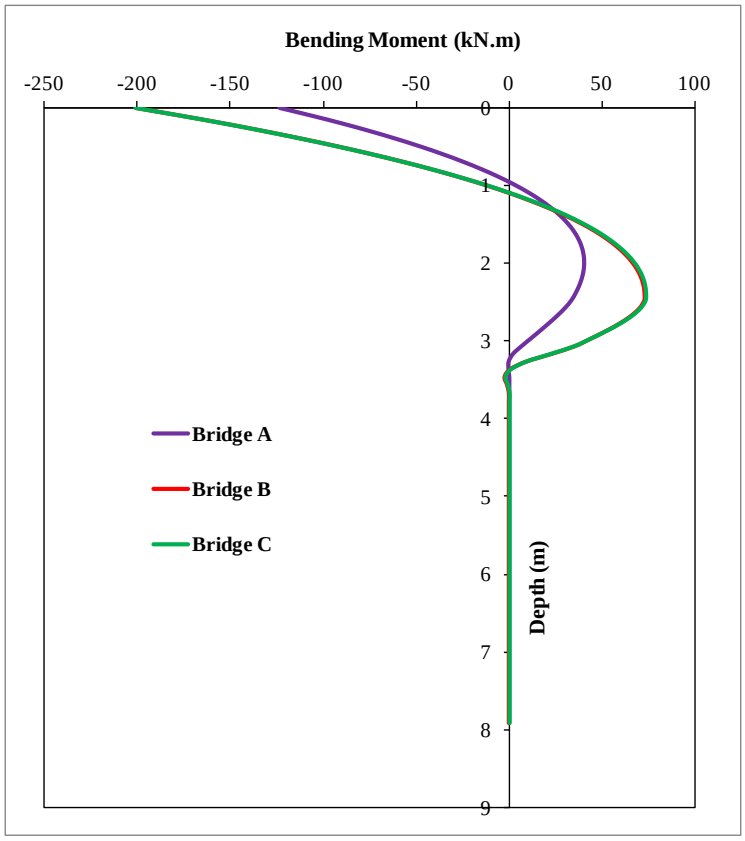

Figure 8.2: Variation in Pile Bending Moments for Different Bridge Configurations

According to Figure 8.2, the bending moment occurring in the abutment piles depends on the total bridge length. For the same bridge length, the computed bending moments are similar. The expansion and contraction of the superstructure were closely related to the total bridge length. The expansion and contraction of Bridge A was approximately half of that of Bridge B.

From the analyses, with the increase of total bridge length from 210 feet to 420 feet; the expansion and contraction of the superstructure and the bending moment in abutment piles increased correspondingly. There is not much variation in the bending moment for Bridge B and Bridge C, however,

using longer spans with larger girders (Bridge C) will increase the axial load on the abutment piles. Furthermore, larger thermal gradients will exist across the depth of superstructure when longer span girders are used for the bridge. Greater thermal gradient will increase the concrete stresses within the superstructure due to the larger depth of girders. Therefore long-span IABs should be designed with caution ensuring that thermally induced abutment pile bending moments and concrete stresses are limited within the allowable ranges.

8.5 Type of Soil Surrounding the Abutment Piles

Since the abutment piles were rigidly connected to the bridge superstructure, the type of soil surrounding the abutment piles has a direct effect on abutment pile behavior and an indirect effect on the behavior of superstructure. The following types of soil were investigated in the parametric study: loose sand, dense sand, soft clay, stiff clay and very stiff clay. A 210 feet long, three-span straight IAB (Bridge A) was considered in this parametric study. Abutment piles (7 HP 10x42 piles) were oriented in week axis bending.

Types and properties of soils surrounding the abutment piles are listed in Table 8.4 (Reese et al. 1974, 1976; Kamel et al. 1996). Computed GROUP pile bending moments for different types of soils are presented in Figure 8.3.

Table 8.3: Properties of Different Types of Soils

Soil Layer	Unit Weight (kN/m^3)	Soil Lateral Stiffness, k (kN/m^3)	Undrained Cohesion, c (kN/m^2)	Internal Friction Angle (o)	Strain Factor, ε_{50}
Loose sand	15.63	6 790	-	30	-
Dense sand	20.72	61 000	-	40	-
Soft clay	17.1	8 140	20	-	0.02
Stiff clay	20.5	136 00	90	-	0.007
Very stiff clay	22.1	271 000	240	-	0.004

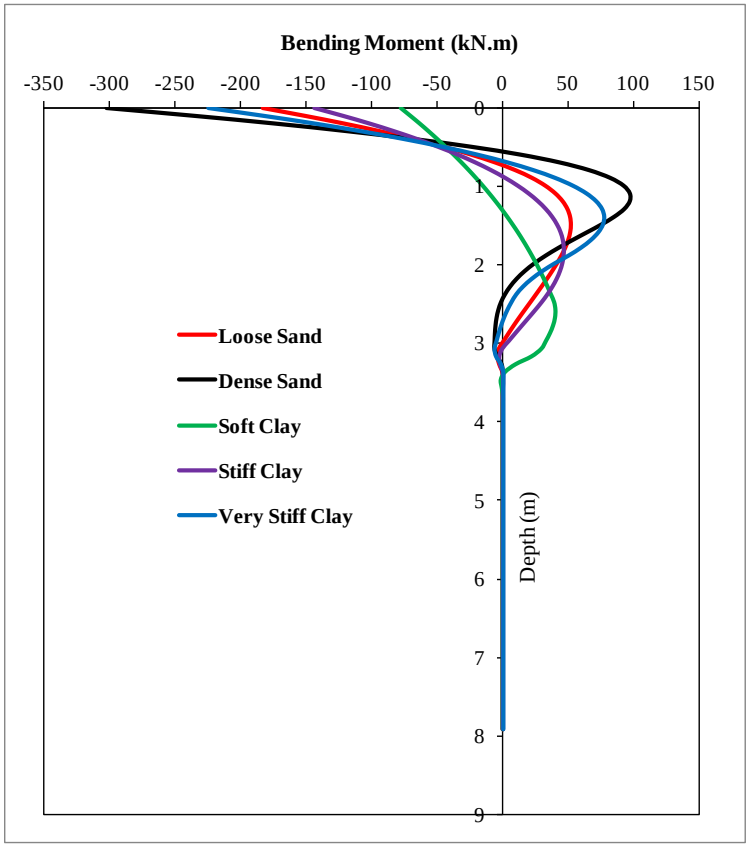

Figure 8.3: Variation in Pile Bending Moments for Different Types of Soils Surrounding the Piles

Soil surrounding the pile had a significant effect on the behavior of the abutment piles. According to Figure 8.3, dense sand and very stiff clay layers surrounding the piles created the largest bending moments in the piles. The stiffness of soil directly affects the abutment pile behavior. When the stiffness of soil is increased, partial flanges of the pile cross section near the pile head will yield and the plastic hinges may occur for longer IABs and larger temperature variations. Pre-drilled holes should be used to improve the behavior of the abutment piles when a stiffer soil layer is located surrounding the piles at shallow depth.

8.6 Pre-Drilled Holes around the Abutment Piles

In IABs, yielding of abutment piles may occur due to the thermally induced deformation of the abutments. To satisfy the safety and durability requirements, the development of plastic hinges should be avoided. The following conditions may favor the yielding of abutment piles: (i) stiff soil conditions (ii) long bridge spans (iii) large environmental temperature changes and (iv) large coefficient of thermal expansion of construction materials. To construct IABs in such conditions, pre-drilled holes may be needed. It should be pointed out that low initial construction and maintenance costs are the two important advantages of IABs. When pre-drilled holes are used, extra cost due to pre-drilling would be added, however, the enhanced in-service performance of IABs will reduce the future maintenance and repair costs.

From the literature, pre-drilling is a measure to improve the performance of piles under lateral loading. Pre-drilled holes filled with a loose material are used to improve the performance of abutment piles that are subjected to lateral loading. Size and depth of the pre-drilled hole, and the material used to fill the hole affect the ductility of the abutment piles subjected to lateral loading.

In this parametric study, the effect of pre-drilled holes on abutment pile behavior was investigated. Pre-drilled holes were modeled for the case of stiff clay condition. Pre-drilled holes with two different diameters (Hole A- diameter 3.0 feet, Hole B – diameter 7.0 feet) and two different lengths (Hole B- length 7.0 feet, Hole C – length 11.0 feet) were investigated in the study. The length of Hole A is 7.0 feet and the diameter of Hole C is 7.0 feet. In practice, pre-drilled holes are often filled with a loose material such as bentonite slurry and in this study, loose sand fill was assumed to be the fill material. A 210 feet long, three-span straight IAB (Bridge A) was considered in this parametric study. Abutment piles (7 HP 10x42 piles) were oriented in week axis bending. Different types of pre-drilled hole configurations considered in this parametric study are summarized in Table 8.3. Note that although 3 feet and 7 feet diameter holes may not be used in practice, they are considered here to study the relative behavior. Using smaller diameter holes in TeraDysac will be computationally time consuming.

Table 8.4: Different Types of Pre-drilled Hole Configurations

Description	Hole A	Hole B	Hole C
Hole Length (ft)	7	7	11
Hole Diameter (ft)	3	7	7

The finite element model developed in TeraDysac was used for this parametric study. The computer program GROUP considers infinitely long soil layers around the piles and therefore a hole cannot be modeled in GROUP. The finite element models developed in TeraDysac are shown in Figures 8.4 and 8.5. Type A hole with a smaller diameter and Type B hole with a larger diameter are shown in Figures 8.4 and 8.5, respectively.

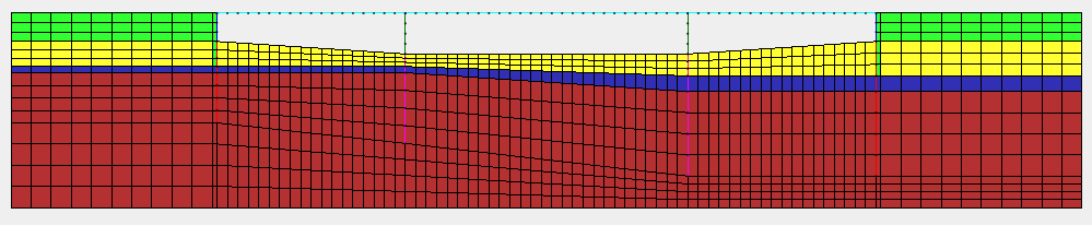

Figure 8.4: Finite Element Model for Hole A

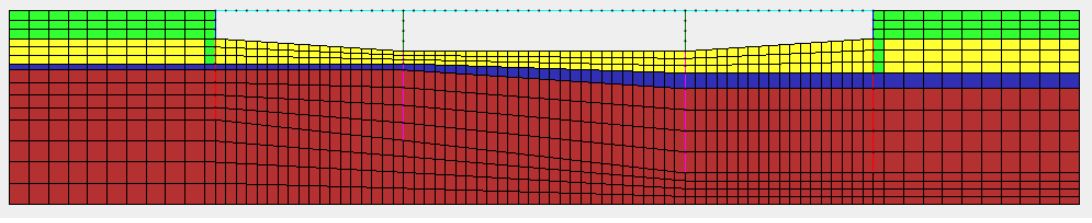

Figure 8.5: Finite Element Model for Hole B

Computed TeraDysac abutment deformations for different diameter of pre-drilled holes are presented in Figure 8.6. Computed TeraDysac pile bending moments in abutment piles for different pre-drilled hole configurations are shown in Figure 8.7.

According to Figure 8.6, there was not much difference in the abutment deformations when the diameter of pre-drilled hole is increased for Hole B. However, as illustrated in Figure 8.7, the bending moment in the abutment piles decreased when the pre-drilled hole diameter is increased for Hole B. The computed bending moments show, for stiff clay, the bending moment of piles were reduced due to the presence of the larger diameter pre-drilled hole. Negligible difference of abutment pile bending moments was observed when the depth of pre-drilled holes was increased from 7.0 feet to 11.0 feet (Holes B and C). When the abutment deformation becomes larger due to the thermal loading, the depth of the pre-drilled hole will also play a role in the bending moment of piles. For long-span IABs, bending moments in the abutment piles due to seasonal temperature changes may become larger and accommodating pre-drilled holes will help to reduce the yielding of the abutment piles.

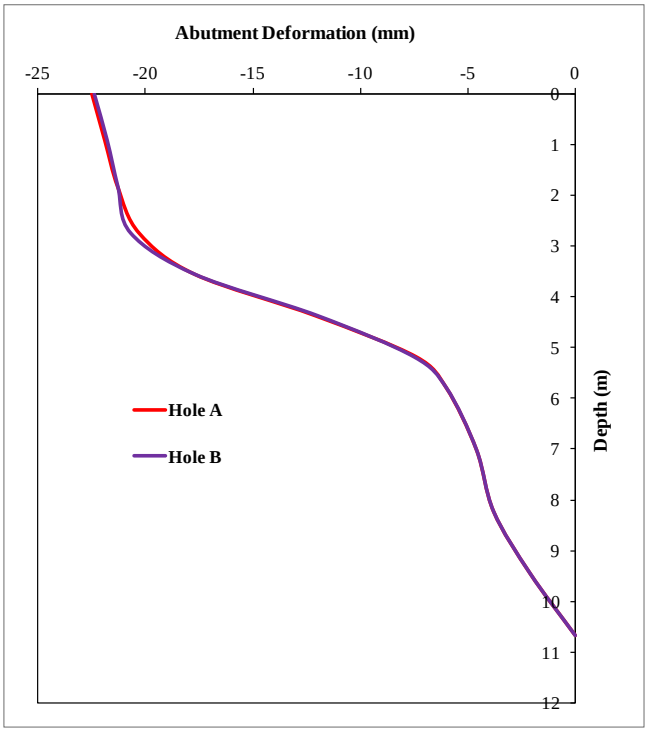

Figure 8.6: Abutment Deformation for Different Hole Configurations

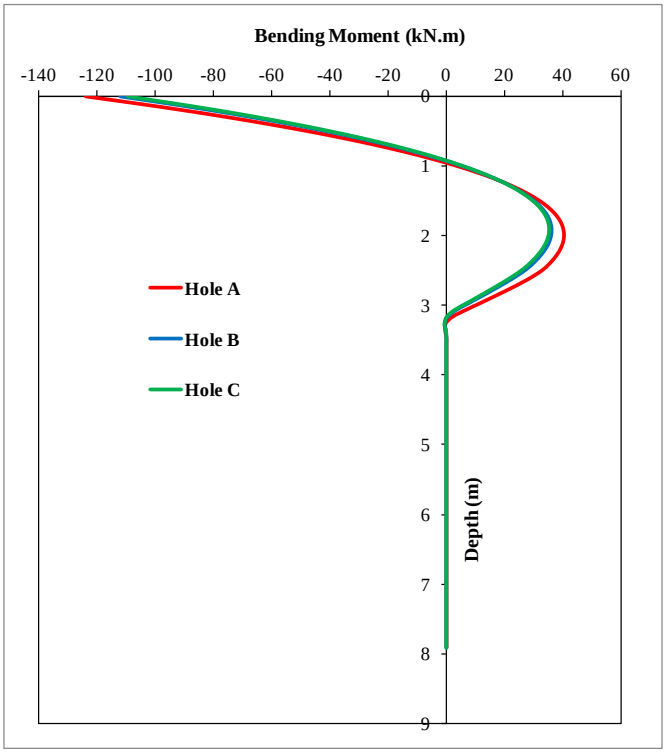

Figure 8.7: Variation in Pile Bending Moments for Different Hole Configurations

8.7 Bridge Skew Angle

In practice, skewed bridges are sometimes unavoidable due to the terrain at the bridge site or road alignment. Behavior of skewed IABs is much more complicated than straight IABs due to the uncertainly of soil-structure interactions. Soil pressure variation behind the abutment backwall is affected by the skew of bridge as the thermal loading of the superstructure is not symmetric in skewed IABs. Changes in soil pressure will also affect the behavior of the abutment piles in skewed IABs.

Very few articles have been found in the literature regarding the behavior of the skewed IABs. The behavior of skewed IABs is not fully understood and design agencies are reluctant to build IABs with larger skew angle. Different from straight IABs, in addition to the normal pressure acting against the surface of the abutments, the friction between the abutment and backfill material becomes very important.

In this study, a 210 feet long three-span IAB with three different skew angles (10^o, 20^o, 30^o) was investigated. Abutment piles (7 HP 10x42 piles) were oriented in week axis bending. The computer program GROUP was used for this parametric study. The variations of pile bending moment in the longitudinal and transverse directions for different skew angles are shown in Figures 8.8 and 8.9, respectively.

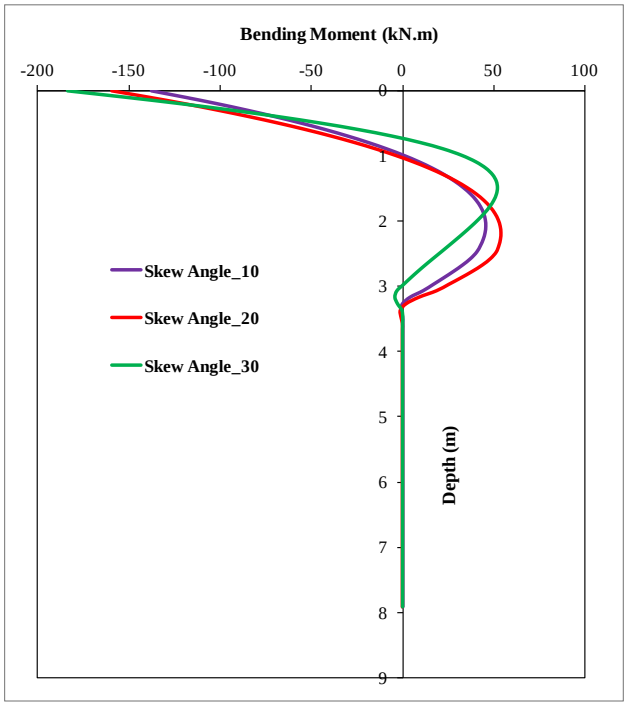

Figure 8.8: Bending Moment Variation in Longitudinal Direction for Different Skew Angles

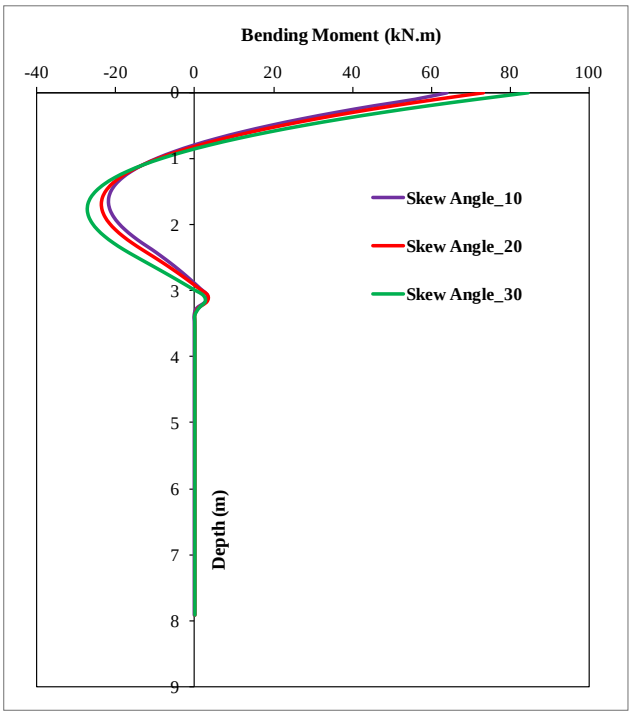

Figure 8.9: Bending Moment Variation in Transverse Direction for Different Skew Angles

According to Figures 8.8 and 8.9, there was an increase in the bending moment in the longitudinal and transverse directions when the skew angle of the bridge is increased. It may be explained that for the skewed bridge, the total force due to the backfill soil pressure was smaller than that of the straight IABs. In the skewed IAB, the reduction in the backfill soil pressure increased the amount of abutment pile bending and thus, larger bending moments were observed. Biaxial bending of abutment piles takes place in the skewed IABs as the thermal loading of the superstructure is not symmetric in skewed IABs.

The biaxial bending of the abutment piles in skewed IABs increases the stresses in the concrete superstructure, especially for long-span IABs and larger seasonal temperature changes. When the bridge skew angle becomes larger, the bending moment in the transverse direction becomes larger than the bending moment in the longitudinal direction. With skewed IABs, the soil passive pressure developed in response to thermal movement has a component in the transverse direction as well. Within certain limits of the skew angle, soil friction on the abutment will resist the transverse component of passive pressure, however, for larger skew angles, the soil friction is insufficient and significant bending moments in transverse direction are generated. Therefore, in such cases, abutment piles should be oriented in weak axis bending along the transverse direction of the bridge in order to accommodate the larger bending moments in the transverse direction. Furthermore, the structural components for the IABs with larger skew angles

have to be designed with caution to accommodate the thermally induced deformations in the superstructure and avoid distresses within the superstructure.

Chapter 9: Conclusions and Recommendations

9.1 Summary

IABs have been developed rapidly over the past 40 years in the United States due to their low initial and maintenance costs, and good earth quake resistance. The behavior of IABs is, however, still not fully understood, especially with respect to thermal movements, soil-structure interactions and skew effects. Due to those uncertainties, ODOT has been reluctant to build longer and skewed IABs. To understand the complex interactions occurring in IABs, a skewed IAB in Oklahoma was instrumented and data were collected over three years. Advanced computer simulation tools, validated with field performance data, were used to understand the soil-structure interactions occurring in IABs. This research provides valuable insight into the complex soil-structure interactions occurring in IABs.

9.2 Conclusions

The Oklahoma IAB was instrumented with 46 separate instruments to capture the behavior during the thermally induced deformation of the superstructure. Five different types of instruments (pile strain gages, earth pressure cells, crack meters, tilt meters, and thermistors) were employed in the bridge instrumentation.

The behavior of Oklahoma IAB for daily temperature variations was studied. The temperature variation across the depth of the superstructure was not uniform and a thermal gradient exists. The largest positive thermal

gradient occurred during summer day and the largest negative thermal gradient occurred during winter day, however, positive thermal gradients are comparatively larger when compared to negative thermal gradients. The cyclic thermal loading of the superstructure that causes the abutments to move towards backfill and then away from backfill results in both positive and negative strains in the abutment piles. The earth pressure measurements showed that the obtuse corner of the skewed IAB will experience larger earth pressure changes.

Since the data for the Oklahoma IAB was collected over three years, the seasonal behavior of the Oklahoma IAB was also studied. The seasonal behavior affects the long-term performance of the IABs. The bridge temperature decreases for six month duration (from July to January) and then increases for the following six month duration (January to July). This cyclic behavior continued from year to year within the measurement time frame. The average seasonal temperature change that the bridge superstructure is experiencing over a six month period of time is 95 ^{0}F. The field measured bridge temperatures for the Oklahoma IAB agree with the temperature range specified in the AASHTO LRFD Specifications (2007).

Earth pressures on the abutments increases as the temperature increases and decreases as the temperature decreases. Maximum changes in earth pressures occurred at the obtuse corner of the north abutment and larger changes in earth pressures were observed near the bridge deck than at a greater depth. Earth pressure measurements show that fairly significant

amount of abutment back pressures have been recorded during summer and also they show increase in abutment back pressures from summer to summer. Recorded readings from the earth pressure cells, tiltmeters, and crackmeters are consistent with the expected behavior of abutments rotating outward during heating and rotating inward during cooling. Crackmeter and tiltmeter measurements show majority of bridge translation is accommodated by the abutment pile movements in IABs. Recorded abutment pile strains show that strains in the piles seem to be accumulating and then stabilizing after a certain time. Furthermore, the abutment piles of IABs are experiencing bending moments beyond the yield bending moment.

The long term behavior of the Oklahoma IAB was studied with the use of computer programs LPILE and GROUP. Computed longitudinal GROUP bending moment are higher than LPILE bending moment since the skew of the Oklahoma IAB is incorporated in the three-dimensional model developed in GROUP. Since the thermal loading of the superstructure is not symmetric in a skewed IAB, biaxial bending (bending in longitudinal and transverse directions) of abutment piles occurs in the Oklahoma IAB. The computed LPILE and GROUP bending moments for abutment piles show the steel HP pile has yielded at shallow depths, however, it has not reached the ultimate bending moment. The comparison of field measured bending moment, and computed LPILE and GROUP bending moment shows field measured bending moments for south abutment pile have lower values than the computed LPILE and GROUP bending moments. Several reasons may be

attributed for the difference between the field measured and computed bending moments and the most important reasons among them are that the south abutment piles were installed in pre-drilled holes and thermal gradients across the depth of superstructure were not considered in the modeling.

A fully coupled finite element computer code, TeraDysac, was also used to study the behavior of Oklahoma IAB for thermal loading. TeraDysac considers the coupled differential equations governing the behavior of the solid skeleton, pore water, and structural elements. Bounding surface elastoplastic constitutive models are used to simulate the stress-strain behavior of soils in TeraDysac. The entire bridge structure was modeled in TeraDysac considering the non-uniform thermal gradient that occurs in the superstructure of the bridge. The computed TeraDysac abutment deformations agree well with the field measurements. The comparison of field measured bending moments, and computed TeraDysac bending moments shows field measured bending moments for south abutment pile have better agreement with the TeraDysac predictions than the computed LPILE and GROUP bending moments.

The results of the Oklahoma IAB were extended to general IABs in order to propose design guidelines to build new IABs with longer lengths and larger skew angles. The validated simulation tools TeraDysac and GROUP were used to understand the long-term behavior of IABs in the parametric study. Steel HP piles are most suitable to support abutments in IABs. The

inherent flexibility of steel HP piles allows them to endure constant flexure induced by the cyclic thermal strains of the superstructure. Using a lighter pile section and orienting HP piles in weak axis bending will ensure the effective performance of IABs for seasonal temperature changes. The expansion and contraction of the superstructure were closely related to the total bridge length. Using longer spans with larger girders will increase axial load on the abutment piles and concrete stresses in the superstructure, and therefore long-span IABs should be designed with caution ensuring that thermally induced abutment pile bending moments and concrete stresses in superstructure are limited within the allowable ranges.

Types of soil surrounding the abutment piles had a significant effect on the behavior of IABs. Stiffer soils created larger bending moments in the abutment piles. When the stiffness of soil is increased, partial flanges of the pile cross section near the pile head will yield and the plastic hinges may occur for longer IABs and larger temperature variations. Pre-drilled holes should be used to improve the behavior of the abutment piles when a stiffer soil layer is located surrounding the piles at shallow depths. For stiffer soils, the bending moment of piles were reduced due to the presence of a pre-drilled hole. When the abutment deformation becomes larger due to the thermal loading, the depth of the pre-drilled hole will also play a role in the bending moment of piles. For long-span IABs, bending moments in the abutment piles due to seasonal temperature changes may become larger

and accommodating pre-drilled holes will help to reduce the yielding of the abutment piles.

Soil pressure variation behind the abutment backwall is affected by the skew of bridge as the thermal loading of the superstructure is not symmetric in skewed IABs. Changes in soil pressure will also affect the behavior of the abutment piles in skewed IABs. There was an increase in the bending moment in the longitudinal and lateral directions when the skew angle of the bridge is increased. Biaxial bending of the abutment piles increases the stresses in the concrete superstructure, especially for long-span IABs and larger seasonal temperature changes. When the bridge skew angle becomes larger, the bending moment in transverse direction becomes significant compared to the bending moment in longitudinal direction. Therefore, in such cases, abutment piles should be oriented in weak axis bending along the transverse direction of the bridge in order to accommodate the larger bending moments in the transverse direction. Furthermore, the structural components for the IABs with larger skew angles have to be designed with caution to accommodate the thermally induced deformations in the superstructure and avoid distresses within the superstructure.

9.3 Design Recommendations

The following recommendations are provided for design and construction of IABs. The deign temperature range of IABs should be selected based on the location of the bridge as specified in AASHTO LRFD Specifications. In order to accommodate the thermal movement in IABs, the upper portion of the abutment pile length should be in a pre-bored hole that is filled with a material that has a very low stiffness (such as bentonite slurry or loose sand) and the piles should be placed in weak axis bending. The temperature variation of superstructure is not uniform along its cross-section and this temperature gradient should be considered in the design of IABs. Comparing IABs with equal total lengths, short spans with shallow girders are recommended over long span deep girders.

The backfill material behind the integral abutments has a significant effect on the performance of integral abutments. Typical soils used in the filling of abutments can exert relatively high passive pressures. Using a compressible material behind the abutments (abutment backwall-backfill interface material) and reinforcing the soil underlying the approach slab with geosynthetics would reduce the passive pressures behind the integral backwall. Materials such as elasticized expanded polystyrene (EPS) can act as a cushion between the abutment backwall and backfill material and reduce the pressure behind the abutment backwall. Geosynthetic reinforcement will create a mechanically stabilized earth mass and also can serve as drain for ground water. It will reduce the settlement of soil behind

the integral backwall. Furthermore, the backfill soil can be replaced with CLSM while deploying compressible EPS geofoam behind the abutment backwall. CLSM is effective in accommodating the displacement of abutments and also minimizes the settlement problem.

Larger differences exist in the design of abutment piles for IABs and not all designers consider lateral loads due to thermal loading. The magnitude of the lateral loads depends on the total length of the bridge, the size and orientation of the piles, the soil condition at the bridge site and the climate. The abutment piles for IABs should be checked for the capacities under combined axial force and bending moments.

Biaxial bending of the abutment piles takes place in skewed bridges. Since the bending moments in both directions increase with the increase of skew angle of the bridge, it causes an increase in stresses in the concrete superstructure, especially for long-span IABs and larger seasonal temperature changes. When the bridge skew angle becomes larger, abutment piles should be oriented in weak axis bending along the transverse direction in order to accommodate the larger bending moments in the transverse direction. The structural components for the IABs with larger skew angles have to be designed carefully to accommodate the thermally induced deformations in the superstructure and avoid distresses within the superstructure.

9.4 Recommendations for Future Research

The fully coupled finite element computer code TeraDysac provides a better prediction of the behavior of the Oklahoma IAB since the entire bridge structure can be modeled in TeraDysac considering non-uniform thermal gradient that occurs in the superstructure of the bridge. Only two-dimensional plane strain analyses were performed in TeraDysac due to the computational complexity involved in three-dimensional analyses. It is recommended that three-dimensional analyses be performed since the skew of the Oklahoma IAB can be incorporated in the modeling. Furthermore, it will provide a better understanding of skewed IABs that are subjected to thermal loading in transverse direction in addition to the thermal loading in longitudinal direction.

The abutment pile behavior is considered as elastic in the numerical models developed for the Oklahoma IAB, however, the piles will undergo non-linear deformations for thermal loading. Non-linear moment-curvature relationships for the HP piles have to be incorporated in the numerical models in order to consider the pile behavior as non-linear.

The backfill material behind the integral abutments has a significant effect on the performance of IABs. Using a compressible material behind the abutments and reinforcing the soil underlying the approach slab with geosynthetics would enhance the in-service performance of IABs. Numerical models that are developed for IABs should incorporate this particular phenomenon in order to study the effectiveness of this modification to the backfill material.

Since only one precast concrete girder IAB was monitored in this research, the experimentally measured temperature changes, displacements, rotations and abutment pile bending moments that are presented in this dissertation may not be entirely representative of those bridge responses and temperatures for other precast concrete girder IABs in Oklahoma. Further experimental studies that involve bridge monitoring programs would contribute to a better understanding of the behavior of IABs with longer lengths and larger skew angles.

References

Alampalli, S. and Yannotti, A. P. In-service performance of integral bridges and jointless decks. Transportation Research Record 1624. Transportation Research Board, National Research Council, Washington, D.C. 1998. Pages 1-7.

American Association of State Highway and Transportation Officials (AASHTO) Load and Resistance Factor Design (LRFD) Specifications, Fourth Edition, Washington, D.C. 2007.

American Association of State Highway and Transportation Officials (AASHTO) Load and Resistance Factor Design (LRFD) Specifications, Third Edition, Washington, D.C. 2002.

American Association of State Highway and Transportation Officials (AASHTO) Load and Resistance Factor Design (LRFD) Specifications, Second Edition, Washington, D.C. 1998.

ANATECH Corporation (formerly TeraScale, LLC.). TeraGrande: A multi-physics finite element program. Albuquerque, New Mexico. 2005.

ANATECH Corporation (formerly TeraScale, LLC.). The TeraScale Framework. Albuquerque, New Mexico. 2001.

Arsoy, S., Ducan, J. M. and Barker, R. M. Performance of piles supporting integral bridges. Transportation Research Record 1808. Transportation Research Board, National Research Council, Washington, D.C. 2002. Pages 162-167.

Canary Systems, Inc. MultiLogger Software User's Guide Version 4.3. New London, New Hampshire. 2008.

Clough, G. W. and Duncan, J. M. Earth pressures. Foundation Engineering Handbook, Second Edition (edited by Fung, H. Y. and Reinhold, V. N.), New York. 1991.

Dafalias, Y.F., and Herrmann, L.R. Bounding surface formulation of soil plasticity. Soil Mechanics – Transient and Cyclic Loads (edited by G.N. Pande and O.C. Zienkiewicz). Wiley. Chichester, England. 1982. Pages 253-282.

Dafalias, Y.F., and Herrmann, L.R. Bounding surface plasticity II: application to isotropic cohesive soils. Journal of Engineering Mechanics 112 n12. December 1986. Pages 1263-1291.

Detournay, E. and Cheng, A.H.-D. Fundamentals of poroelasticity. Comprehensive rock engineering principles, practice and projects, analysis and design methods (Fairhurst, C. ed). Pergamon. Oxford. 1993. Pages 113-171 (Chapter 5).

Duncan J.M., and Arsoy, S. Effect of bridge-soil interaction on behavior of piles supporting integral bridges. Transportation Research Record 1849. Transportation Research Board, National Research Council, Washington, D.C. 2003. Pages 91-97.

ENSOFT, Inc. Computer program LPILE^{PLUS} 5.0 for Windows. Austin, TX. 2007.

ENSOFT, Inc. GROUP 8.0 for Windows Manual. Austin, TX. February 2010. Pages 3-111.

ENSOFT, Inc. LPILE^{PLUS} 5.0 for Windows Technical Manual. Austin, TX. July 2004. Pages 3-33.

Geokon, Inc. Instruction Manual for Model 3800 Thermistors & Thermistor Strings. Lebanon, New Hampshire. 2008.

Geokon, Inc. Instruction Manual for Model 4420 VW Crackmeter. Lebanon, New Hampshire. 2008.

Geokon, Inc. Instruction Manual for Models 4800, 4810, 4815, 4820, and 4830 VW Earth Pressure Cells. Lebanon, New Hampshire. 2008.

Geokon, Inc. Instruction Manual for Model 6350 Vibrating Wire Tiltmeter. Lebanon, New Hampshire. 2007.

Geokon, Inc. Instruction Manual for Model 8032 Terminal Board and 16/32 Channel Multiplexer. Lebanon, New Hampshire. 2007.

Geokon, Inc. Instruction Manual for Model 8021-1 Micro-1000 Datalogger. Lebanon, New Hampshire. 2007.

Geokon, Inc. Instruction Manual for Model 4000 Vibrating Wire Strain Gage. Lebanon, New Hampshire. 2005.

Girton, D. D., Hawkinson, T. R. and Greimann, L. F. Validation of design recommendations for integral abutment piles. Journal of Structural Engineering. American Society of Civil Engineers 117 (7). 1991. Pages 2117-2134.

Girton, D. D., Hawkinson, T. R. and Greimann, L. F. Validation of design recommendations for integral abutment piles. Final Report. Iowa DOT Project HR- 292, Highway Division, Iowa Department of Transportation, Ames, Iowa. 1989.

Greimann, L. F., Yang, P. S., Edmunds, S. K., and Wolde-Tinsae, A. M. Design of piles for integral abutment bridges. Final Report. Iowa DOT Project No. HR-252, Iowa Department of Transportation, Ames, Iowa. 1984.

Greimann, L. F., Wolde-Tinsae, A. M. and Yang, P. S. Skewed bridges with integral abutments. Transportation Research Record 903. Transportation Research Board, National Research Council, Washington, D.C. 1986. Pages 64-72.

Hanlon, B. Instrumentation to study thermal loading of a skewed integral abutment bridge. M.S. Thesis. School of Civil Engineering and Environmental Science, University of Oklahoma, Norman, Oklahoma. 2010.

Huang, J., French, C. and Shield, C. Behavior of concrete integral abutment bridges. Final Report. Minnesota Department of Transportation, St. Paul, Minnesota. 2004.

Jorgenson, J. L. Behavior of abutment piles in integral abutment in response to bridge movements. Transportation Research Record 903. Transportation Research Board, National Research Council, Washington, D.C. 1983. Pages 72-79.

Kamel, M. R., Benak, V. J., Tadros, M. K. and Jamshidi, M. Prestressed concrete piles in jointless bridges. Prestressed concrete institute journal. 1996. Pages 56-67.

Kirupakaran, K. Finite element modeling of borehole stability in poroelastoplastic media. M.S. Thesis. School of Civil Engineering and Environmental Science, University of Oklahoma, Norman, Oklahoma. 2011.

Krier, D. Modeling of integral abutment bridges considering soil-structure interaction effects. Ph.D. Dissertation. School of Civil Engineering and Environmental Science, University of Oklahoma, Norman, Oklahoma. 2009.

Kunin, J. and Alampalli, S. Integral abutment bridges: current practice in the United States and Canada. Special Report 132. New York State Department of Transportation. 1999.

Kunin, J. and Alampalli, S. Integral abutment bridges: current practice in the United States and Canada. Journal of Performance of Constructed Facilities, American Society of Civil Engineers 14 (3). 2000. Pages 104-111.

Lawver, A., French, C. and Shield, C. K. Field performance of an integral abutment bridge. Transportation Research Board. 79th Annual Meeting, Washington, D.C. 2000.

Lehane, B. M., Keogh, D. L. and O'Brien, E. J. Simplified elastic model for restraining effects of backfill soil on integral bridges. Computers and Structures. Pergamon, Elsevier Services Ltd., New York 73 (1-5). 1999. Pages 303-313.

Loveall, C. L. Jointless bridge decks. Civil Engineering. American Society of Civil Engineers. November 1985. Pages 64-67.

Mistry, V. C. Integral abutment and Jointless bridges. Proceedings of the Federal Highway Administration Conference on Integral Abutment and Jointless Bridges, Baltimore, Maryland. March 2005. Pages 3-11.

Muraleetharan, K.K., Deshpande, S, and Adalier, K. Dynamic deformations in sand embankments: centrifuge modeling and blind, fully coupled analyses. Canadian Geotechnical Journal, 41(1). 2004. Pages 48-69.

Muraleetharan, K.K., Mish, K.D., and Arulanandan, K. A fully coupled non-linear dynamic analysis procedure and its verification using centrifuge results. International Journal for Numerical and Analytical Methods in Geomechanics 18. 1994. Pages 305-325.

Muraleetharan, K.K., Ravichandran, N., and Taylor, L.M. TeraDysac: TeraScale dynamic soil analysis code. Computer Code. School of Civil Engineering and Environmental Science, University of Oklahoma. Norman, Oklahoma. 2003.

Oesterle, R. G., Tabatabai, H., Lawson, T. J., Refai, T. M., Volz, J. S. and Scanlon, A. Jointless and integral abutment bridges. Summary Report. Construction Technology Laboratories, Skokie, Illinois. 1999.

Pentas, H. A., Avent, R. R., Gopu, V. K. A. and Rebello, K. J. Field study of longitudinal movements in composite bridges. Transportation Research Record 1476. Transportation Research Board, National Research Council, Washington, D.C. 1994a. Pages 117-128.

Pentas, H. A., Avent, R. R., Gopu, V. K. A. and Rebello, K. J. Field study of bridge temperatures in composite bridges", Transportation Research Record

1460. Transportation Research Board, National Research Council, Washington, D.C. 1994b. Pages 42-52.

Pugasap, K., Kim, W. and Laman, J. A. Long-term response prediction of integral abutment bridges. Journal of Bridge Engineering. American Society of Civil Engineers 14 (2). 2009. Pages 129-139.

Ravichandran, N. A framework-based finite element approach for solving large deformation problems in multi-phase porous media. Ph.D. Dissertation. University of Oklahoma, Norman, OK. 2005.

Reese, L. C., Cox, W. R. and Koop, F. D. Analysis of lateral loaded piles in sand. Offshore technical conference, Dallas, Texas, Paper No. OTC 2080. 1974.

Reese, L. C., Touma, F. T. and O'Neill, M. W. Behavior of driven piers under axial loading. Journal of the geotechnical engineering division, proceedings of the American society of civil engineers, 102(GT5). 1976. Pages 493-510.

Reid, R. A., Soupir, S. P. and Schaefer, V. R. Mitigation of void development under bridge approach slabs using rubber tire chips. Recycled materials in geotechnical applications, Vipulanandan, C. and Elton, D. J. (eds.), proceedings of the American society of civil engineers. 1998. Pages 37-50.

Russell, H. G. and Gerken, L. J. Jointless bridges – the knowns and the unknowns. Concrete International. American Concrete Institute, 16 (4). 1994. Pages 44-48.

Stanford, T. C. and Elgaaly, M. Skew effects on backfill pressures at frame bridge abutments. Transportation Research Record 1415. Transportation Research Board, National Research Council, Washington, D.C. 1994. Pages 1-11.

Siros, K. A. Three dimensional analysis of integral bridges. Ph.D. Dissertation. West Virginia University, Morgantown, West Virginia. 1995.

Thippeswamy, H. K., Raju, P. R. and GangaRao, H. V. S. Parametric study of single-span jointless steel bridges. Transportation Research Record 1460. Transportation Research Board, National Research Council, Washington, D.C. 1994. Pages 1-11.

Thippeswamy, H. K. and GangaRao, H. V. S. Analysis of in-service jointless bridges. Transportation Research Record 1476. Transportation Research Board, National Research Council, Washington, D.C. 1995. Pages 162-170.

Wasserman, E. P. Jointless bridge decks. Engineering Journal. American Institute of Steel Construction, Chicago, Illinois, 24 (3). 1987. Pages 93-100.

Wolde-Tinsae, A. M., Greimann, L. F. and Yang, P. S. Nonlinear pile behavior in integral abutment bridges. Final Report. Iowa DOT Project HR-227, Highway Division, Iowa Department of Transportation, Ames, Iowa. 1982.

Wolde-Tinsae, A. M., Klinger, J. E. and White, E. J. Performance of jointless bridges. Journal of Performance of Constructed Facilities. American Society of Civil Engineers, 2 (2). 1988. Pages 111-124.

Yang, P. S., Wolde-Tinsae, A. M. and Greimann, L. F. Effects of pre-drilling and layered soils on piles. Journal of geotechnical engineering, 111(1). 1985. Pages 18-31.

Yogachandran, C. Numerical and centrifuge modeling of seismically induced flow failures. Ph.D. Dissertation, University of California, Davis, California. 1991.

Appendix A: Borehole Logs

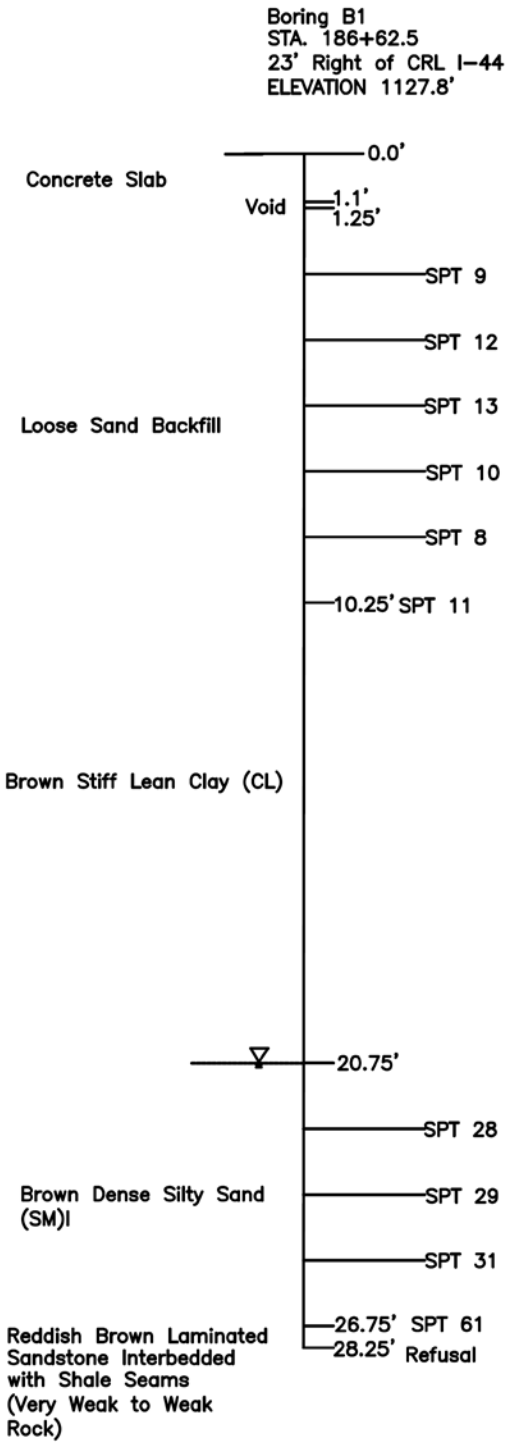

Figure A.1: Boring B1

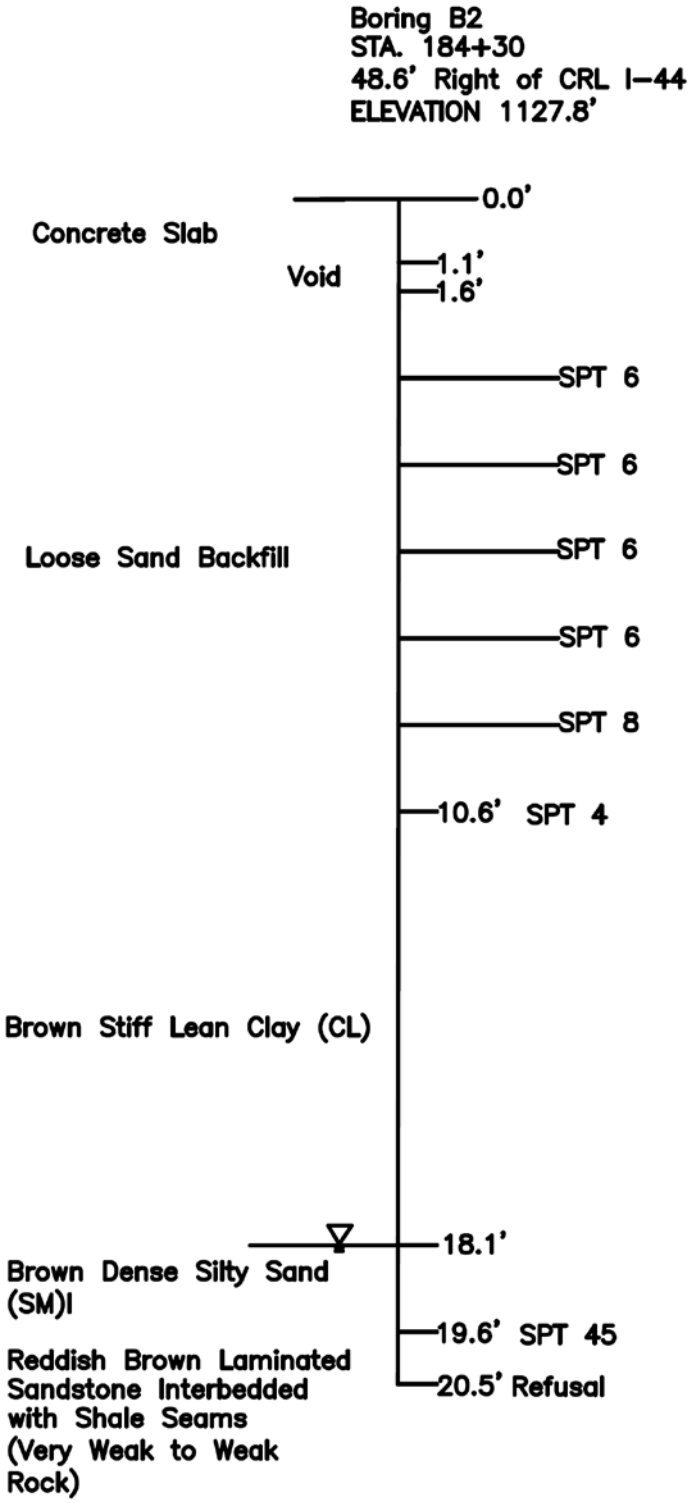

Figure A.2: Boring B2

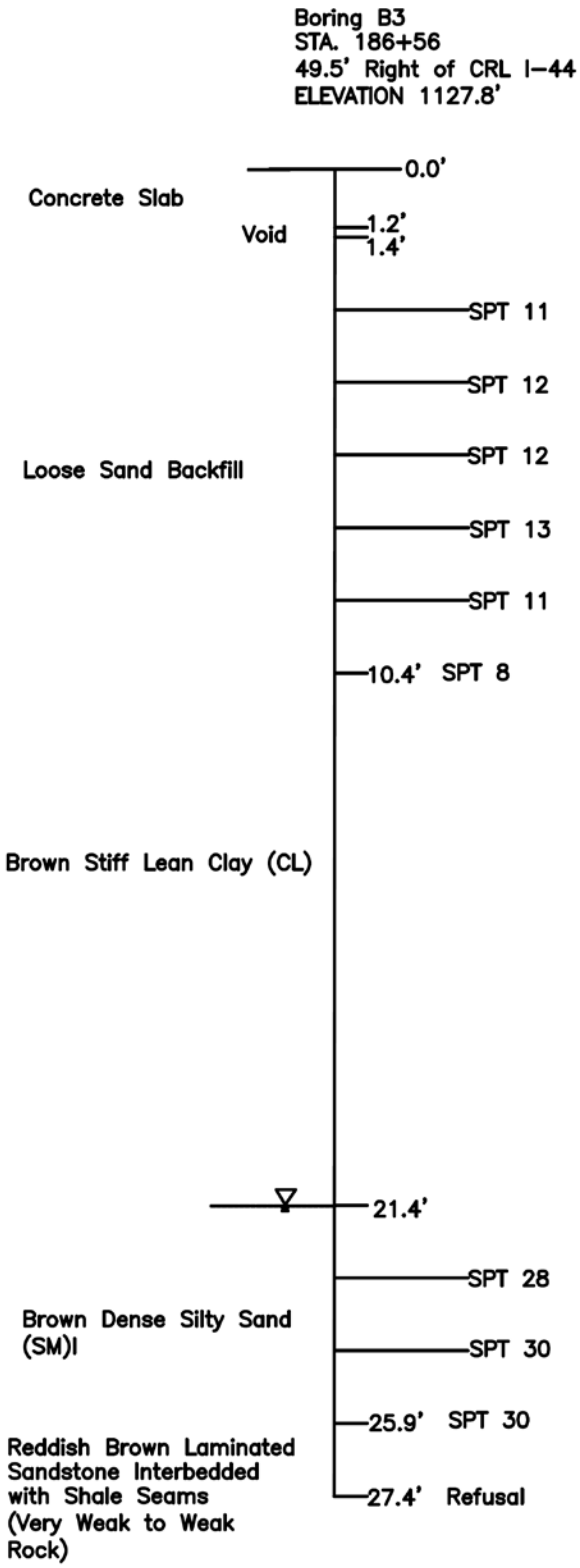

Figure A.3: Boring B3

Appendix B: CPT Logs

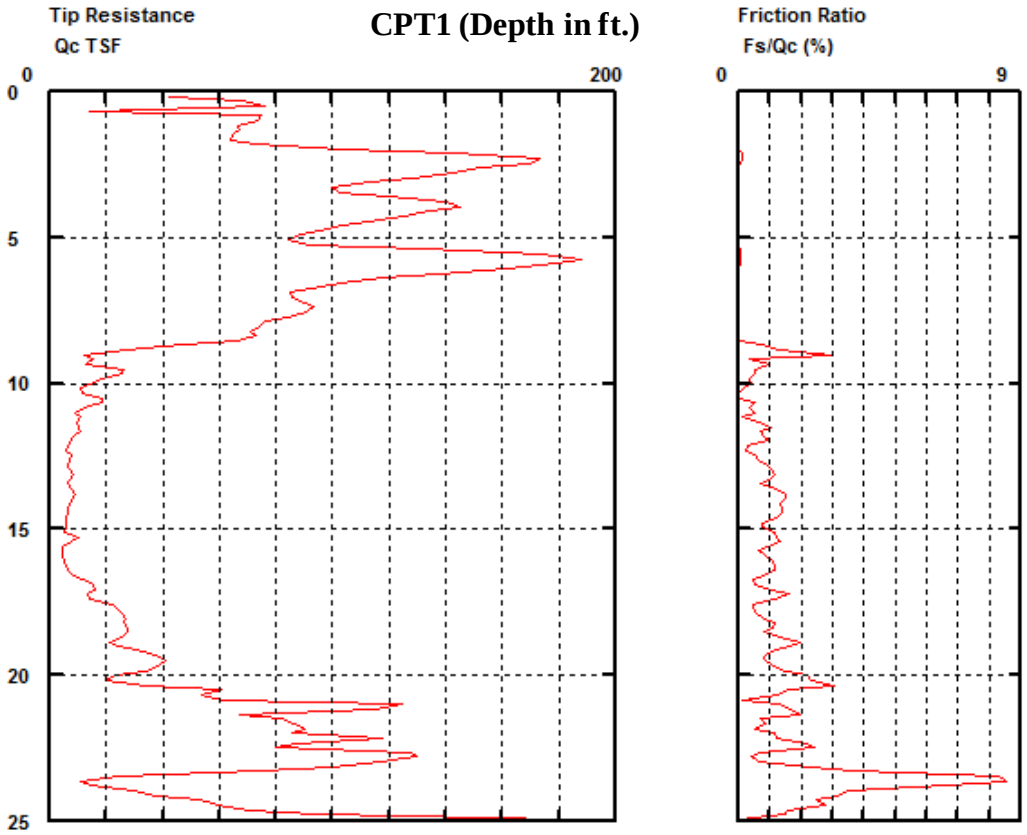

Figure B.1: CPT1

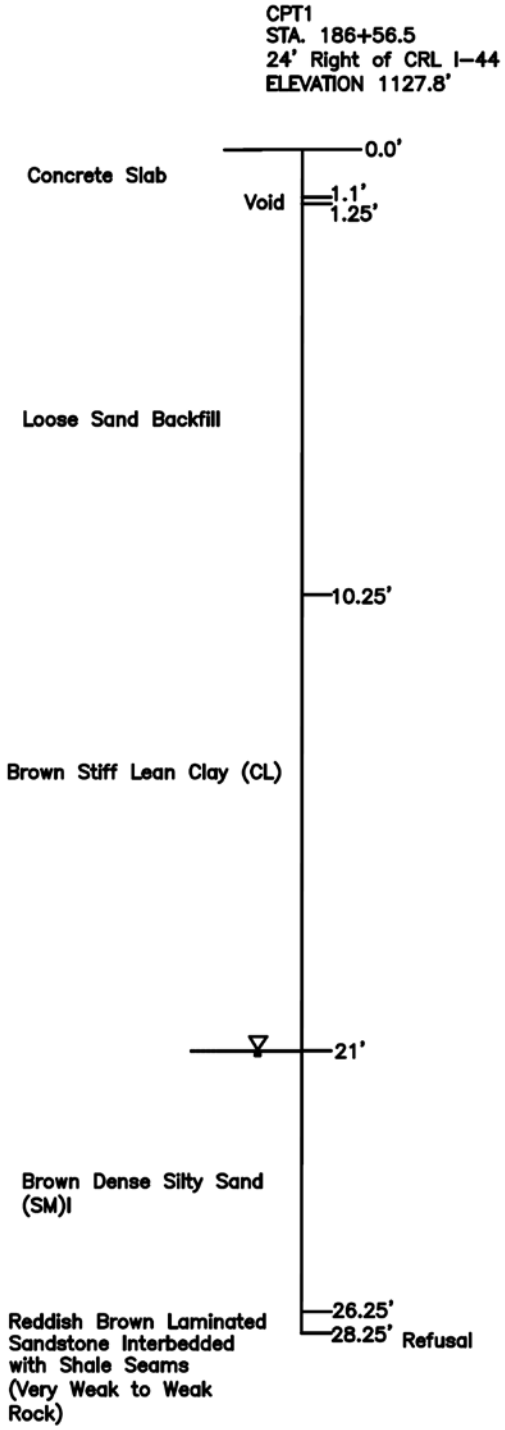

Figure B.2: CPT1

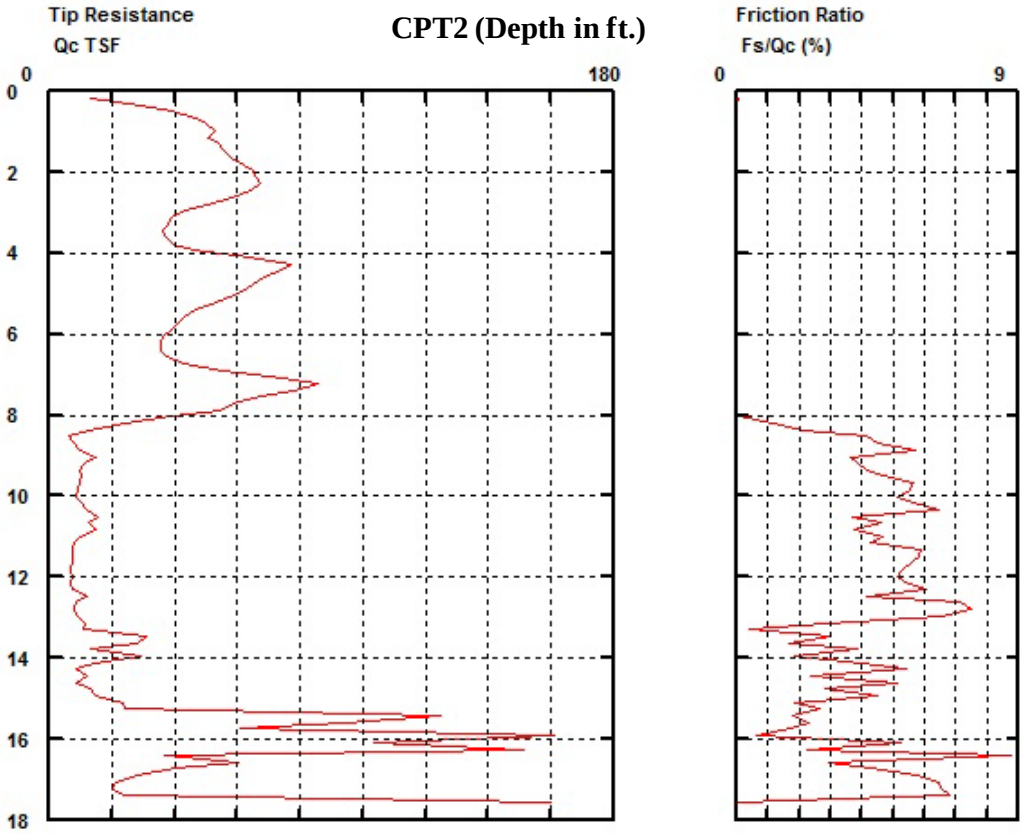

Figure B.3: CPT2

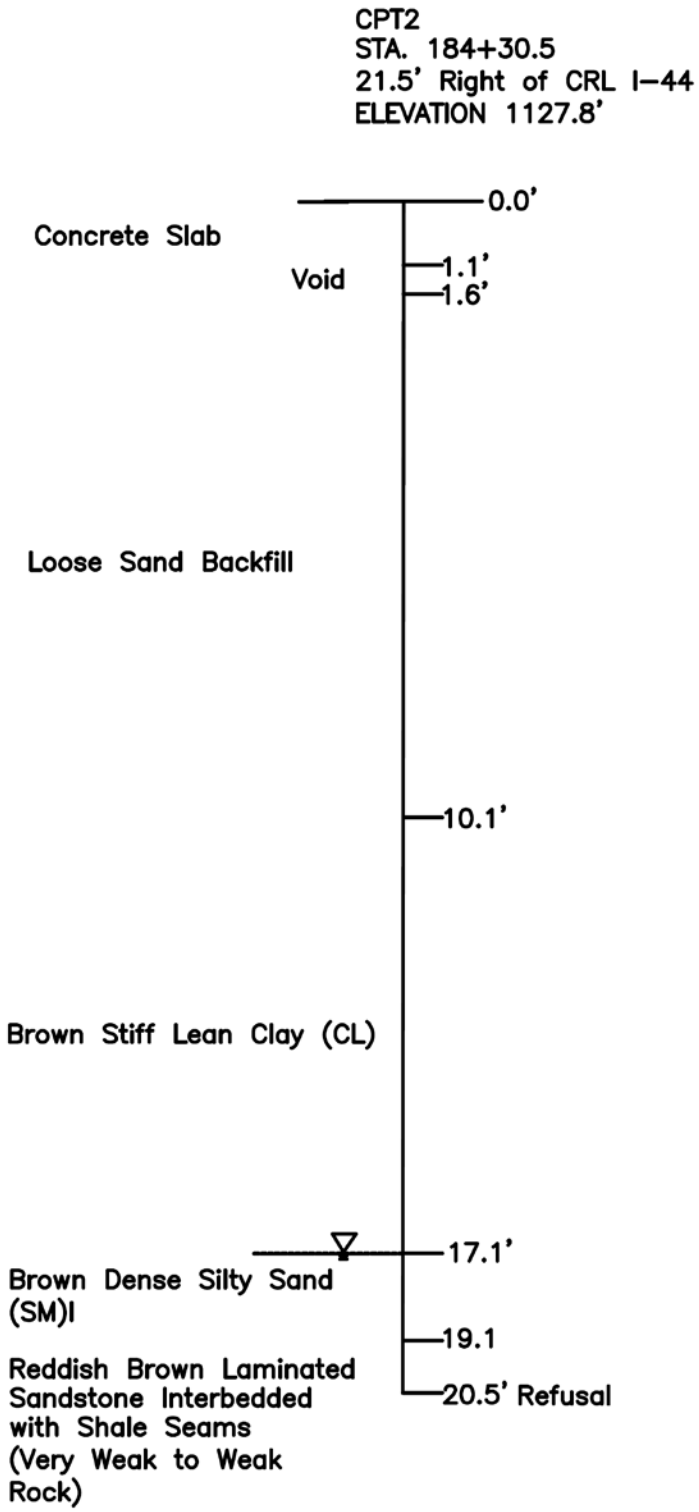

Figure B.4: CPT2

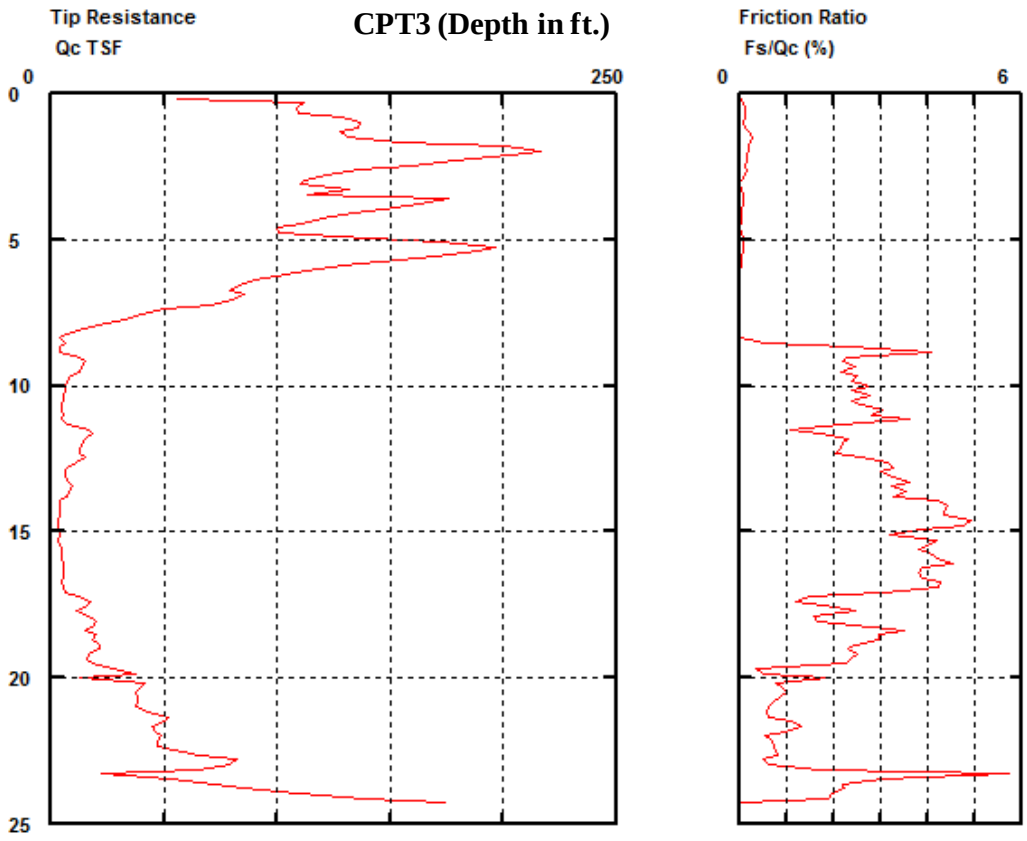

Figure B.5: CPT3

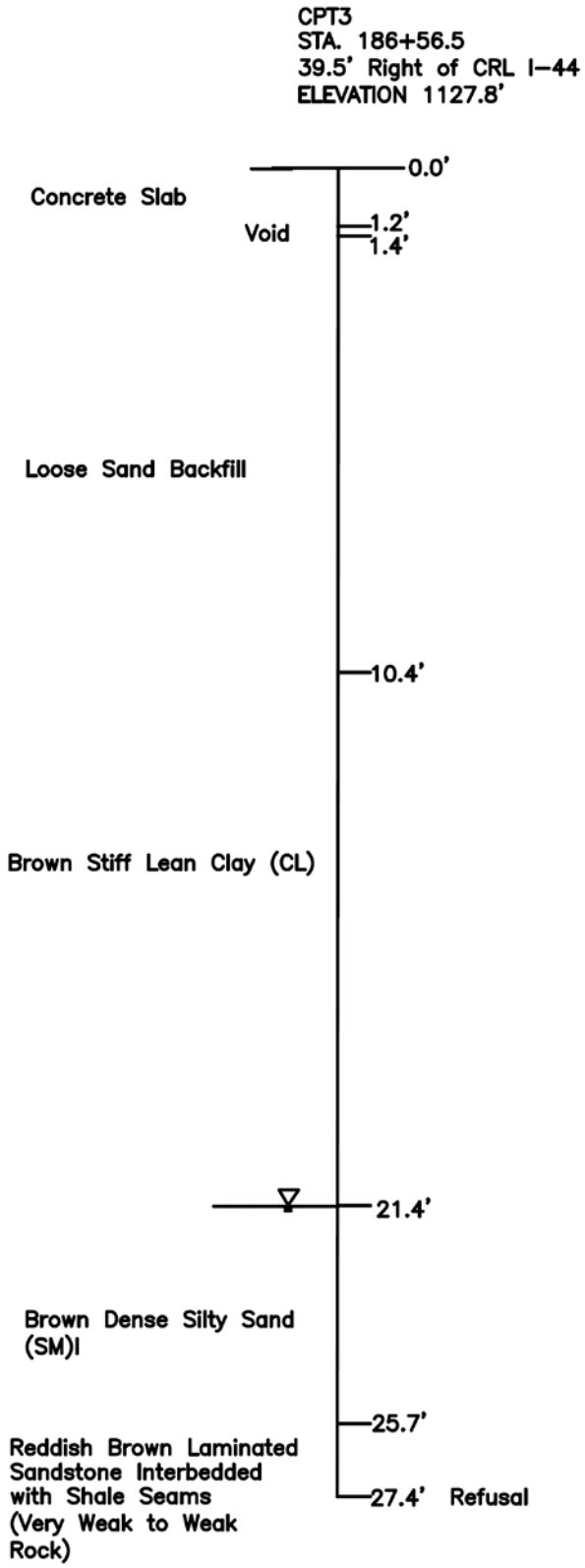

Figure B.6: CPT3

Appendix C: Laboratory Test Results

Table C.1: Moisture, Gradation and Atterberg Limit Test Results

Borehole	Sample Depth (ft)	Moisture (%)	% Passing #10	I% Passing #40	% Passing #200	Liquid Limit (LL)	Plasticity Index (PI)
BH1	22	16.5	100	100	24.9	-	-
BH3	12	26.5	100	100	83.3	37.9	18.6

Oedometer Test Results (Borehole B2, Sample Depth 12 feet)

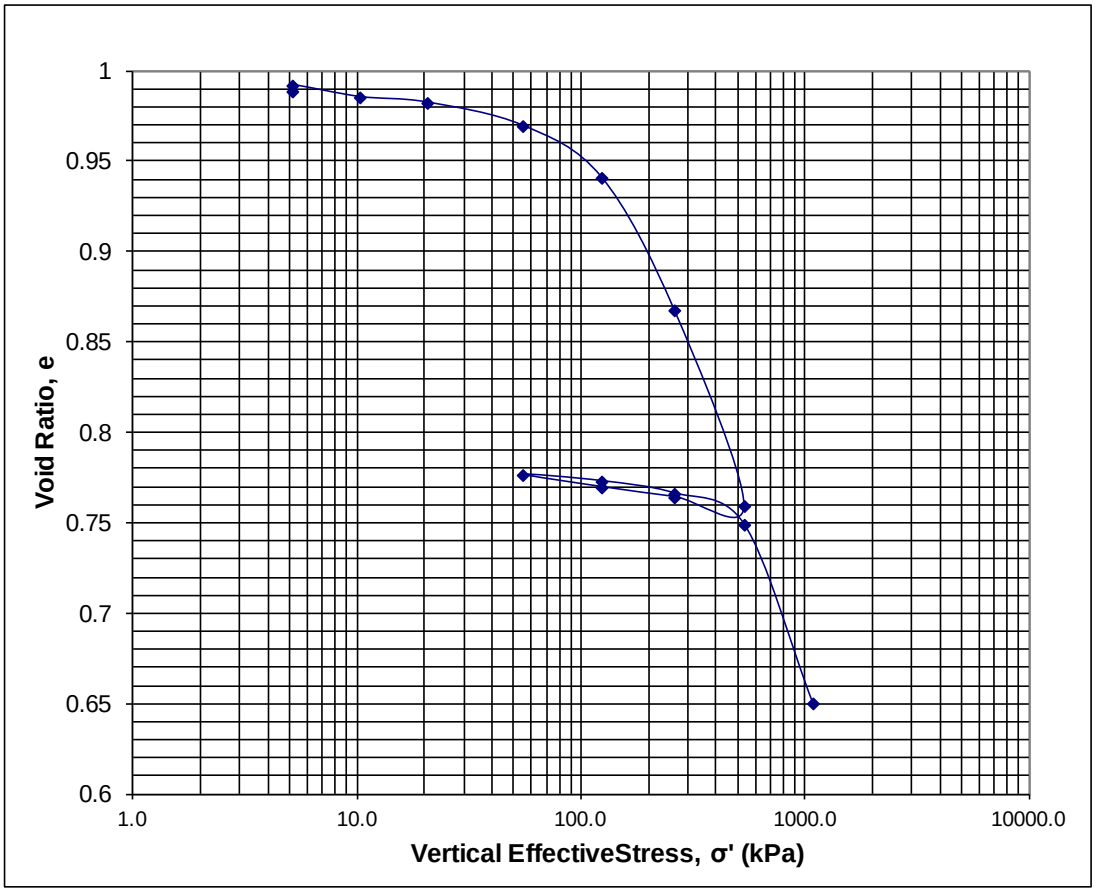

Figure C.1: Variation of Void Ratio with Applied Stress

CIUC Test Results (Borehole B3, Sample Depth 14 feet)

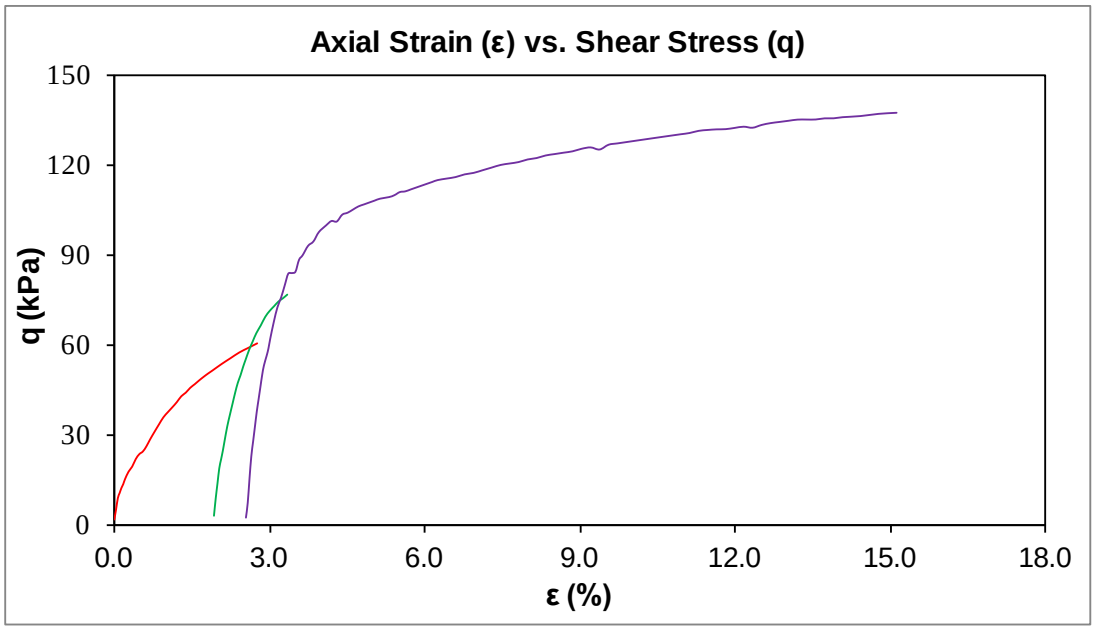

Figure C.2: Variation of Deviatoric Stress with Axial Strain

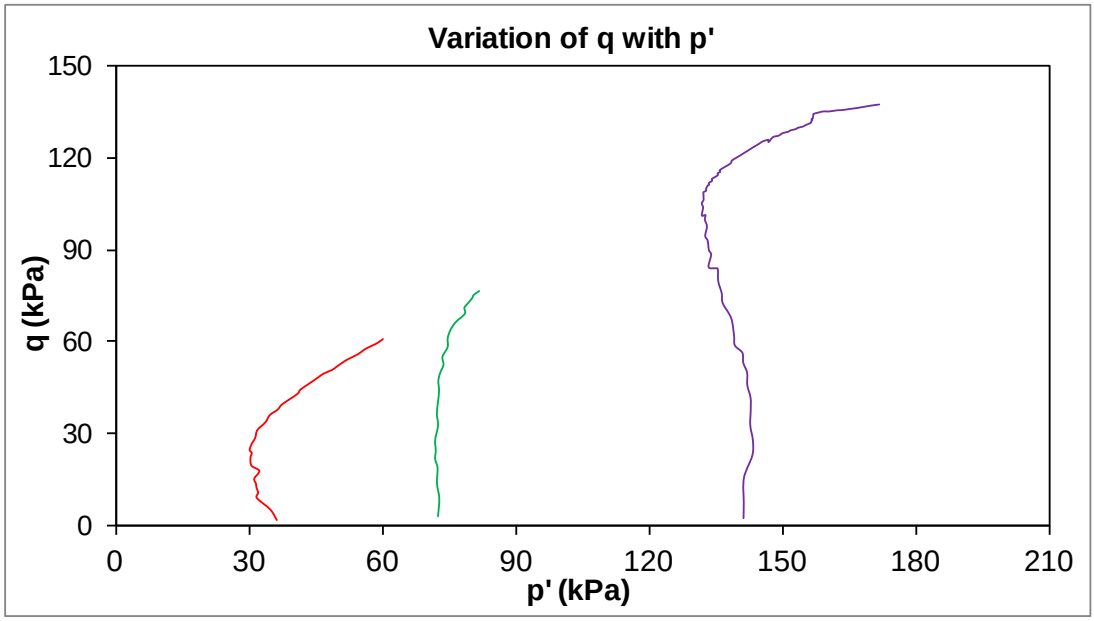

Figure C.3: Stress Path

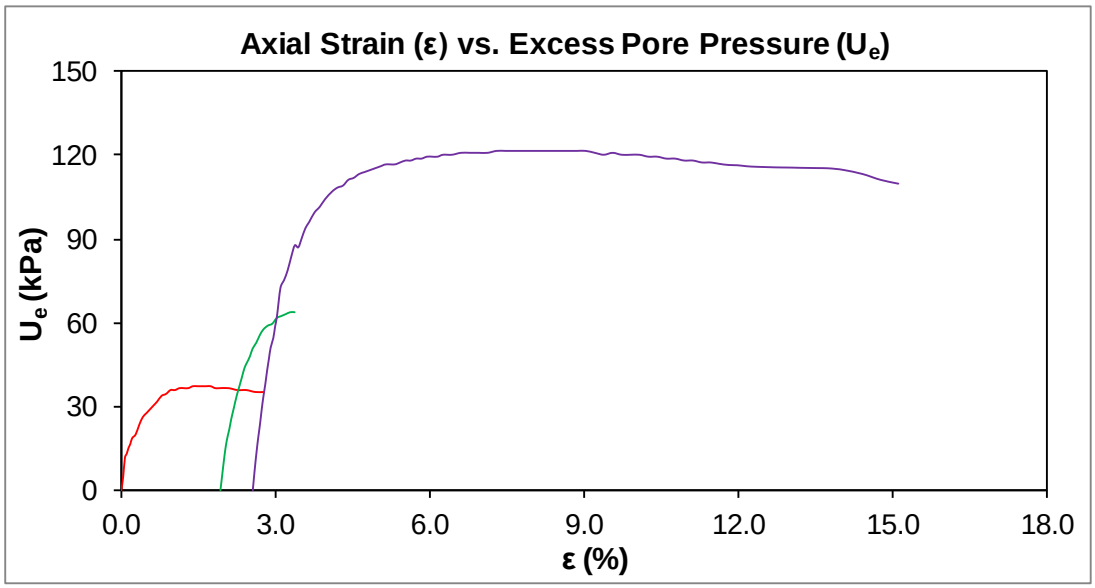

Figure C.4: Variation of Excess Pore Pressure with Axial Strain